Simulations of Saltwater Upconing in the Great Bend Prairie Unconfined Aquifer

Kansas Geological Survey Open-File Report 94-28f

T-S. Ma and M. A. Sophocleous

A cooperative investigation by

The Kansas Geological Survey and
Big Bend Groundwater Management District No. 5

Table of Contents

List of Tables

List of Figures

I. INTRODUCTION

1.1 Statement of the Problem

The major source of fresh water in the Big Bend Groundwater Management District #5(GMD5) is provided by the Great Bend Prairie aquifer. There is concern that the increasing withdrawal of groundwater in the Big Bend Groundwater Management District #5(GMD5) may cause significant decline of groundwater levels and contribute to the rising of the freshwater-saltwater interface from the saltwater source in the underlying geologic formation. A decline in the available groundwater supply and the deterioration of water quality would eventually result in shortages of freshwater supply in the district if the trend is not stopped by a sound management strategy. However, a clear understanding of the present quantity and quality of the groundwater in the district is necessary before a management plan for sustainable supply can be adequately designed.

The purpose of this research is to study the dynamics of the groundwater system by using available historical data in the region, mathematical modeling, and geostatistical analysis. The results of this research are intended to provide technical support for a management policy for the long-term sustainable groundwater supply.

1.2 Objectives of Study

The specific objectives of this research are:

1. To estimate the aquifer parameters for the study area based on the existing data.
2. To compute the groundwater quantity and quality by using an existing 3-D finite-difference model (SWIFT II).
3. To use the conditional simulation technique to account for the uncertainty of aquifer parameters used in the groundwater flow model.
4. To develop a groundwater management model and to estimate the sustainable groundwater supply under various management policies.

II. GEOHYDROLOGICAL FEATURES AND DATA OF STUDY AREA AND METHODOLOGY

2.1 Geohydrological Features of Study Area

The study area is situated in the northern part of the Big Bend Groundwater Management District #5 (GMD5) of the state of Kansas as shown in Fig. 1. The area is bounded by the Arkansas River and the Rattlesnake Creek and is approximately 625 mi^2 (1600 km^2) which covers parts of Barton, Rice, Reno, and Stafford counties. According to the 1990 census of population in Kansas, the total population in Barton, Rice, Reno, and Stafford counties was approximately 100,000. The main agricultural crops are wheat, grain sorghum, corn, and alfalfa hay. Groundwater is used for urban household, livestock, industry, and irrigation. Most of the precipitation falls during the growing season from April through September. The precipitation records from 1955-1992 at the Hudson climatic station show that the mean annual precipitation is about 27.74 in. The study area has a typical continental climate with a wide range of temperatures, rapid evaporation, and variable precipitation. Recharge is mainly from the precipitation and the annual recharge only ranges from 1 to 3 inches, approximately 10% of the annual precipitation (Sophocleous, 1991). Groundwater discharge occur in the vicinity of the Quivira Marsh, and the Arkansas River downstream from the Great Bend and Rattlesnake Creek (Sophocleous, 1992). The primary source of freshwater in the eastern portion of the GMD5 (Fig. 2) is the Great Bend Prairie aquifer which is underlain by Permian red beds (Fig. 3A & 3B) containing brines. There is no effective separation between the Great Bend Prairie aquifer and the Permian red beds east of the boundary of the Cretaceous bedrock. The continuous extraction of fresh water in the upper aquifer may cause upward movement of the deeper saltwater resulting in the deterioration of water quality. Consequently, to maintain a sustainable supply of water of good quality becomes a serious concern to the GMD5 and the State. In 1993, an intensive study site, the Siefkes site (Fig. 4), was developed to provide much needed field data on saltwater intrusion into the freshwater aquifer.

The main geologic units in the Great Bend Prairie aquifer are described by Latta (1950), Layton and Berry (1973), Fader and Stullken (1978), and Cobb (1980) (Figs. 3A and 3B.). The major geologic units (Fig. 3A) in descending order are the Great Bend Prairie aquifer, the Cretaceous Formations, and the Permian rocks.

The Great Bend Prairie aquifer is in the drainage basin of the Arkansas River in south-central Kansas. The aquifer consists of alluvial sand, gravel, silt, and clay which were deposited by the ancestral Arkansas River. The thickness of the deposits range from several tens of feet to over 200 feet. The Cretaceous Formation which is known as the Dakota Formation is generally considered a confining or leaky confining layer; it effectively separates the Great Bend Prairie aquifer and the underlying Permian water bearing units. The Permian formations consist of reddish-brown sandstone, siltstone,

shale, salt, gypsum, anhydrite and limestone and are known to contain salt water. The saline water rises upward into the unconsolidated aquifer in the lower reaches of the Rattlesnake Creek and increases the salinity of the available groundwater. Roughly east of US-281, the surface aquifer directly contacts with the Permian formation, and a threat of saltwater from the Permian bedrock is a major concern in this area. In addition, Gillespie et al. (1991) indicated that in some places the hydraulic heads in the Permian bedrock are higher than the freshwater table. This phenomenon was verified with observations of the KGS/GMD5 monitoring-well network at sites 2, 4, 5, 15, 41, and 49 (Fig. 4). The direction of groundwater flow can be determined by water level at different locations. The 1991 water-table contour for GMD5 (Buddemeier et al, 1992) indicates that the direction of ground water flow is generally eastward. The upward leakage from the Permian Bedrock has been studied by Cobb et al. (1982). However, the aquifer hydrogeologic properties and hydraulic relationships are still not clear. In addition, unplugged wells, sinkholes, boreholes, and fractures may provide pathways for more rapid contaminant transport (Young, 1992); therefore, estimation of total leakage from Permian bedrock is a difficult task at this time.

2.2 Field Data

The ground-water-level data in the GMD5 are collected by the Kansas Geological Survey, the Division of Water Resources, GMD5, and the U.S. Geological Survey. Most of the wells are measured annually, some are quarterly, and a few well sites are equipped with continuous recorders. In order to avoid the influence from the irrigation pumping, most of the wells are measured in mid-winter. The water level data are published annually by the Kansas Geological Survey.

The bedrock elevation data were collected from the data used by Fader and Stullken (1978); the water-quality monitoring network established by the GMD5 since 1974; and the Kansas Geological Survey bulletins.

The natural gamma activity and formation conductivity in the monitoring well network (Fig. 4) is measured by using an electromagnetic (EM) logging tool (Young, et al., 1993). The data are collected at 0.1 foot intervals to obtain a vertical profile of conductivity. Water levels are also measured and recorded for each well before logging is conducted. The measured conductivity can be converted into its corresponding chloride concentration. A groundwater chloride concentration less than 500 mg/L is good for most general uses and is considered as the target for sustainable groundwater. Because of the noisy conductivity profile form the field measurements, the lowest conductivity value that can be reliably read is about 100 ms/m and this value corresponds to a chloride concentration of about 3300 mg/L, which is too salty for most uses. A curve fitting technique is employed to produce a smoothly fitted curve and the location of the 500 mg/L chloride concentration can be estimated (Garneau et al., 1994). The first logging was conducted in March, April, and May, 1993. The Permian well and the deep-aquifer well were logged for most of the well

sites; however, well sites 5, 39, and 49 were not logged due to inaccessibility. The results of the logging are documented by Buddemeier et al (1993).

The water level and the location of the saltwater-freshwater interface may vary from year to year, mainly due to the pumpage and yearly recharge. The observed water heads in the shallow aquifer and Permian monitoring wells in January 1994 were greater than or approximately equal to January 1993 due to the unusually high precipitation (high recharge) in 1993. At the Siefkes site, the water level increased 6 feet between April and October 1993, and the measured water level in March-April 1994 was still approximately 4 feet higher than the March-April 1993 level. Although groundwater heads had significant change in 1993, the amount of salt and the characteristics of most transition zones in the Great Bend Prairie aquifer remained rather stable. All the field data discussed above will be analyzed for the numerical model discussed later.

2.3 Methodology

The purpose of this research is to develop a quantitative relationship between groundwater withdrawal and saltwater intrusion based on field data and modeling. The results will then be used to investgate possible best management practices for attaining optimal sustainable groundwater supply for the study area. Sustainable groundwater supply is an estimated amount of supply of freshwater for the study area that is sustainable for a relatively long term without substantial saltwater intrusion.

Because the field data in the study area have been collected for quite a long period of time by the GMD5 and the KGS, the management model will integrate the existing data, knowledge, and the mathematical model for evaluating the effects of various management options. The focus will be on the assessment of sustainable groundwater and water quality. Pumping patterns (demand) and precipitation are considered as the two major factors for aquifer discharge and recharge, respectively. Several scenarios will be proposed and based on these two factors to predict the movement of the saltwater-freshwater interface 10 years after the present operating conditions. The usable groundwater is the saturated thickness between the top of the freshwater body to the upper part of the transition zone. Figure 5 is the general structure of this microcomputer-based decision support system. The whole structure consists of the following modules:

1. Database:

The database contains the information on the characteristics of the aquifer, groundwater quality and quantity.

2. Geostatistics:

The geostatistics base serves as a tool for the estimation of the value of each grid point for the simulation model. Three components are included which are the kriging, the cokriging, and the conditional simulation.

3. Simulation Model:

The SWIFT-II model (Reeves, et al., 1986) is a fully-coupled, transient , three-dimensional finite-difference model. This code has been verified against eight analytical solutions for heat flow and laboratory results (Ward et al., 1984). In addition, it has been applied to studies of nuclear waste isolation, deep injection (Ward et al., 1987) and mineral intrusion problems (Butow and Holzhecher, 1987). This model is apparently suitable for this study for the simulation of the present condition and trends of salt water interface of the Great Bend Prairie Aquifer

4. System Module

The system module is an user interface and serves as a bridge between the users and the whole system, which allows the users to perform the following tasks:

A. To define the region that will be analyzed.

B. To query the correct input data from the database.

C. To extract the data from the database.

D. To format the data for use by the simulation model.

5. Output Module:

The output module contains several programs to extract and clearly display output from numerical model.

Finally, the system manager will be developed based on the above five components. This will be able to generate feasible decision and to evaluate the various management options.

III. LITERATURE REVIEW

3.1 Literature on Saltwater Intrusion

Two approaches are generally used in analyzing the salt water intrusion. One assumes that there exists a sharp interface between saltwater and freshwater without mixing of these two fluids. The other is the solute-transport approach to include a transition zone with continuous variability of salinity created by the mixing of saltwater and freshwater and its dispersion. The latter approach is closer to reality and is preferred.

In certain special cases, the sharp interface approach can be applied to a large physical system for gaining some information on the general behavior of the interface under various stresses. The solute-transport approach uses a system of numerical methods to solve complex transport equations. Numerical instabilities and cost of computation time are two major concerns.

Sharp Interface Approach

This approach is employed when the thickness of the transition zone is small compared to the whole depth of the aquifer and the interface serves as a boundary where the flux and pressure is continuous. Solution of this approach will become difficult in three dimensional analysis due to the highly nonlinear interfacial boundary condition (Bear, 1979). Ghyben (1888) and Herzberg (1901) modeled coastal aquifers and simply assumed a static equilibrium and a hydrostatic pressure distribution in the freshwater and saltwater, that the depth of the interface can be determined by saltwater and freshwater densities, and that the freshwater head on the interface at a certain point is the same as the head on the water table at the same point which implied that no vertical head gradient was considered. The major criticism of this approach is that as the freshwater approaches the coast, the Ghyben-Herzberg relation is not satisfied. Muskat (1937) and Hubbert (1940) improved the Ghyben-Herzberg relation; the saltwater and freshwater interface was treated as a boundary with the pressure in equilibrium condition at a point on the interface. Many other studies have been developed based on the sharp interface approach. Wang (1965) used an analytical approach to determine the critical pumping rate in an unconfined aquifer. Sahni (1972) conducted experiments to study salt water upconing, and his experimental results were compared with the numerical results obtained by Chandler and McWhorter (1975). Wirojanagud and Charbeneau (1985) adopted finite difference and finite element techniques to investigate both steady-state and transient salt water upconing.

Density-Dependent, Solute-Transport Approach

In this approach, two nonlinear partial differential equations (the groundwater flow equation and the advection-diffusion (transport) equation) must be solved simultaneously by iteration. The governing equations are expressed in terms of

pressure (p) and intrinsic permeability (κ) because the total head (h) and hydraulic conductivity (K) are functions of density (ρ).

Many studies have been conducted based on this approach. Henry (1964) derived an analytical solution to describe the movement of a diffused saltwater wedge in a confined aquifer. Van der Veer (1977) also used a closed form solution to describe the flow of salt water and fresh water. Bear and Dagan (1964) conducted laboratory experiments by using a Hele-Shaw model to measure the advance of a salt water interface. Bennett et al. (1968) investigated the brine upconing in the Punjab Region of West Pakistan by using an electric-analog model. Reilly and Goodman (1987) used the Voss (1984) finite element model based on axisymmetric, linear, triangular elements in a cylindrical coordinate system to study a saltwater upconing interface, and the results were compared with the sharp interface approach.

Many numerical groundwater models have been developed in the past several decades. Mangold and Tsang (1991) provided a summary of 56 existing numerical codes along with a general description of the methods of analysis and capabilities. All these codes can be broadly classified into geochemical models, solute transport models, and hydrochemical models. The effect of salinity on fresh water is the major concern in this research, therefore, a solute transport model coupled with a groundwater flow model is the one adopted to simulate the salt water intrusion.

3.2 Review of Geostatistical Analysis

The mineral intrusion problem is solved numerically by two coupled partial differential equations, the fluid flow equation and solute transport equation. Since no closed form solution is obtainable for complex field problems such as the one under investigation here, these two coupled equations are solved numerically by using the finite-difference technique. The numerical technique divides the aquifer model into a finite number of grid cells, the aquifer geometry and properties for each discrete cell have to be estimated.

Henley (1981) and Davis (1986) described several estimation techniques. Generally, all these estimation techniques are to determine the weights for each available sampled data within the predefined search area. Estimation is the sum of the available data multiplied by their corresponding weights. Because the properties of an aquifer (permeability, storativity, transmissivity) usually exhibit a significant spatial variability, direct measurements of each point in space is practically impossible. Geostatistics is used to generate realizations of the regionalized variables (variables of interest) for the deterministic model.

Geostatistics has been applied to a variety of estimation problems in geohydrology since it was first developed by Georges Matheron (1963, 1971) and applied to the mining industry. In groundwater hydrology, the mapping of spatial

transmissivity and piezometric heads was performed by Delhomme (1978, 1979) and Palumbo and Khaleel (1983); Delhomme (1978) and Mantoglou and Wilson (1982) used conditional simulation to generate transmissivity fields; Ahmed and De Marsily (1987) adopted the cokriging technique to interpolate transmissivities by using the transmissivity and the specific capacity data; Smyth and Istok (1989) also used the cokriging technique to investigate a groundwater contamination problem.

Geostatistics is the statistics of spatially correlated data and the estimation is to solve a set of equations that describes the expected autocorrelation between values of sampled variables and samples to be estimated. The regionalized variables are assumed to be second-order stationary. Estimation of water level and bedrock is performed by the ordinary kriging technique; the semivariance, which describes the rate of change of regionalized variables, is the fundamental part of using kriging. Cokriging is adopted to estimate the saltwater freshwater-interface because the primary variable (saltwater freshwater interface) is undersampled. Similar to the variogram for spatial continuity of a single variable, the cross-variogram describes the cross-continuity between primary and secondary variables and is necessary for the cokriging technique. Conditional simulation will be performed to investigate the spatial distribution of permeability. The theory of geostatistics is well documented (Journel and Huijbregts, 1978; Carr et al., 1985). The geostatistical techniques used in this research will be discussed in chapter IV.

IV. GEOSTATISTICAL ANALYSIS OF FIELD DATA

Geostatistics initially (Matheron, 1963) stood for estimation problems in two- or three-dimensional fields using probabilistic tools. More recently, the term has been used more generally to describe all applications of statistics in hydrogeology and geology. For the groundwater flow, the heterogeneity of the subsurface often cannot be adequately characterized for use in deterministic models. Geostatistical simulations must be used to generate realizations of the random model parameters involved in the mathematical model. In this study, a method of optimal estimation of random fields called kriging is used to estimate groundwater level and bedrock elevation at unsampled locations based on values at sampled locations. The cokriging technique is adopted to estimate the undersampled saltwater-freshwater interface by utilizing the secondary, highly correlated bedrock elevation data. Finally, the conditional simulation technique is employed to generate the spatial realization of the hydraulic conductivity honoring the observed measurements. These geostatistical methods and applications are described in the following sections.

4.1 Ordinary Kriging

The objective of kriging is to find the best linear unbiased estimate of a random field which is assumed to be second-order stationary. A random field is said to be second-order stationary if it satisfies the following conditions in its mean, variance and covariance:

Stationarity is defined through the first- and second-order moments of the observed random function. For the first-order moment, the expected value of the random variable x must be constant.

$$\text{Mean} \quad : E\{Z(x)\} = m(x) = \text{m}, \qquad \text{independent of x} \qquad 4.1$$

$$\text{Variance} \quad : Var\{Z(x)\} = \sigma^2(x) = \sigma^2, \qquad \text{independent of x} \qquad 4.2$$

For the second-order moment requires that:

$$\text{Covariance} \quad : Cov\{Z(\vec{x}_1), Z(\vec{x}_2)\} = Cov(\vec{x}_1 - \vec{x}_2) = Cov(\vec{h}) = C(\vec{h}) \qquad 4.3$$

where $\vec{h} = \vec{x}_1 - \vec{x}_2$, *i.e.*, the covariance between the process at $\vec{x}_1$ and $\vec{x}_2$ is independent of the individual locations $\vec{x}_1$ and $\vec{x}_2$ and dependent only on their difference.

The variance is:

$$Var\{Z(x)\} = E\{[Z(x) - m(x)]^2\} = C(0) \qquad 4.4$$

and the semivariogram is:

$$\gamma(h) = \frac{1}{2} E\left\{\left[Z(x+h) - Z(x)\right]^2\right\} \qquad 4.5$$

Under the conditions of second-order stationarity, Eq. 4.2 can be introduced into Eq. 4.5, the relationship of the covariance and the semivariogram functions is as follows:

$$C(h) = \sigma^2 - \gamma(h) \qquad 4.6$$

In practical application, the semivariogram or the covariance is unknown and must be estimated from the sampled data using the following equation:

$$\hat{\gamma}(h) = \frac{1}{2N(h)} \sum_{i=1}^{N(h)} \left[Z(x_i) - Z(x_i+h)\right]^2 \qquad 4.7$$

where $\hat{\gamma}(h)$ is the value of the estimated variogram at lag h and $N(h)$ is the number of pairs of sampled values with a distance approximately h apart.

Since numerical difficulties, multiple solutions, or negative variance may occur when directly using the estimated semivariogram, an admissible semi-variogram model which fits the estimated semivariogram points and satisfies the positive definiteness condition is an alternative solution to guarantee an unique kriging solution (Christakos, 1984). Some of the most common semivariogram models which satisfy the constraint of positive definiteness are power, spherical, exponential, and Gaussian models (Cressie, 1991) and a linear combination of any of the above models is still positive definite. Figure 6 shows a typical semivariogram plot with computed points from sampled data and a Gaussian model. The three major components of a semivariogram model are the nugget, range, and sill. Theoretically, at zero distance, the semivariance is zero because the measurement is compared to itself. However, in application, sampling errors and small scale variation may result in a sharp discontinuity near zero distance. Therefore, the semivariance will extrapolate to a y-intercept and this is termed the nugget effect. As the separation distance increases, the corresponding variogram value also generally increase because the difference between variable measurements becomes larger. Beyond a certain separation distance, the corresponding value of the variogram will no longer be increasing and stays constant (plateau). The distance before the variogram reaches a plateau is termed the range, the value at which the variogram reaches the plateau is termed the sill.

Once the pattern of spatial continuity (semivariogram model) has been determined, ordinary kriging can be used to perform estimation. The idea of this method is to linearly determine the weights of the available data; the sum of weights is equal to one. In addition, it tries to have zero mean residual (error) and to minimize the variance of the errors. The ordinary kriging estimator is as follows:

$$\hat{Z}(x_0) = \sum_{i=1}^{n} \lambda_i Z(x_i) \qquad 4.8$$

where $\hat{Z}(x_0)$ is the kriging estimate at location x_0, λ_i is the weights for the location x_i, and $Z(x_i)$ is the observation at sampling location x_i.

To satisfy the second-order stationarity, $\hat{Z}(x_0)$ must be unbiased, therefore, the estimation error (difference between the estimate and the true value) is:

$$R(x_0) = \sum_{i=1}^{n} \lambda_i \cdot Z(x_i) - Z(x_0) \qquad 4.9$$

and substituting Eq. 4.1 to the above equation:

$$E\{R(x_0)\} = m(x)\left[\sum_{i=1}^{n} \lambda_i - 1\right] = 0 \qquad 4.10$$

where $R(x_0)$ is the estimation error, and $Z(x_0)$ is the true value.
therefore:

$$\sum_{i=1}^{n} \lambda_i = 1 \qquad 4.11$$

The estimation based on this technique is to have minimum variance of estimation error, unbiased linear estimator:

$$E\left[\left(\sum_{i=1}^{n} \lambda_i Z(x_i) - Z(x_0)\right)^2\right] = Minimum \qquad 4.12$$

The minimization of the above equation with the constraint (Eq. 4.11) can be done by introducing a Lagrange multiplier, μ:

$$\frac{\partial\ Var\left[\sum_{i=1}^{n}\lambda_i Z(x_i) - Z(x_0)\right]}{\partial\ \lambda_i} - 2\mu = 0 \qquad \text{for } i = 1,2,3,\ldots,n \tag{4.13}$$

and the ordinary kriging system in matrix form is:

$$\begin{bmatrix} \gamma_{11} & \gamma_{12} & \cdots & \gamma_{1n} & 1 \\ \gamma_{21} & & & \gamma_{2n} & 1 \\ \vdots & & & \vdots & \vdots \\ \gamma_{n1} & \gamma_{n2} & \cdots & \gamma_{nn} & 1 \\ 1 & 1 & \cdots & 1 & 0 \end{bmatrix} \begin{bmatrix} \lambda_1 \\ \lambda_2 \\ \vdots \\ \lambda_n \\ \mu \end{bmatrix} = \begin{bmatrix} \gamma_{01} \\ \gamma_{02} \\ \vdots \\ \gamma_{0n} \\ 1 \end{bmatrix} \tag{4.14}$$

With the γ's estimated from the variogram for the sampled data, γ's and μ can be formed from the solution of the above equation. The kriged value at any location can be calculated from Eq. 4.8.

The variance of the estimation error is:

$$\hat{\sigma}^2_{OK} = \sum_{i=1}^{n}\lambda_i\,\gamma_{0i} + \mu \tag{4.15}$$

The ordinary kriging is used to estimate 1992 and 1993 groundwater levels and bedrock elevations. The kriged 1992 groundwater level is used for the initial condition in the three-dimensional numerical simulation and the kriged 1993 groundwater level is used for the purpose of water head calibration. The kriged bedrock elevation is used for the bottom boundary of the Permian bedrock.

Application of Ordinary Kriging

The study area is 25x25 mi^2 (1600 km^2). To take the advantage of measurements outside the study area, the sample area was enlarged to 37x37 mi^2 (3505 km^2). For the extended area, there are 71 and 97 measured groundwater levels in 1992 and 1993, respectively, and 564 measured values of bedrock elevation. The locations of observation wells measured in 1992 and 1993 are shown in Figs. 7 and 8, respectively. The measurements for 1992 and 1993 do not exactly match because bad weather made some well sites inaccessible during measurement period. The locations of measured bedrock elevations are shown in Fig. 9. These measured values at sampled sites will be used to obtain the optimal estimates of the values at unsampled locations by kriging.

The first step of the estimation procedure is to find semivariograms which characterize the spatial variability of the groundwater level elevation and the bedrock elevation. Once a suitable semivariogram model is determined, the model is evaluated by cross validation (Davis, 1987). The objective of cross validation is to krige the known data one at a time based on the fitted model. If the mean and variance of the estimation error based on the semivariogram model are close to zero and one, respectively, the model is judged to be acceptable. In other words, the results of cross validation can be presented as a scatterplot of the estimated values versus the measured values and the plotted points should lie close to the 45-degree line. The ordinary kriging based on the obtained best fitted semivariogram model is then employed to estimate the values at unsampled locations. These computations can be performed using the GSLIB (Deutsch & Journel, 1992) software.

Estimated Bedrock Elevations for the Study Area

Cumulative probability and a histogram with the sample mean, variance, standard deviation, and quartiles of the bedrock elevations are shown in Fig. 10A and Fig. 10B, respectively. These plots are used to determine whether the observed data are normally distributed. The plotted points in Fig. 10A show convincingly that the bedrock elevation data are normally distributed except for a few very low and very high values. The Kolmogorov-Smirnov test is performed at a significance level of 5%. The test value for the sampled data is 0.039, which passes the value of the 5% significance level, 0.057, for normal distribution.

The measured bedrock elevations decrease in their values from west to east. All semivariograms are calculated with lag 1.4 miles and a tolerance ± 0.7 mile; for directional semivariograms an angular tolerance of ± 22.5 degrees is used. Fig. 11 is the plot of the calculated omnidirectional and directional semivariograms along E-W, NE-SW, N-S, and NW-SE directions. All semivariogram plots show an increasing trend except in the N-S direction perpendicular to the main trend of bedrock. In geostatistics, the continuous rise of the semivariance on Figs. 11A, C, D, and E indicate that no limited range can be specified; therefore, the sampled data exhibit a significant dip (descending trend) in the bedrock surface along the east, the north-east, and the south-east directions. Therefore, the fitting of a semivariogram model is determined by adopting the calculated semivariograms along the N-S direction due to its good continuity at the origin and nearly constant semivariance. In addition, the accuracy of kriged values depends mostly on the semivariograms at small lags, therefore, the best fitted semivariogram model is determined based on the first few semivariogram points. The final semivariogram model selected for kriging is the following spherical model:

$$\gamma(h) = \begin{cases} C\left(1.5\,\frac{h}{a} - 0.5\left(\frac{h}{a}\right)^3\right), & h \le a \\ C, & h > a \end{cases} \qquad 4.16$$

where the sill C is 2100; the lag distance h is in miles; the range a is 6 miles.

Cross validation was performed for the best-fit model. The fitted curve is shown in Fig. 11B. The kriged values at sampling locations are plotted versus the sampled values in Fig. 12. Figure 12 shows that the plotted points cluster around the 45-degree line. This means that the kriged values based on the spherical model are unbiased and the model is adequate for estimating the bedrock elevations at unsampled sites to provide a detailed pattern of the bedrock topography.

The bedrock surface obtained from the kriged values is shown in Fig. 13. A plot of contours of bedrock elevation is shown in Fig. 14. Figures 13 and 14 show the ragged features of the bedrock with higher elevations at the south-west and lower elevations in the east. The variability of the bedrock elevation will be included in developing a three-dimensional numerical model and will be used for interpretation of saltwater intrusion.

Analysis of Groundwater Level Data

Previous analysis of the measured groundwater levels indicates that the groundwater level generally dips from west to east (Mitchell, et al., 1993), and that a significant spatial trend exists in the groundwater level data. Thus the calculated semivariogram is expected not to reach a constant sill as the distance increases because of the non-stationarity of the data. Consequently, the trend must be estimated and be removed from the original data so that the residuals required for kriging satisfy the stationarity condition thus allowing the semivariogram model to be found. To accomplish this, both linear and nonlinear trends are fitted with a first-degree and a second-degree polynomials as follows:

Linear trend:

$$\textit{Water level elevation} = -7.47\,X - 1.72\,Y + 1909.93 \qquad 4.17$$

Non-linear trend:

$$\textit{Water level elevation} = -7.66\,X^2 - 1.62\,Y^2 - 0.020\,X + 0.068\,XY - 0.034\,Y \qquad 4.18$$

where X and Y are the coordinate along the east and the north direction, respectively.

The goodness-of-fit of Eq. 4.18 is 0.98 which is slightly better than the first-order with 0.97 and Eq. 4.18 is used to remove the estimated trend from the data at sampled locations.

After the nonlinear trend was removed from the original data set, a cumulative probability plot and histogram plot with sample mean, variance, standard deviation, and quartiles of the residuals are plotted and shown in Fig. 15. The Kolmogorov-Smirnov test indicates that the residuals of piezometric heads are normally distributed at a significance level of 5 %. Figure 16 is a plot of omnidirectional and directional semivariograms of residuals along E-W, NE-SW, N-S, and NW-SE directions with a lag of 3.2 miles and a tolerance of ± 1.6 miles. For the directional semivariograms, an angular tolerance of ± 22.5 degrees is used. The best fitted model is the spherical model (Eq. 4.16) along the E-W direction with a sill equal to 120 and a range of 12 miles.

Again, cross validation is carried out based on the best fitted model and the results are shown in Fig. 17. There are a few points deviating substantially from the 45-degree line. It is reasonable to adopt the spherical model for kriging.

The final results are obtained by adding the removed trend back to the kriged residuals. The 1992 groundwater surface is shown in Fig. 18 and a plot of groundwater level elevation contours is shown in Fig. 19. The number on each contour in Fig. 19 indicates the water level elevation. The highest elevation is 1900 ft designated as B and the lowest elevation is 1700 ft designated as 1. Unlike the bedrock contours shown in Figs. 13 and 14, the surface for the piezometric heads is very smooth with higher values at the southwestern corner and gradually decreasing eastward. The trend is quite similar to that of the bedrock elevation as one would expect.

The data of the 1993 piezometric heads is analyzed in the same manner to obtain the estimated values for comparing the results from the numerical model using the 1992 values as the initial values. The results will be presented and discussed later.

4.2 Cokriging

When the primary variable of interest is undersampled, but the secondary variables are spatially cross-correlated with the primary variable, then the secondary variables can be utilized to improve estimates of the primary variable. To ensure that the cokriging technique can be performed properly, the modeling of the auto- and cross-variograms of two or more variables have to be performed; second-order stationarity is also assumed.

Similar to the one-variable case (kriging), for m regionalized variables and n sample locations ($Z_j(x_i)$, $j = 1,2,...,m$; $i = 1,2,...,n$), the cross-covariance is:

$$C_{jk}(h) = E\{Z_j(x) \cdot Z_k(x+h)\} - m_j\, m_k \qquad 4.19$$

the cross-variogram is

$$\gamma_{jk}(h) = \frac{1}{2} E\{[Z_j(x+h) - Z_j(x)][Z_k(x+h) - Z_k(x)]\} \quad 4.20$$

If $j = k$ then the above equation reduces to Eq. 4.5. The cross-semivariogram is symmetric, however, the cross-covariance is not. The matrices of cross-covariances or cross-semivariograms are used for estimation. The relationship between the cross-covariance and the cross-semivariogram is as follows:

$$2\gamma_{jk}(h) = 2C_{jk}(0) - C_{jk}(h) - C_{kj}(h) \quad 4.21$$

The difficulty is not to find all the models but to ensure the model is positive definite (Myers, 1982), otherwise, negative variance, numerical difficulties, or multiple solutions may occur.

Cokriging is similar to kriging, however, the data that are being estimated are based on different attributes. The cokriging estimator for $Z_1(x_0)$ is:

$$\hat{Z}(x_0) = \sum_{i=1}^{n} \Gamma_i Z(x_i) \quad 4.22$$

where $Z = (Z_1, Z_2, ..., Z_m)^T$; each Γ_i is an unknown m x m weight matrix which needs to be determined.

Under the constraint of unbiasedness:

$$E\{\hat{Z}(x_0)\} = E\{Z(x_0)\} \quad 4.23$$

therefore, the estimation error can be minimized.

$$\min E\{Z_1(x_0) - \hat{Z}_1(x_0)\}^2 \quad 4.24$$

As discussed above, the modeling of the spatial correlation for the primary and secondary variables and the cross-correlation between these two are the fundamental part of obtaining the optimal cokriging weights. A detailed discussion of this approach is given by Myers (1982).

Locations of the saltwater-freshwater interface will be estimated by using the cokriging technique and the estimated interface will be used for the initial interface condition in the three-dimensional numerical simulation.

Saltwater-Freshwater Interface

Young et al. (1993) conducted a linear regression analysis of the measured locations of the saltwater-freshwater interface. The interface is somewhat arbitrarily set at a place where the measured conductivity equal to 100 mS/m. They proposed the following empirical formula for the interface as a linear function of piezometric head and bedrock elevation:

$$Z = -76.0271 + 0.4873\, Z_W + 0.5331 Z_B \qquad 4.25$$

where

Z = the elevation of the saltwater freshwater interface (ft, MSL).
Z_W = the elevation of groundwater level (ft, MSL).
Z_B = the elevation of the top of the bedrock (ft, MSL).

It is interesting to note that Eq. 4.25, generally, gives a value of the elevation of the interface equal to the average of the groundwater surface elevation and the elevation of bedrock. In this study, the saltwater freshwater interface data is determined by adopting the previously kriged groundwater level and bedrock elevations and the results are shown in Fig. 20 (3-D surface plot) and Fig. 21 (2-D contour). Basically, the interface follows the topography of the bedrock, Fig. 14, but is smoother than the bedrock surface due to very smooth surface of piezometric head, Fig. 19.

Since 1993, field measurements of the saltwater-freshwater interface, piezometric heads, and bedrock elevations have been obtained at a limited number of sampling locations. The sampling location and the measured values are shown in Fig. 22 and listed in Table 1. The correlation between the bedrock and interface and the water table and interface is shown in Fig. 23. The correlation coefficients and the rank correlation are also presented in Fig. 23. It is seen that the correlation coefficients between the bedrock and interface is about 0.79 and that between the interface and the water level is 0.59 and the rank correlation is 0.644. Instead of using both bedrock and groundwater level two secondary variables to estimate the location of saltwater-freshwater interface, only the bedrock elevation is used in the cokriging technique to estimate the elevation of the interface.

In cokriging, in addition to the semivariogram model for the bedrock elevation, Eq. 4.16, the semivariogram model for the interface and the cross-variogram model between the bedrock and the interface are also needed. The calculated results are shown in Fig. 24 and Table 2. The fitted models for both cases are the spherical model.

The semivariogram model for the saltwater-freshwater interface was estimated using a distance lag of 5.5 miles, and a tolerance ± 2.75 miles. The fitted omnidirectional spherical model is:

$$\gamma(h) = \begin{cases} 2200\left(1.5\,\frac{h}{10} - 0.5\left(\frac{h}{10}\right)^3\right), h \le 10 \\ 2200 \qquad\qquad\qquad\quad , h > 10 \end{cases} \qquad 4.26$$

Due to limited number of measured values, the fitted model does not match well the sample variograms for distance lag beyond 20 miles. For lags less than 10 miles, the semivariograms compared well with the sample. Therefore, Eq. 4.26 is still considered as an acceptable semivariogram model.

The cross-variogram for the interface and the bedrock was calculated with lag 5.5 miles, tolerance ± 2.75 miles. The following spherical model with sill 1300 and range 12 miles is selected as the fitted cross-variogram model.

$$\gamma(h) = \begin{cases} 1300\left(1.5\,\frac{h}{12} - 0.5\left(\frac{h}{12}\right)^3\right), h \le 12 \\ 1300 \qquad\qquad\qquad\quad , h > 12 \end{cases} \qquad 4.27$$

Based on the linear combination of the above fitted models, Eqs. 4.16, 4.26, and 4.27, cokriging is performed and the estimated elevations of the saltwater-freshwater interface are shown in Figs. 25 and 26. The corresponding standard deviation is also estimated. The contour of the estimated standard deviation is shown in Fig. 27.

Because of the high correlation between the bedrock and the interface, the contours of the interface are similar in pattern to the contours of the bedrock elevation shown in Fig. 14. The contour of estimation error (Fig. 27) shows that in an approximately square area defined by four measured wells, the error increases sharply from the location of the well to a maximum located around the center of the square area. A reasonable solution would be to place an additional observation well near the center of each square (highest estimation error).

4.3 Stochastic Simulation by Simulated Annealing

The kriging techniques described above focus on the accuracy (minimizing the variance of the estimate error) of the estimated value of the random variable at a location with little concern about whether the estimated random process would be the same as the real stochastic process. In fact, estimated values of the random field tend to smooth out local variations.

If such estimates of hydraulic conductivity of the system were used in the governing equations, these parameters would not predict well the large-scale effects of local spatial variability. Therefore, a simulation technique is required for generating a parameter field that possess fluctuation patterns similar to the real process. If the generated parameter field also honors the sampled values at sampled locations, then it is called the conditional simulation.

The conditional simulation is another geostatistical approach to generate the realization of a random function. Unlike the kriging estimation that the histogram of the estimated data is not the same as the histogram of the sampling. The realization generated from the conditional simulation has the same structure as the experimental data; in other words, both the estimated and observed data have the same mean, variance, histogram, and variogram. The theoretical fundamentals of this technique was presented by Matheron (1973). Basically, the semivariogram model which describes the spatial variability of the random variable is used by this technique to reproduce values at unsampled locations honoring the observed values of a regionalized variable, and the processes of this approach are to calculate the unconditional simulated values at each point first, after which the simulated values are adjusted based on the observed values.

Some of the commonly used simulation methods are as follows:

1. The turning bands method (Matheron, 1973).
2. The lower-upper decomposition method (Davis, 1987).
3. The simulated annealing (Kirkpatrick, et al., 1983)

Any of the above techniques can generate an infinite number of different solutions; however, the constraint that the simulation must honor the observed data will reduce the number of solutions. The simulated annealing technique is employed in this study and the theory of this technique is briefly discussed below.

The Simulated Annealing

Since the simulated annealing (SA) was first introduced by Kirkpatric, Gelatt, and Vecchi (1983) for solving the combinatorial optimization problems, the SA has been applied to a wide variety of problems. The concept of this technique is based on an analogy between the physical annealing process of solids and the combinatorial optimization problems. Annealing is a thermal process that first increases the temperature high enough so that the particles of the solid are in a highly mobile status, then slowly decreases the temperature to allow the particles to align themselves until a highly structured lattice is reached (Press et al., 1992).

The SA first assigns a value randomly based on the cumulative density function of the sampled data to each grid point in the simulated area, and then pairs of nodal values z_i and z_j are chosen randomly and swapped. The swap of pairs of nodal values is

to adjust the semivariogram model $\gamma^*(h)$ of the simulated realization and finally match the semivariogram model $\gamma(h)$ of the observed data. Therefore, the objective function O can be defined as:

$$O = \sum_h \frac{\left|\gamma^*(h) - \gamma(h)\right|^2}{\gamma(h)^2} \qquad 4.28$$

The square of the $\gamma(h)$ at each lag is to standardize the units and give more weight to closely spaced (low variogram) values. Every swap of the pairs of nodal values will update the objective function and whether the swap will be accepted or not is determined by the following acceptance criterion:

$$P\{accept\} = \begin{cases} 1 & \text{if } O_{new} \le O_{old} \\ \exp\left(\frac{O_{old} - O_{new}}{t}\right) & \text{if } O_{new} > O_{old} \end{cases} \qquad 4.29$$

where the $\frac{O_{old} - O_{new}}{t}$ is known as the Boltzmann Probability distribution (Aarts and Korst, 1989). t is the control parameter which is similar to the temperature parameter in the Boltzmann distribution and must be lowered slowly to avoid convergence to a local minimum.

The swapping process will continue and the objective function O will gradually decrease until it approaches zero, in other words, the semivariogram model $\gamma^*(h)$ of the simulated realization matches the semivariogram model $\gamma(h)$ of the observed data.

Spatial Realization of the Permian Bedrock Permeability

The sources of the permeability data of the Permian bedrock in the study area are from the previous reports of field tests (Gillespie and Hargadine, 1911, Cobb, 1980), and the field tests carried out by Butler et al (1993). The locations and the field test data are shown in Fig. 28. The limited number of data are anamorphosed to satisfy the constraints that the random function is second order stationary and univariate standard normally distributed. The histogram plot of the obtained normal scores with sample mean, variance, standard deviation, and quartiles are plotted and shown in Fig. 29. The omnidirectional semivariograms based on the normal scores are calculated and listed in Table 3. The best fitted semivariogram model is determined based on the first few semivariogram points, and the fitted exponential model is shown in Fig. 30. The fitted exponential model was estimated by using distance lag of 3.6 miles and a tolerance of ± 1.8 miles as follows:

$$\gamma(h) = C\left[1 - \exp\left(-\frac{h}{a}\right)\right] \qquad 4.30$$

where the sill C is 1; the lag distance h is in miles; the range a is 3.2 miles.

As can be seen from Fig. 30, the calculated semivariograms matched well for lags less than 8 miles, therefore, Eq. 4.30 is considered as an acceptable semivariogram model.

The initial realization of the study area is generated by assigning a value randomly to each node from the cumulative density function of the normal score data; however, the conditioning data are assigned to the nearest grid nodes. The initial realization is updated by swapping pairs of nodal values randomly, however, the conditioning data remain constant, and the acceptance of the swap of the nodal values is determined by Eq. 4.29. Once the swap of the nodal values is accepted the semivariogram model $\gamma^*(h)$ will be updated and the objective function (Eq. 4.28) will be decreased. The process will be terminated as the objective function O finally approaches zero. Fig. 31 shows the comparison of the calculated semivariograms, $\gamma^*(h)$, and of the simulated realization to the semivariogram model, $\gamma(h)$, based on the observed data. Because the $\gamma^*(h)$ is not obtained from the whole realization, the local $\gamma^*(h)$ does not match perfectly with the global $\gamma(h)$. The final optimal normal scores are backtransformed to the original space and the realization of the Permian bedrock permeability is shown in Fig. 32. From the results, the Permian bedrock permeability can be categorized into two groups: the more permeable area around the lower south and the east part of the study area with the average permeability around 0.5 ft/day ($\geq$0.1 ft/day) and the rest of the study area with the average permeability around 0.05 ft/day ($\leq$0.1 ft/day).

The conditional simulation approach adopted in this study takes the spatial attributes of the sampled data and reproduces the realistic realization of the natural variability of the Permian bedrock formation, however, the simulated realization can be significantly improved if a few more field test data can be obtained as suggested and shown in Fig. 28.

V. NUMERICAL MODEL FOR SALTWATER INTRUSION

5.1 Numerical Model

The groundwater flow in the Great Bend Prairie aquifer is stratified with freshwater in the upper region and saltwater near the bedrock. The source of the saltwater is the highly mineralized water of the Permian rocks. The whole aquifer is considered as unconfined. The stratified flow is governed by Darcy's law, the conservation of mass of fluid and the conservation of mass of salt in a porous medium. The governing equations, the initial and boundary conditions are described as follows:

Conservation of Mass of Fluid

The conservation of mass is to express the balance of water and solute mass in a solid matrix. The ground water equation is based on the conservation of mass coupled with Darcy's law for flow in a porous medium. The general equation is:

$$-\nabla \cdot (\rho \underline{u}) - Qw + Rc' = \frac{\partial}{\partial t}(\Phi \rho) \qquad 5.1$$

where

ρ : fluid density (ML^{-3}).

$\underline{u}$: fluid velocity vector (LT^{-1}).

Qw : sink or source [$(M(L^3T)^{-1}$], a positive sign denotes a sink, a negative sign denotes a source.

Φ : porosity.

Rc' : salt dissolution [$(M(L^3T)^{-1}$].

$$\nabla = \left(\frac{\partial}{\partial x}\right) i + \left(\frac{\partial}{\partial y}\right) j + \left(\frac{\partial}{\partial z}\right) k \ .$$

i, *j*, and *k* are unit vectors in the Cartesian coordinates.

The scalar product of ∇ operator and $\rho \underline{u}$ gives the mass flux per unit volume at each point. The term on the right hand side is an unsteady term which states the rate of change of fluid mass per unit volume. Sinks or sources are used to represent the recharge or discharge wells in the interior grid of the model.

The flow equation is the Darcy's law:

$$\underline{u} = \left(\frac{\kappa}{\mu}\right) \cdot (\nabla p - \rho g \nabla z) \qquad 5.2$$

where

κ : solid matrix permeability (L^2), a vector quantity.

μ : fluid viscosity [$M(LT)^{-1}$].
g : gravitational acceleration (L/T^2).
z : potential head (L).

Fluid density is assumed to be a function of salt concentration and pressure and the equation of fluid density is given as:

$$\rho = \rho_o \left[1 + C_w(p - p_0) + C_c\hat{C}\right] \qquad 5.3$$

and

$$C_c = \frac{(\rho_I - \rho_N)}{\rho_0} \qquad 5.4$$

where

ρ_I : fluid density at reference temperature and pressure at unit brine concentration (M/L^3).
ρ_N : freshwater density at reference temperature and pressure (M/L^3).
ρ_0 : the fluid density for the initial conditions (M/L^3).
$\hat{C}$: local salt concentration (M/L^3).
C_W : compressibility of the water $[M/(LT^2)]^{-1}$.
p : local pressure in the aquifer $[M/(LT^2)]$.
p_0 : reference pressure $[M/(LT^2)]$.

The fluid viscosity depends on the salinity concentration and the temperature of the fluid and is expressed as

$$\mu = \mu_R\left(\hat{C}\right)\exp\left[B\left(\hat{C}\right)\left(T^{-1} - T_R^{-1}\right)\right] \qquad 5.5$$

where T_R is the reference temperature of rock surrounding the wellbore; the relationship between $\mu_R(C)$ and B(C) is determined from the available viscosity, μ, temperature, T, and concentration, $\hat{C}$, data. The determination of fluid viscosity is discussed by Reeves et al. (1986), and internally included in SWIFT II code.

Porosity Φ is a function of pressure p:

$$\Phi = \Phi_0\left[1 + C_R(p - p_0)\right] \qquad 5.6$$

where

Φ_0 : the dimensionless porosity at the reference pressure.
C_R : the compressibility of the pores (Pa^{-1}).

Conservation of Mass of Salt

The solute mass balance is expressed as:

$$-\nabla\cdot\left(\rho\,\hat{C}\,\underline{u}\right) + \nabla\cdot\left[\rho\,(D + D_m I)\cdot\nabla\hat{C}\right] - Q_w\hat{C}_1 = \frac{\partial}{\partial t}\left(\Phi\,\rho\,\hat{C}\right) \qquad 5.7$$

where

D_m : molecular diffusivity (L^2T^{-1})
D : dispersion tensor (L^2T^{-1})
I : identity tensor

The above equation describes the rate of change of solute in the fluid phase in terms of the net dispersive and diffusive flux, the net advective flux, and the solute source or injection rate.

The dispersion coefficient is originally from Bear (1961) and Scheidegger (1961). For an isotropic porous medium, the dispersion tensor D is a function of velocity of groundwater flow, and can be expressed by the longitudinal dispersivity α_L (m) and the transverse dispersivity α_T (m):

$$D_{ij} = (\alpha_L - \alpha_T)\frac{v_i\,v_j}{v} + \alpha_T v\delta_{ij} \qquad 5.8$$

where

$v_i(x,y,t)$: velocity in the i the direction.
δ_{ij} :Kronecker delta function.
$v = \left(v_1^2 + v_2^2 + v_3^2\right)^{1/2}$
i and j are unit vectors in the Cartesian coordinates.

Initial and Boundary Conditions

For the problem of interest, supplementary information (initial and boundary conditions) has to be provided for the solution of the above equations.

Hydrostatic equilibrium is assumed for the initial pressure distribution. However, if the constant flux Darcy flux is specified as the initial condition, Eq. 5.2 will be performed to adjust the hydrostatic pressure. In addition, brine concentration is initially specified at appropriate locations to represent the initial saltwater distribution.

The boundary condition is to specify that the dependent variables are known functions of space and time in the simulated domain. The boundary conditions can be generally classified into Dirichlet, Neumann, and Cauchy three types of boundary conditions.

The initial and boundary conditions and the above two partial different equations (Eq. 5.1 & Eq. 5.7) are solved by the finite-difference scheme to determine the piezometric heads and the concentrations at nodes inside the aquifer boundary.

The numerical algorithm and its associated computer code is referred to as SWIFT II (Reeves et al., 1986). The SWIFT II model is a three-dimensional, fully transient, finite-difference approximation and is well documented by Reeves et al. (1986). Numerical procedures for solving the governing equations require an appropriate mesh in space and time steps. The set of linear equations generated by spatial discretization have to be solved repeatedly as the simulation time advances. To solve the partial differential equations (Eqs. 5.1 & 5.7) by using the finite difference technique, the two-line, successive overrelaxation method (Varga, 1962) is employed. It is a block-iterative method, the optimal overrelaxation factor is firstly estimated to increase convergence; then two neighboring lines of nodes are oriented and solved together by direct elimination. Once the optimal relaxation parameters and the optimal directions are determined at the time step for each transport equation, a convergent solution can be achieved. Although this matrix solver is efficient, numerical dispersion and oscillations will occur and accumulate at each time step due to the truncation of the high order derivatives of the Taylor series. The finite difference equations are considered to be stable if the numerical dispersion and oscillations are less than a certain tolerance. The numerical instability is mainly from the diffusion-convection equation (Price, et al., 1966); therefore, stability analysis is recommended before the numerical simulation is implemented.

The application of the von Neumann method is one of the ways to check the stability. This method is straightforward, however, the derivation of the stability criteria may be tedious and it can only be applied to linear problems with constant coefficients (Noye, 1981).

A general guide to avoid numerical problems is to check the Courant number (CO) which controls numerical oscillation from the discrete approximation of the time derivative, and the Peclet number (PE) which controls oscillations from spatial discretization. These two constraints provide a general guide for the selection of the local grid spacing in x, y, and z directions and for the time step Δt (Frind, 1982). These two criteria corresponding to the x coordinate direction are:

$$Co_x = \frac{v_x \Delta t}{\Delta x} \leq 1 \qquad 5.9$$

$$Pe_x = \frac{v_x \Delta x}{D_{xx}} \leq 2 \qquad 5.10$$

The same criteria also apply to y and z coordinate directions. For multi-dimensional transport, stability criteria are functions of variables in all directions.

The flow equation (Eq. 5.1) does not involve the convective diffusion term; therefore, the numerical instability is not significant and can be usually ignored.

5.2 Modeling Saltwater Upconing Beneath a Pumping Well

The saltwater upconing under a single pumping well is simulated numerically to understand the basic characteristics of the upconing phenomenon and to provide information for guiding the future study of more complex situations such as three-dimensional effects. Because of the uncertainty of the aquifer parameters, a sensitivity analysis is performed to investigate the effect of aquifer parameters on the upconing of the saltwater.

An axisymmetrical flow model including the density-dependent solute-transport which discretizes the partial-differential equations and boundary conditions in time and space into the cylindrical-coordinate system (Fig. 33) is used to investigate the saltwater upconing. A second-order correct central difference approximation in both time and space is used to eliminate numerical dispersion with carefully chosen grid size and time step during simulation. The model mesh for an area of 3200 meters by 74 meters is shown in Fig. 34A and 34B. In the radial direction, variable spacing ranging from 0.4 meter to 200 meters was employed. In the vertical z direction, variable spacing varying from 3 meters in the top two rows to 2 meters in the next two rows and 1 meter for the rest was employed. The pumping well has a radius of 0.4 meter with the center at radius equal to zero. The pumping well is screened from 23 to 32 meters below the initial water table.

Eight simulation cases are considered and summarized in Table 4. Case #1 will be used as a reference model and the sensitivity analysis will be performed to investigate the impact of the aquifer parameters and clay layers on the upconing of the saltwater. The values of variables and parameters and the boundary conditions used in case #1 are summarized in Table 5 and Table 6, respectively. The initial water table condition is assumed to be horizontal and is allowed to vary due to the change of fluid pressure. The total simulation period is one year; a constant, continuous pumpage of 0.05 m^3/s (~800gpm) is applied throughout the whole simulation period. Saltwater initially starts at 54 meters below the initial water table and a transition zone with linearly varying brine concentration from 0.0 to 0.025 is assumed. The physical system of case #1 is shown in Fig. 35A. Case #2 is to investigate the impact of the continuous and discontinuous clay layers on the upconing of the saltwater under pumping stress. All the input parameters and boundary conditions are the same as case #1 except for the continuous clay layer is placed 49 meters below the initial water table (Fig. 35B) and the discontinuous clay layer is also placed 49 meters below the initial water table with a 20 meter-wide discontinuity located 35 meters away from the pumping well

(Fig. 35C). The clay layer is 10 meters in thickness with radial conductivity, Kr, and vertical conductivity, Kz, equal to 0.023 m/d, and effective porosity equal to 0.02. The typical saltwater upconing at 7th and 30th day and their corresponding water drawdown from the simulation are shown in Figs. 36A, B, C and Figs. 37A, B, C, respectively. A plot of brine concentration versus time (Fig. 38) shows the effect of clay layer. As can be seen from Figs. 36A, saltwater with lower concentration initially moves upward faster and the mixing process between that saltwater and freshwater is more significant than that involving the higher concentration saltwater in the deeper aquifer. Once the lower concentration saltwater reaches the well screen (Fig. 37A), the movement of the lower concentration saltwater stays around the well screen due to the upward flow below the well screen. The higher concentration saltwater subsequently approaches the well screen. The amount of discharged salt continuously increases, nonlinearly, in the early pumping stage and gradually reaches a constant value (steady state). Fig. 36B and 37B show that the continuous clay layer serves as a barrier which protects the upper part of the freshwater alluvial aquifer from salt intrusion. Fig. 36C and 37C show that the discontinuity provides an access for the saltwater to move freely up the upper aquifer under pumping stress. From the results of Fig. 38, the discontinuous clay layer case has a sharper brine concentration increase at the early stage than the no clay layer one; this is because a higher flow velocity passes through the discontinuity, which causes a faster movement of the saltwater upconing in the discontinuous clay layer case than the no clay layer one. However, the discharged salt is limited due to the limited source of salt in the discontinuous clay layer case and the long term salinity problem in the discontinuous clay layer case is less than the no clay layer one. The continuous clay layer does effectively prevent the saltwater from intruding into the upper freshwater aquifer, however, the water drawdown is the most significant.

Case #3 is to investigate the effect of porosity by changing the values of porosity from 0.002 to 0.4 and Fig. 39 is the plot of brine concentration versus time in the discharged water. In a unit aquifer volume, lower porosity means less water content and the mixing of freshwater and saltwater will be less significant due to the limited supply of water. Therefore, under a constant pumping stress, the movement of the upconing saltwater will be faster than the case with higher porosity and this is clearly demonstrated in Fig. 39. The realistic range of the effective porosity is around 0.15 to 0.35 and it is usually considered as a constant parameter, therefore, the effect of the effective porosity is not as significant as the hydraulic conductivity which will be discussed next.

Case #4 is to investigate the effect of radial conductivity by changing the values of radial conductivity form 0.23 m/d to 2300 m/d and Case #5 is to investigate the effect of vertical conductivity by changing the values of vertical conductivity from 0.23 m/d to 2300 m/d. The hydraulic conductivity with the value of 2300 m/d for both cases is an unrealistic value; however, it is used for the purpose of comparison. The

results are shown in Fig. 40 and Fig. 41. The hydraulic conductivity can vary several orders of magnitude in some cases, and is usually considered as the most uncertain parameter. From the results, the saltwater upconing is directly controlled by the vertical conductivity (Fig. 41), however, the mixing of freshwater and saltwater is dominated by the radial conductivity and the upconing of the saltwater is inversely controlled by the radial conductivity (Fig. 40).

Case #6 is to investigate the effect of the well screen location by shifting the well screen 10 meters up and down. Fig. 42 is the plot of brine concentration versus time with 3 different well screen locations. As can be seen from the results, the discharged saltwater is somewhat sensitive to the locations of the well screen and a nonlinear relationship between the location of the well screen and the discharged saltwater is existed.

Case #7 is to investigate the effect of recharge by increasing the recharge from 0 in./year to 15 in./year. Fig. 43 is the plot of brine concentration versus time with 4 different recharges. The four curve lines in Fig. 43 practically overlapped, which explains that the recharge can only very slightly alleviate the problem of the saltwater upconing.

Case #8 is to investigate the effect of pumpage by changing the pumping rate from 0.01 m^3/s to 0.19 m^3/s. A family of nonlinear relationship of the brine concentration versus time under various pumpages at the 10th, 30th, 50th, 100th, 200th, and 300th days is shown in Fig. 44. The result from this simulation can help to determine appropriate discharge rates for a safe yield of the groundwater resources.

The above investigation provides some information on the relationships between saltwater and freshwater in groundwater systems. The saltwater upconing is sensitive to the hydraulic conductivity, the clay layer, and the pumping rate. Once the hydraulic conductivity and clay layer can be determined the only significant parameter which will have a great impact to the salinity is the pattern of pumpage.

5.3 Three-Dimensional Simulation

Model Design

The study area (Fig. 1) is situated on the north part of GMD5 which is bounded by the Arkansas River and the Rattlesnake Creek; the total area is 25x25 mi^2 (1600 km^2). The Siefkes site is located near the center of the study area.

Three dimensional Cartesian geometry was adopted for regional numerical simulation. The whole study area is meshed as 25 x 25 x 19 (Fig. 45) and discretised with a uniform grid of 1,600 m x 1,600 m (1 mile x 1 mile) in the X-Y direction and a variable spacing in the vertical direction (6 m from the top to 12 m depth, 4 m from 12 m to 24 m, 3 m from 24 m to 54 m, and 4 m fro 54 m to 70 m). The kriged 1992

water level and saltwater-freshwater interface are used for the initial condition and the kriged bedrock elevation is used for the bottom bedrock boundary condition. The major natural recharge is from precipitation and the amount of recharge is assumed to be uniformly distributed throughout the whole year and is used as the input recharge data in simulation. The locations of irrigation wells are shown in Fig. 46; however, to accommodate the model grid, the groundwater rights were lumped as shown in Fig. 47. The lumped pumping rate for initial regional simulation is shown in Table 7. The grid block regions indicated as "inactive" (Fig. 47) are removed from the simulation by setting pore volumes to zero to reduce computer resource requirements.

To satisfy numerical stability, the time step is chosen to be not greater than 1 day, and the total simulation period is initially chosen as 1 year. The simulation area outside the Arkansas river and the Rattlesnake creek are set to be inactive. The boundary condition along the Arkansas River and the Rattlesnake Creek is assumed to be constant pressure. Because the area of most interest is around the Siefkes site, the boundary condition at the left outer edge is also assumed to be constant pressure. Constant pressure and brine concentration are assumed at the bottom bedrock boundary. All pumping wells are located above the saltwater-freshwater interface. Pumping stress is divided into three stress periods. The first stress period is from the first day of simulation to the 120th day; no pumpage is assumed during this stress period. The second stress period is from the 120th day of simulation to the 300th day, and spatially variable pumping stress is used based on the lumped groundwater rights. The third stress period starts from the 300th day of simulation to the last day of simulation and no pumpage is assumed. Required input data for the saltwater intrusion model are summarized as follows:

1. the areal aquifer parameters (hydraulic conductivity, porosity, longitudinal and transverse dispersivity).
2. bedrock elevation.
3. water level elevation.
4. saltwater-freshwater interface elevation.
5. locations of pumping wells and pumping rates.
6. initial and boundary conditions.
7. natural recharge.

The value of input parameters are shown in Table 8. Numerical computation is performed on the Sun Sparc 10 workstation and the whole simulation takes approximately 16 hours to complete.

The mechanism of the saltwater upconing is still not clear, the only factors considered in this simulation are the location of the pumping well and pumpage. Presentation of the three-dimensional simulations are still in progress.

VI. CONCLUSIONS

6.1 Upconing Under a Pumping Well

The density-dependent solute-transport approach is the most realistic way to simulate the saltwater intrusion problem. However, because the actual physical system is usually very complicated and some parameters are difficult to obtain (in particular, the coefficient of dispersivity), the simulation of the real physical systems is quite costly. A simplified axisymmetrical model is used to investigate the local saltwater upconing problem and some conclusions can be drawn from the results.

1. Saltwater upconing is very sensitive to the pumping rate, clay layer presence and continuity, and the hydraulic conductivity. The location of the well screen certainly affects the saltwater upconing, however, it is not as significant as the three parameters discussed above.
2. The transition zone is not symmetrical around the 50% isobar, and it is more significant when the transition zone approaches the pumping well due to the relatively higher velocity field around the pumping well. The spreading of brine is wider in the higher velocity zone than in the lower velocity zone.
3. The clay layer (low hydraulic conductivity) serves as a protection that greatly retards the upward movement of saltwater under pumping stress. However, the discontinuous clay layer fails to protect the fresh water from the upconing saltwater.

This study gives an inexpensive way to understand the basic characteristics of the saltwater upconing and also provides some general guides for well design to maintain a long term supply of groundwater resources. In addition, the effort on the more complex three-dimensional simulation can be reduced based on the information obtained from this study. However, this conceptual model can not handle the interaction of saltwater upconing under the multi-well system, the three-dimensional numerical model will be used to investigate this problem.

6.2 Three-Dimensional Numerical Simulation

The three-dimensional numerical model has the advantages in simulating problems that two dimensional simulations can not address; however, its application can be limited by the computing facilities. A finer model is necessary for better simulation results; however, the computation time and computer storage are two major concerns. Since the recent development of computer technology, the above limitations are not crucial. The SWIFT II model is suitable for three-dimensional simulation, however, results are still in progress and will be discussed in a later report.

6.3 Future Work

The following are the tasks that will be studied in the future:

1. Numerical simulation of the three-dimensional saltwater intrusion.
2. Development of the decision support system.

REFERENCES

Aarts, E. and Korst, J., "Simulated Annealing and Boltzmann Machines," John Wiley, New York, 1989, 272 pp.

Ahmed, S. and De Marsily, G., "Comparison of Geostatistical Methods for Estimation Transmissivity Using Data on Transmissivity and Specific Capacity," Water Resource Research, Vol. 23, No. 9, 1987, pp. 1117-1137.

Bear, J., "On the Tensor Form of Dispersion," Journal of Geophysical Research, Vol. 66, No. 4, 1961, pp. 1185-1197.

Bear, J., "Hydraulics of Groundwater," McGraw-Hill Book Company, New York. 1979, 569 pp.

Bear, J. and Dagan, G., "Moving Interface in Coastal Aquifers," ASCE Journal of the Hydraulics Division, Vol. 90 No. HY4, 1964, pp. 193-216.

Bennett, G. D., Mundorf, M. J. and Hussain, S. A., "Electric-Analog Studies of Brine Coning Beneath Fresh-Water Wells in the Punjab Region, West Pakistan," U.S. Geological Survey Water-Supply Paper 1608-J, 1968, pp. J1-J31.

Buddemeier, R. W., Sophocleous, M. A., and Whittemore, D. O., "1992, Mineral intrusion: Investigation of salt contamination of ground water in the Eastern Great Bend Prairie Aquifer," Kansas Geological Survey, Open-File Report 92-25, 1992.

Buddemeier, R. W., Garneau, G., Healey, J. M., Ma, T. S., Sophocleous, M. A., Whittemore, D. O., Young, D., and Zehr, D., "The Mineral Intrusion Project: Report of Progress During Fiscal Year," 1993, 157 pp.

Butler, J. J. Jr., Liu, W., and Young, D. P., "Analysis of October 1993 Slug Tests in Stafford, Pratt, and Reno Counties," Kansas Geological Survey, Open-File Report 93-52, 1993.

Butow, E. and Holzbecher, E., "On the modeling of groundwater flow under the Influence of salinity," Ground water contamination : Use of models in decision making, Kluwer Academic Publishers, 1987, pg. 263-271.

Carr, J. R., Myers, D. E., and Glass, C. E., "Co-kriging - A Computer Program," Computers and Geosciences, Vol. 11, No. 2, 1985, pp. 112-127.

Chandler, R. L. and McWhorter, D. B., "Upconing of the Saltwater-Freshwater Interface Beneath a Pumping Well," Ground Water, Vol. 13, No. 4, 1975, pp. 354-359.

Christakos, G., "On the Problem of Permissible Covariance and Variogram Models," Water Resource Research, Vol. 20, No. 2, 1984, pp. 251-265.

Cobb, P. M., "The Distribution and Mechanisms of Salt Water Intrusion in the Fresh Water Aquifer and in rattlesnake Creek, Stafford County, Kansas." MS thesis, Department of Civil Engineering, University of Kansas, Lawrence, 1980, 176 pp.

Cobb, P. M., Colarullo, S. J., and Heidari, M., "A Groundwater Flow Model for the Great Bend Aquifer, South-Central Kansas," Open-File Report 83-3, Kansas Geological Survey, 1982, 12 pp.

Cressie, N. A. C., "Statistics for Spatial Data," John Wiley and Sons, Inc., New York, 1991.

Davis, B. M., "Uses and Abuses of Cross-Validation in Geostatistics," Mathematical Geology Vol. 19 No. 3, 1987, pp. 241-248.

Davis, M., "Production of Conditional Simulations via the LU decomposition of the Covariance Matrix," Mathematical Geology, Vol. 19, No. 2, 1987, pp. 91-98.

Davis, J., "Statistics and Data Analysis in Geology," 2nd ed., John Wiley and Sons, Inc., New York, 1986.

Delhomme, J. P., "Kriging in the Hydrosciences," Advances in Water Resources, Vol. 1, No. 5, 1978, pp. 251-266.

Delhomme, J. P., "Spatial Variability and Uncertainty in Groundwater Flow Parameters: A Geostatistical Approach" Water Resources Research, Vol. 15, No. 2, 1979, pp. 269-280.

Deutsch, C., and Journel, A., "GSLIB: Geostatistical Software Library and User's Guide," Oxford University Press, New York, 1992.

Fader, S. W., and Stullken, L. E., "Geohydrology of the Great Bend Prairie, South-Central Kansas," Irrigation Series 4, Kansas Geological Survey, 1978, 19 pp.

Frind, E. O., "The Principal Direction Technique: A New Approach to Groundwater Contaminant Transport Modeling. In: Finite Elements in Water Resources,"

Mangold, D. C. and Tsang, C. F., "A Summary of Subsurface Hydrological and Hydrochemical Models," Reviews of Geophysics, Vol. 29, No. 1, Feb. 1991, pp.51-79.

Mantoglou, A. and Wilson, J., "The Turning Bands Method for Simulation of Random Fields Using Line Generation by a Spectral Method," Water Resource Research, Vol. 18, No. 5, 1982, pp. 1379-1394.

Matheron, G., "Principles of Geostatistics," Economic Geology, Vol. 58, 1963, pp. 1246-1266.

Matheron, G., "The Theory of Regionalized Variables and Its Applications," Ecole Des Mines, Fontainebleau, France, 1971.

Matheron. G., "The Intrinsic Random Functions and Their Applications," Advances in Applied Probability, No. 5, 1973, pp. 439-468.

Mitchell, J. E., Woods, J., McClain, T. J., and Buddemeier, R. W., "January 1992 Kansas Water Levels and Data Related to Water-Level Changes," Technical Series 3, Kansas Geological Survey, 1993, 130 pp.

Muskat, M., "The Flow of Homogeneous Fluids Through Porous Media," McGraw-Hill, New York, N.Y., 1937, pp. 763.

Myers, D. E., "Matrix Formulation of Co-Kriging," Mathematical Geology, Vol. 14, 1982, pp. 249-257.

Noye, J., "Numerical Solutions of Partial Differential Equations," North-Holland Publishing Company, Amsterdam, New York, Oxford, 1981.

Palumbo, M. R., and Khaleel, R., "Kriged Estimates of Transmissivity in the Mesilla Bolson, New Mexico," Water Resource Bulletin, Vol. 19, No. 6, 1983, pp. 929-936.

Press, W. H., Teukolsky, S. A., and Vetterling, W. T., Flannery, B. P., "Numerical Recipes in Fortran: The Art of Scientific Computing," Cambridge University Press, 2nd edition, New York, 1992, 962 pp.

Price, H. S., Varga, R. S., and Warren, J. E., "Application of Oscillation Matrices to Diffusion-Convection Equations," Journal of Mathematics and Physics, Vol. 45, No. 3, 1966, pp. 301-311.

Reeves, M., Ward, D. S., Johns, N. D., and Cranwell, R. M., "Theory and Implementation for SWIFT II, the Sandia Water-Isolation Flow and Transport Model

for Fractured Media," Rep. NUREG/CR-3328 and SAND83-1159, Sandia National Lab., Albuquerque, N. M., 1986.

Reilly, T. E. and Goodman, A. S., "Quantitative Analysis of Saltwater-Freshwater Relationships in Groundwater Systems - A Historical Perspective," Journal of Hydrology, Vol. 89, No. 3/4, 1987, pp. 169-204.

Sahni, B. M., "Salt Water Coning Beneath Fresh Water Wells," Water Management Technical Report No. 18, Colorado State Univ., Fort Collins, CO., 1972.

Scheidegger, A. E., "General Theory of Dispersion in Porous Media," Journal of Geophysical Research, Vol. 66, No. 10, 1961, pp. 153-162.

Smyth, J. D. and Istok, J. D., "Multivariate Geostatistical Analysis of Groundwater Contamination by Pesticide and Nitrate: A Case History, in Armstrong, M., ed.," Geostatistics, Vol. 2, 1989, pp. 713-724.

Sophocleous, M. A., "Recharge Estimation for the Groundwater Management District No. 5: A Six-Year Record," Open-File Report 91-1, Kansas Geological Survey, 1991.

Sophocelous, M. A., "A Quarter-Century of Ground-Water Recharge Estimates for the Great Bend Prairie Aquifer of Kansas (1967-1992)," Open-File Report 92-17, Kansas Geological Survey, 1992.

Van der Veer, P., "Analytical Solution for a Two-fluid Flow in a Coastal Aquifer Involving a Phreatic Surface with Precipitation," Journal of Hydrology, Vol. 35, 1977, pp. 271-278.

Varga, R. S., "Matrix Iterative Analysis," Prentice-Hall, Inc., Englewood Cliffs, N. J., 1962, 322 pp.

Voss, C. I., "A Finite-Element Simulation Model for Saturated-Unsaturated, Fluid-Density-Dependent Groundwater Flow with Energy Transport or Chemically-Reactive Single-species Solute Transport," U.S. Geological Survey, Water Resources Investigations Report 84-4369, 1984.

Wang, F. C., "Approximate Theory for Skimming Well Formulation in the Indus Plain of West Pakistan," Journal of Geophysical Research, Vol. 70, No. 20, 1965, pp. 5055-5063.

Ward, D. S., Reeves, M., and Duda, L. E., "Verification and Field Comparison of the Sandia Waste-Isolation Flow and Transport Mdel (SWIFT)," Rep. SAND83-1154 and NUREG/CR-3316, Sandia National Lab., Albuquerque, N. M., 1984.

Proceedings of the 4th International Conference, Hannover, Springer-Verlag, Berlin, 1982, pp. 13/25-13/42.

Garneau, G. W., Buddemeier, R. W., and Young, D. P., "Characterization of the Saltwater Interface and Related Parameters," Kansas Geological Survey, Open-File Report 94-28b, 1994.

Gillespie, J. B., Hargadine, G. D., Myers, N. C., and Hargadine, D. A., "Geohydrologic Data for the South Fork Ninnescah River Valley and Adjacent Plains in Pratt and Kingman Counties, South-Central Kansas," Open-File Report 91-186, U.S. Geological Survey, Lawrence, Kansas, 1991, 55 pp.

Ghyben, W. B., "Nota in Verband Met de Voorgenomen Putboring Nabij Amsterdam (Notes on the Probable Results of Well Drilling Near Amsterdam)," Tijdschrift van Let Koninklijk Inst., Van Ing, 1888, pp. 8-22.

Henley, S., "Nonparametric Geostatistics," London: Applied Science Publishers, 1981.

Henry, H. R., "Effects of Dispersion on Salt Encroachment in Coastal Aquifers," in U.S. Geological Survey Water Supply Paper 1613-C, Sea Water in Coastal Aquifers, 1964, pp. 70-84.

Herzberg, A., "Die Wasserversorgung Einiger Nordseedbader (The Water Supply on Parts of the North Sea Coast in Germany)," J. Gasbeleucht. Wasserversorg., Vol. 44, 1901, pp. 815-819; 824-844.

Hubbert, M. K., "The Theory of Ground-Water Motion," Journal of Geology, Vol. 48 No. 8, 1940, pp. 785-944.

Journel, A. G., and Huijbregts, C. J., "Mining Geosatistics," Academic Press, London, 1978.

Kirkpatrick, S., Gelatt, C. D., and Vecchi, M. P., "Optimization by Simulated Annealing," Science, Vol. 220, No. 4598, 1983, pp. 671-680.

Latta, B. F., "Geology and Ground-Water Resources of Barton and Stafford counties," Kansas Geological Survey Bulletin 88, Lawrence, KS, 1950.

Layton, D. W., and Berry, D. W., "geology and Ground-Water Resources of Pratt County, South-Central Kansas," Bulletin 205, Kansas Geological Survey, 1973, 33 pp.

Ward, D. S., Buss, D. R., Morganwalp, D. W., and Wadsworth, T. D., "Waste Confinement Performance of Deep Injection Wells," paper presented at solving ground water problems with models, National Water Well Association, Denver, Colo., Feb. 1987, pp. 10-12.

Wirojanagud, P. and Charbeneau, R. J., "Saltwater Upconing in Unconfined Aquifers," Journal of Hydraulic Engineering, Vol. 111, No. 3, 1985, pp. 417-434.

Young, David P., "Mineral Intrusion: Geohydrology of Permian Bedrock Underlying the Great Bend Prairie Aquifer in South-Central Kansas," Kansas Geological Survey, Open-File Report 92-44, 1992.

Young, D. P., Garneau, G. W., Buddemeier, R. W., Zehr, D., and Lanterman, J., "Elevation and Variability of the Freshwater-Saltwater Interface in the Great Bend Prairie Aquifer, South-Central Kansas," Kansas Geological Survey, Open-File Report 93-55, 1993.

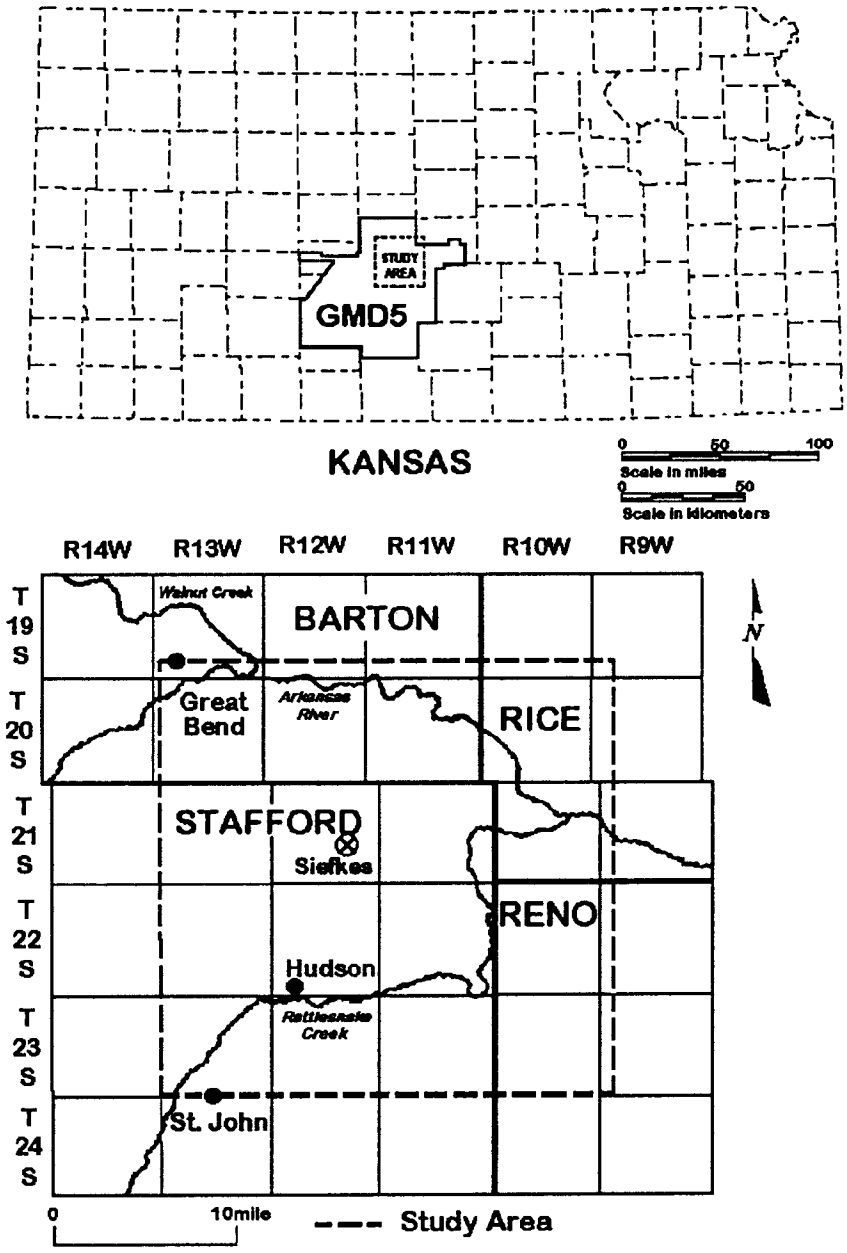

Figure 1. Region of the study area located at the north part of the Groundwater Management District #5.

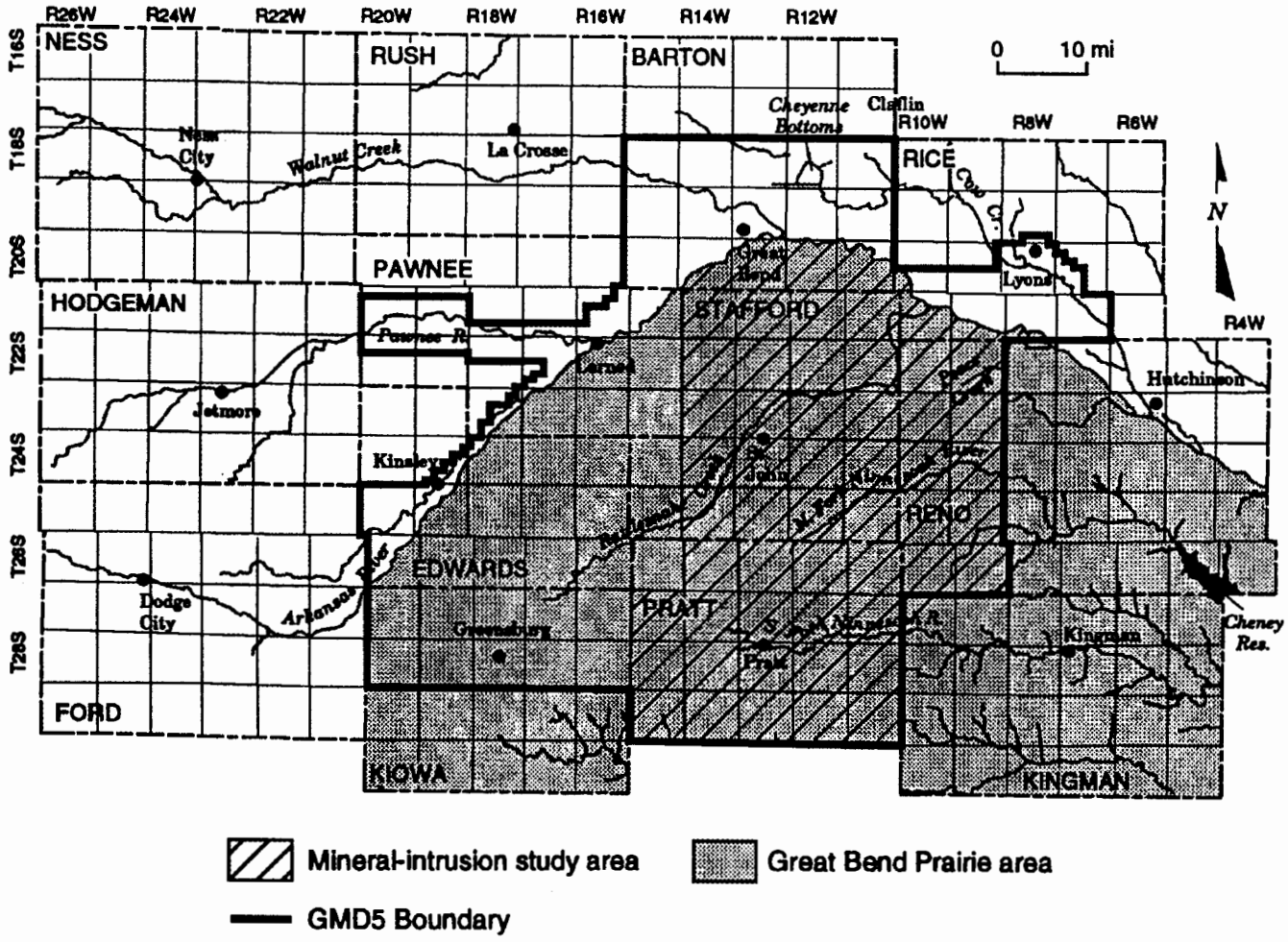

Figure 2. Region of Groundwater Management District #5 and the observed mineral intrusion area.

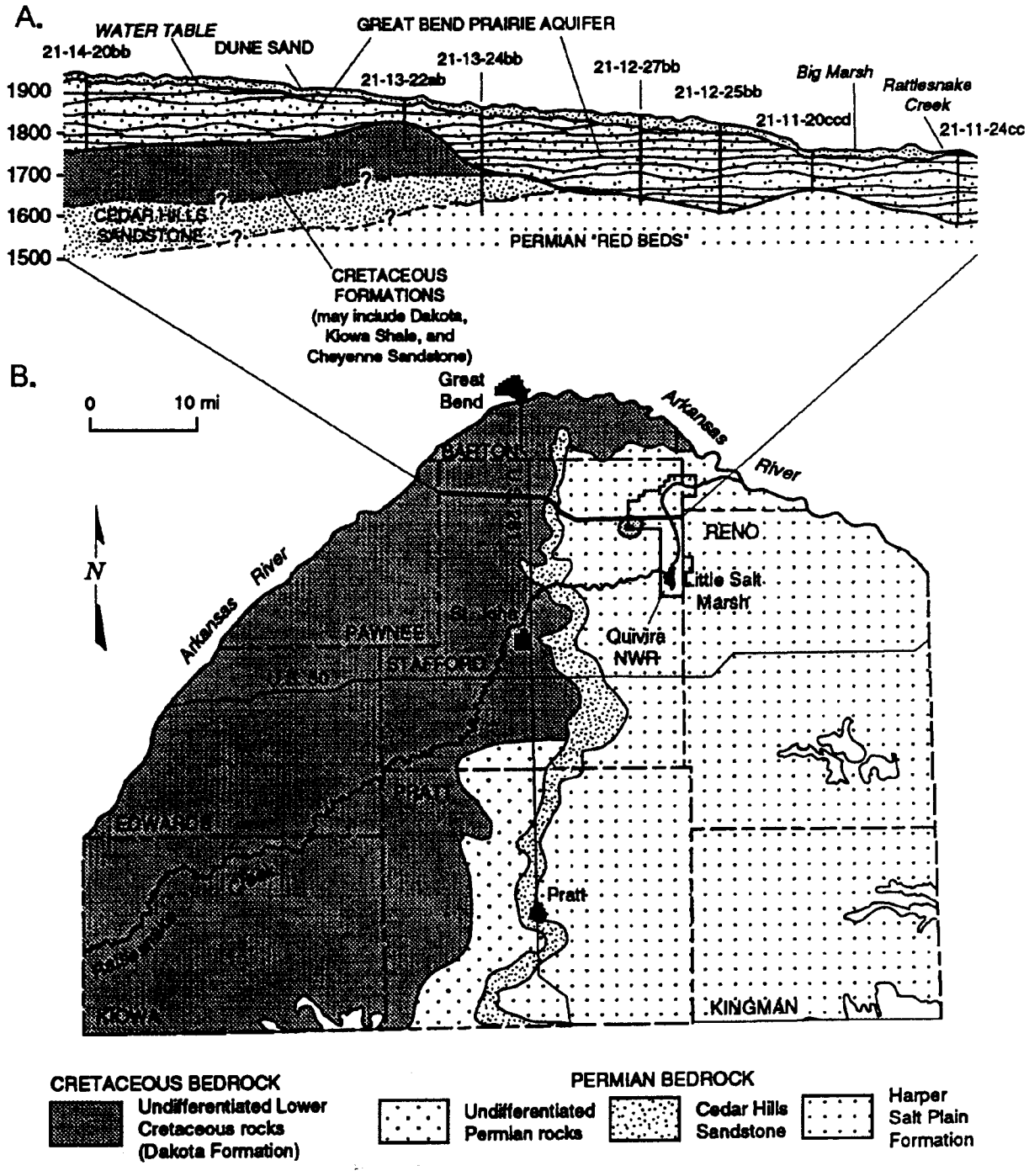

Figure 3. Geologic formations of the Big Bend aquifer

A. Vertical section from west to east across the region, showing the relation of the alluvial Big Bend Prairie aquifer to the underlying Cretaceous and Permian strata (Latta, 1950).

B. Bedrock geology underlying the Big Bend Prairie aquifer and areas in which the Permian bedrock has the potential to contribute saltwater to the overlying aquifer (Fader and Stullken, 1978).

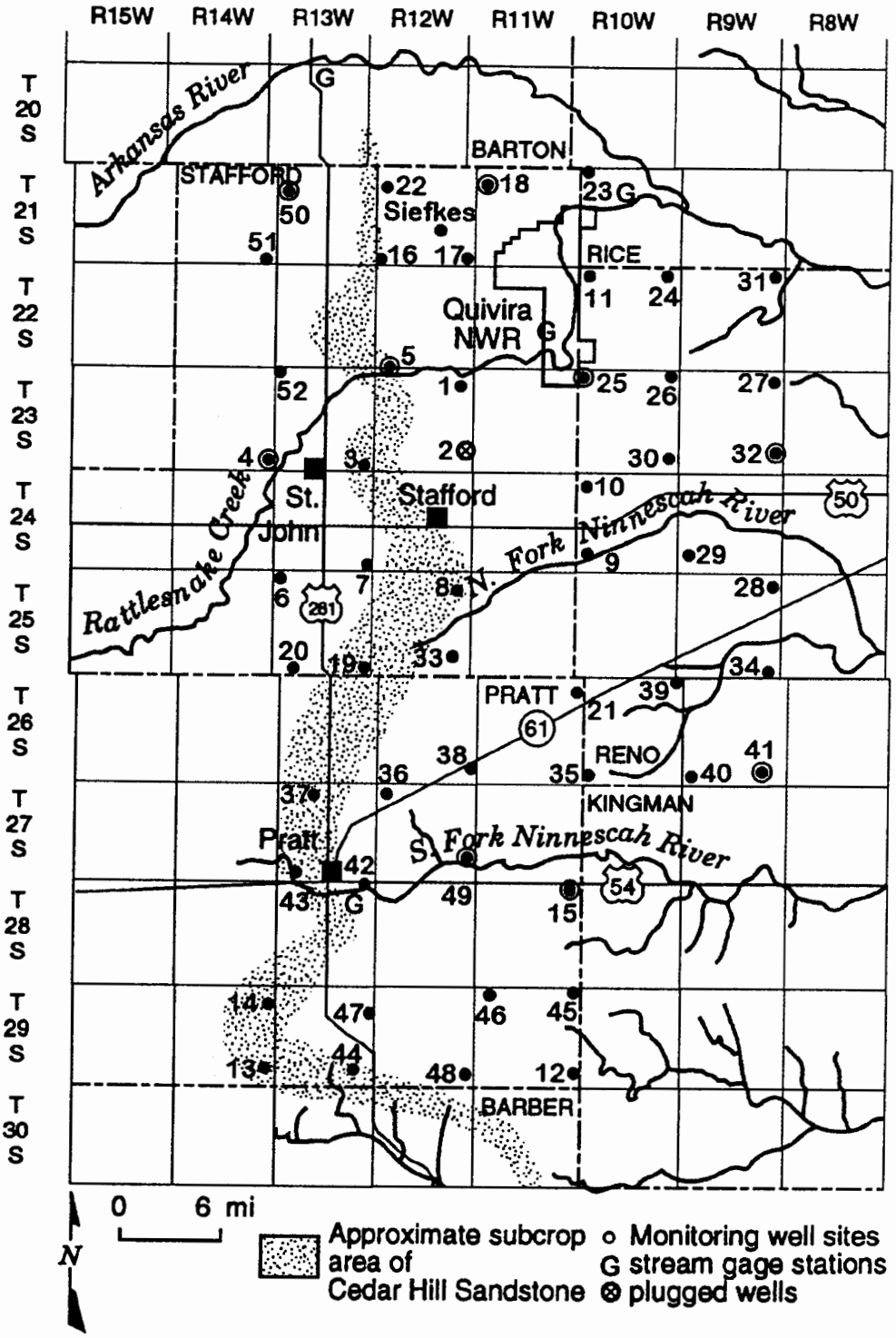

Figure 4. The location of Siefkes site and the observation well and other physical features in the area of the KGS/GMD5 monitoring-well network.

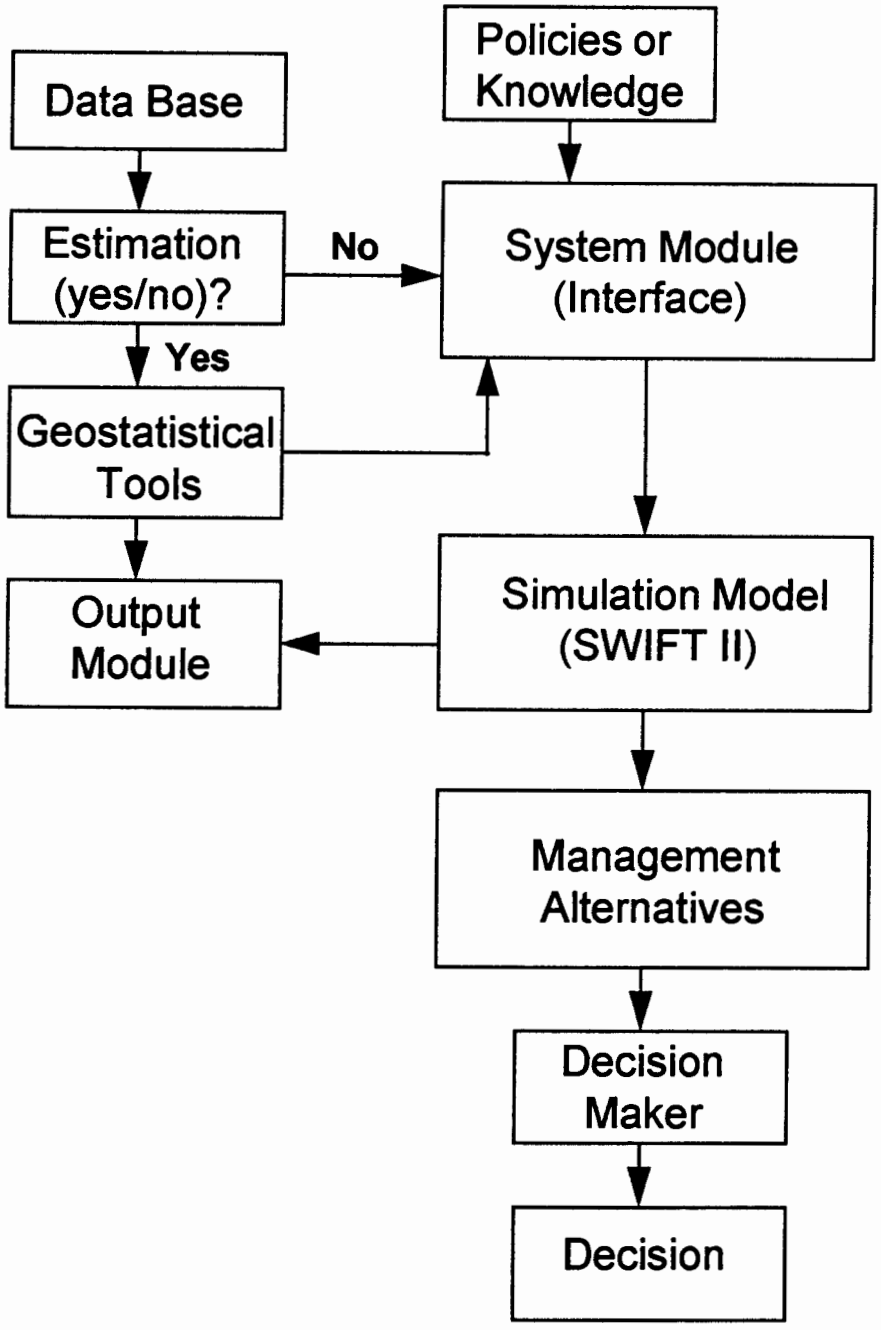

Figure 5. The general structure of the microcomputer-based decision support system. Database, Geostatistics, Simulation model, System module, and Output module are the five major components in the system.

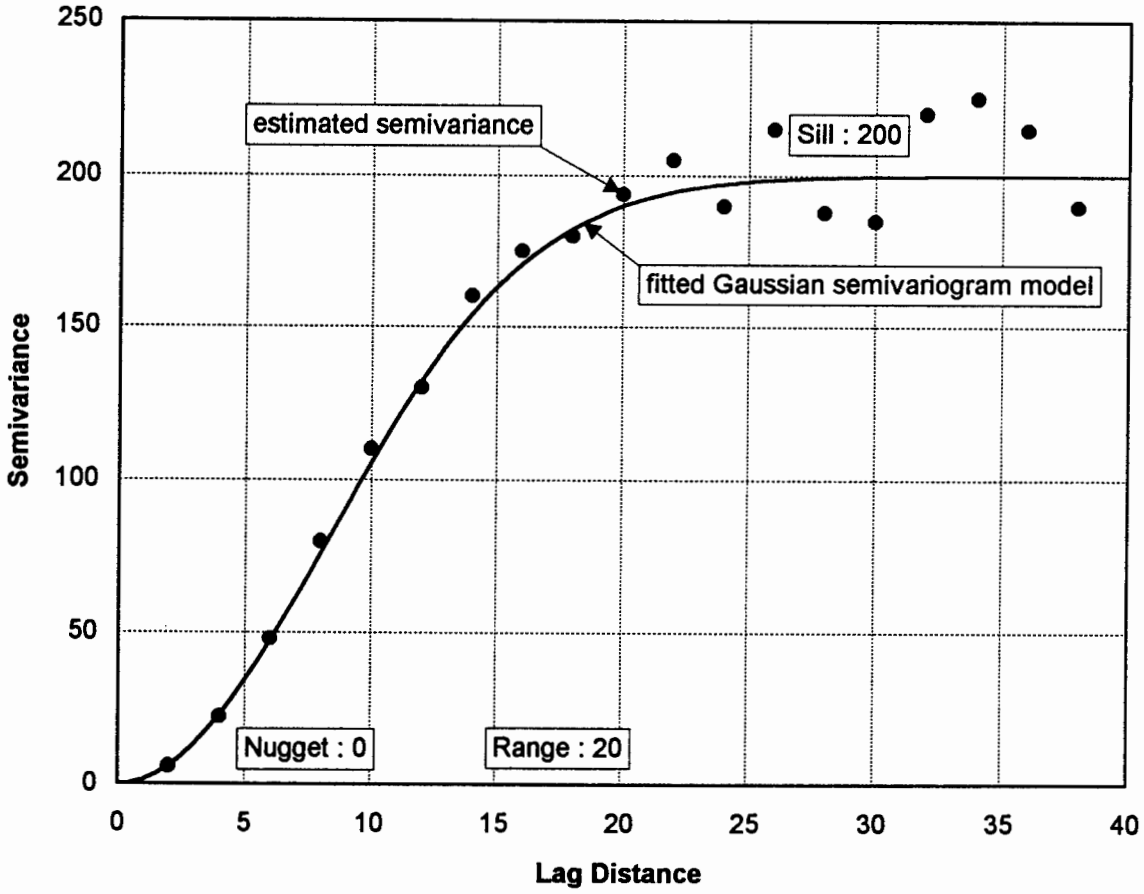

Figure 6. A typical semivariogram plot, three major components are nugget, range,and sill.

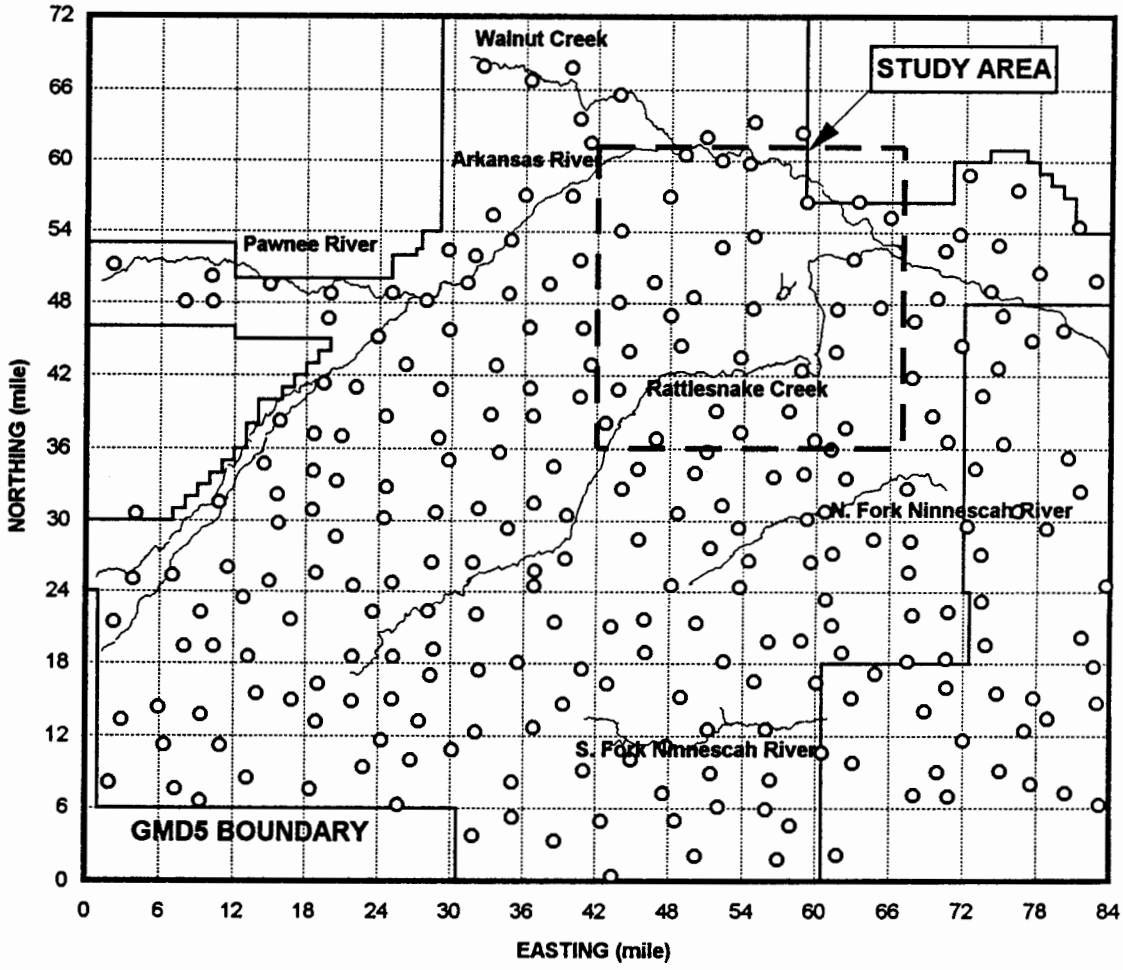

Figure 7. Location of measured piezometric heads in 1992, shown as open circle.

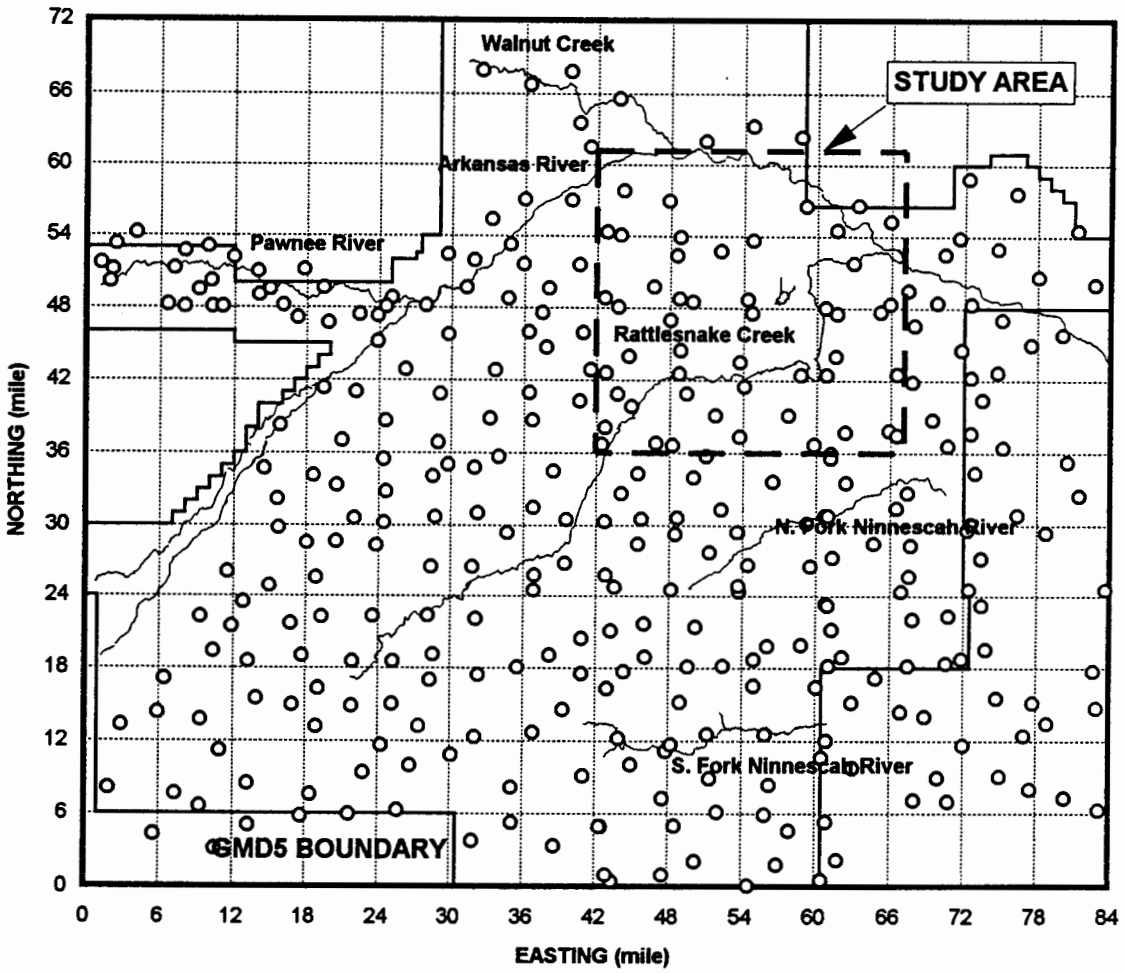

Figure 8. Location of measured piezometric heads in 1993, shown as open circle.

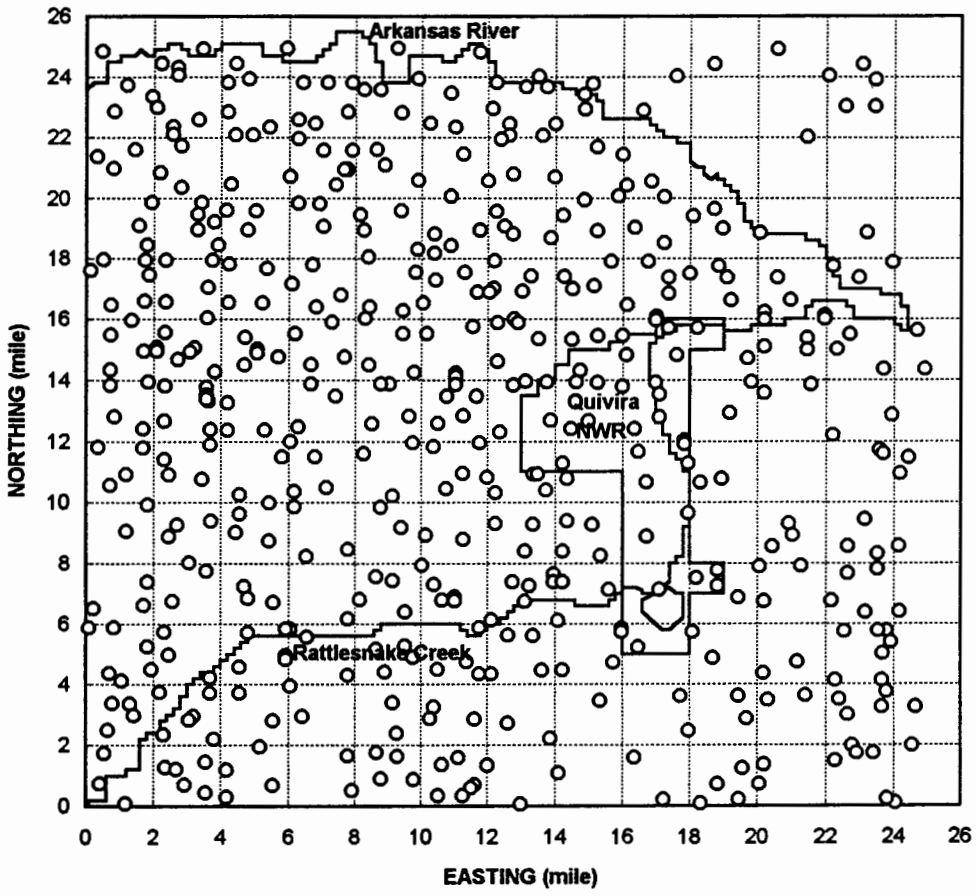

Figure 9. Locations of measured bedrock elevations in the study area, shown as open circle.

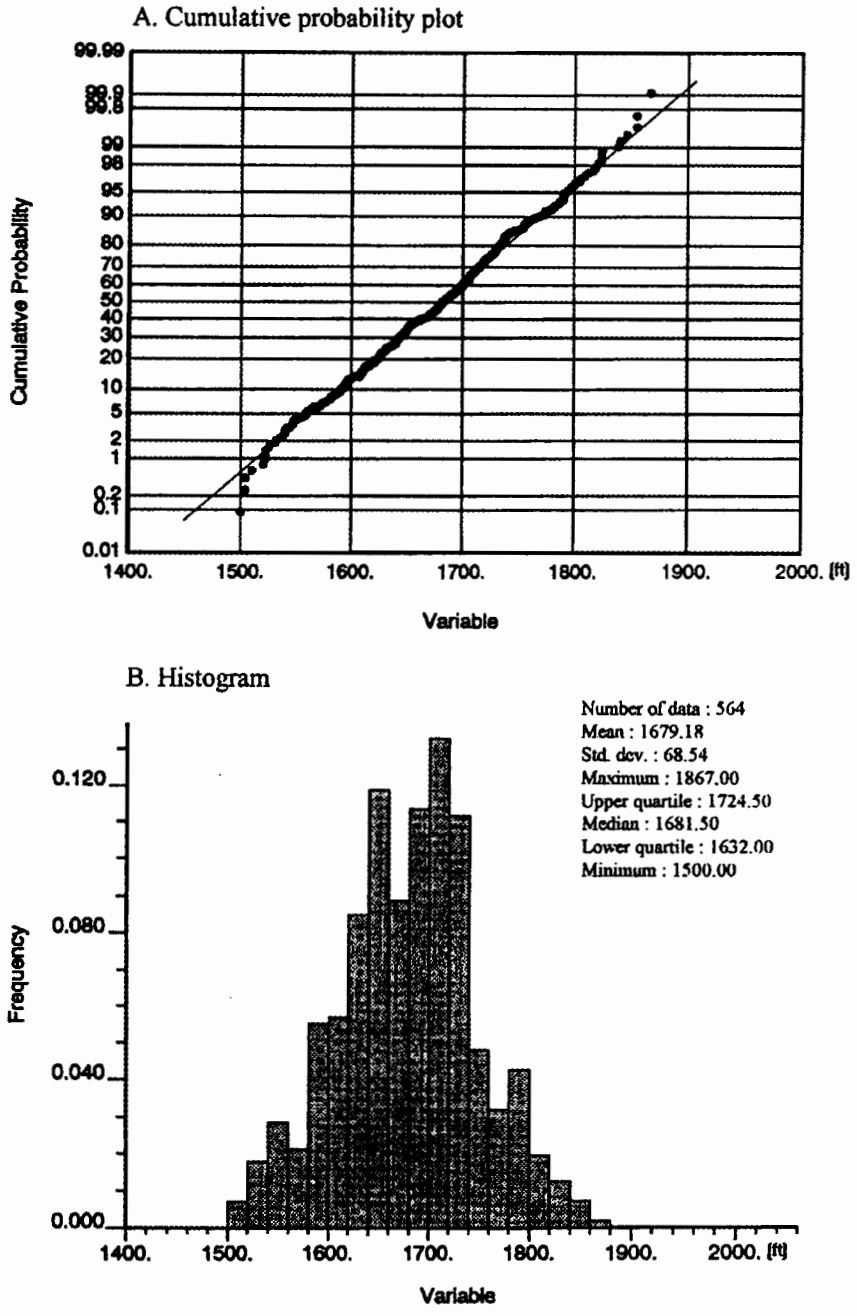

Figure 10. Cumulative probability and histogram of 564 measurements of bedrock elevation in the study area.

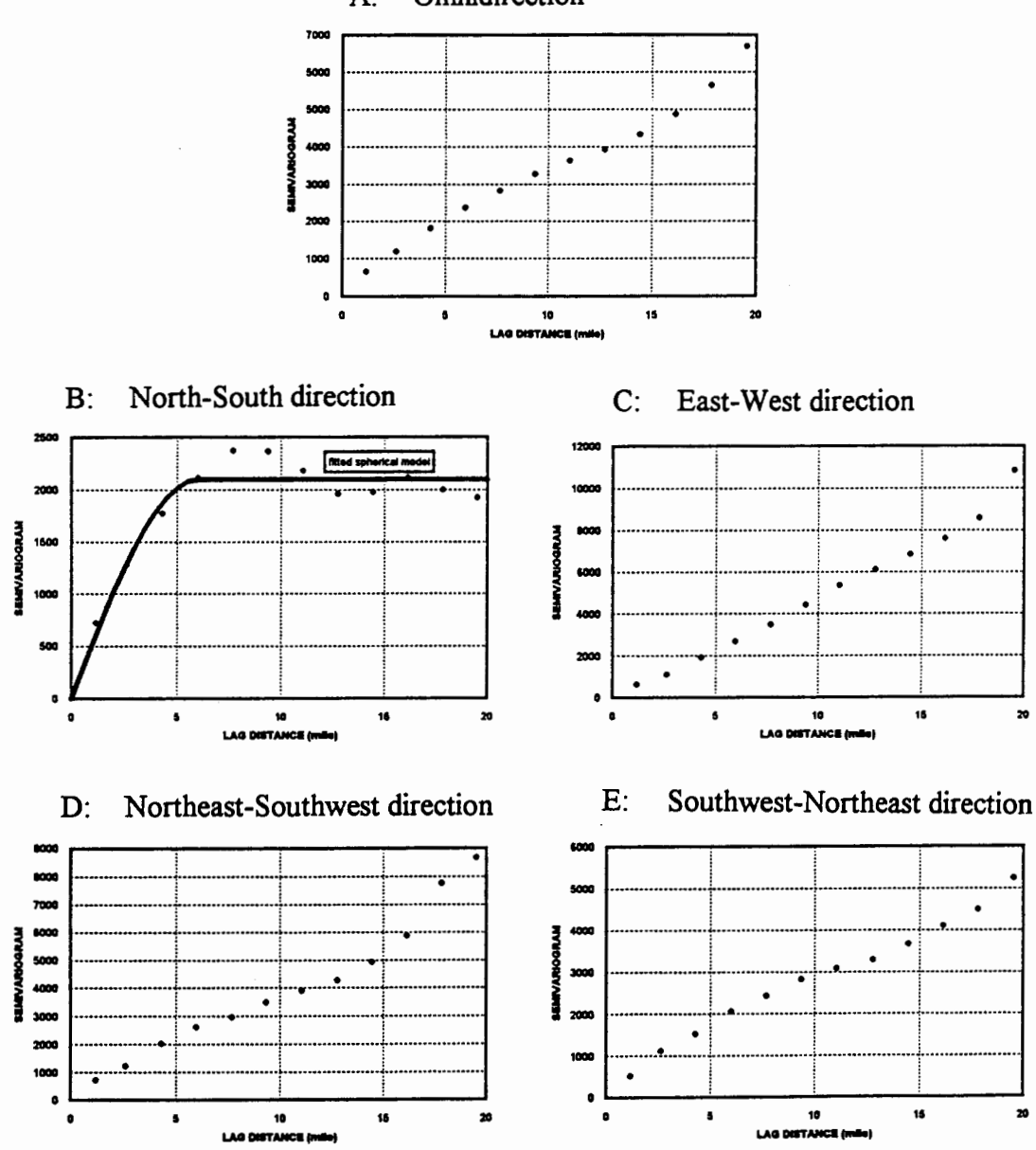

Figure 11. Plots of calculated semivariograms based on the sampled values of bedrock elevation, and the fitted spherical model (B).

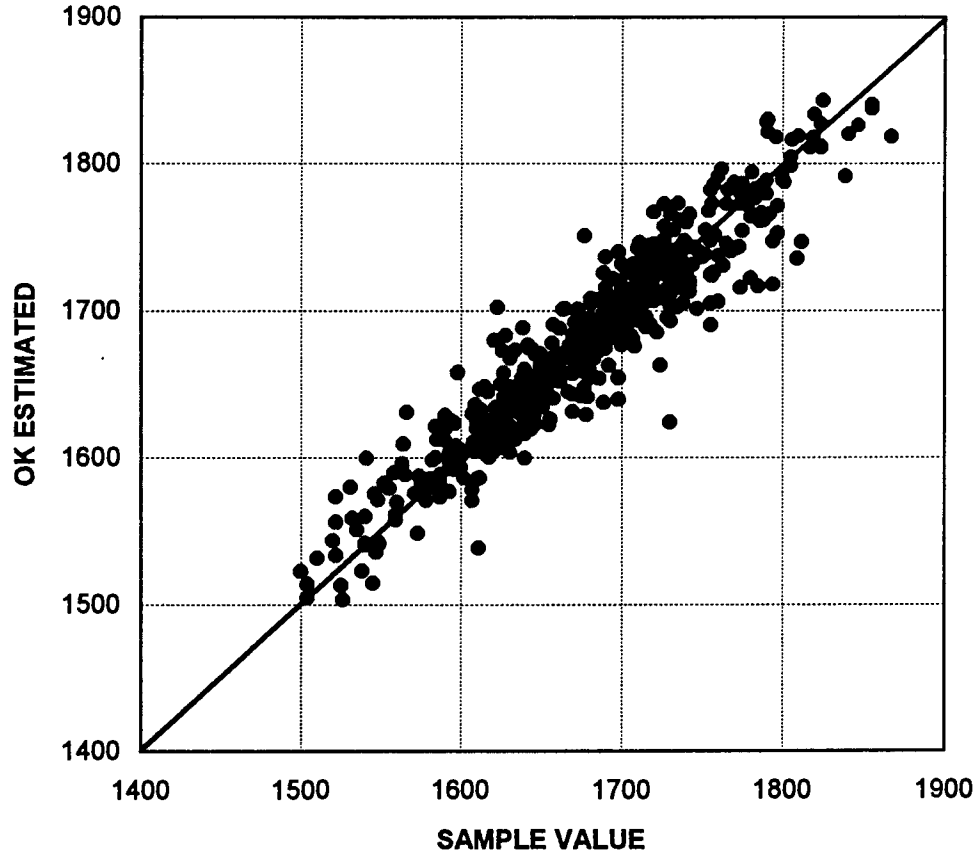

Figure 12. Scatter plot of measured bedrock elevations versus kriged values at sampled sites..

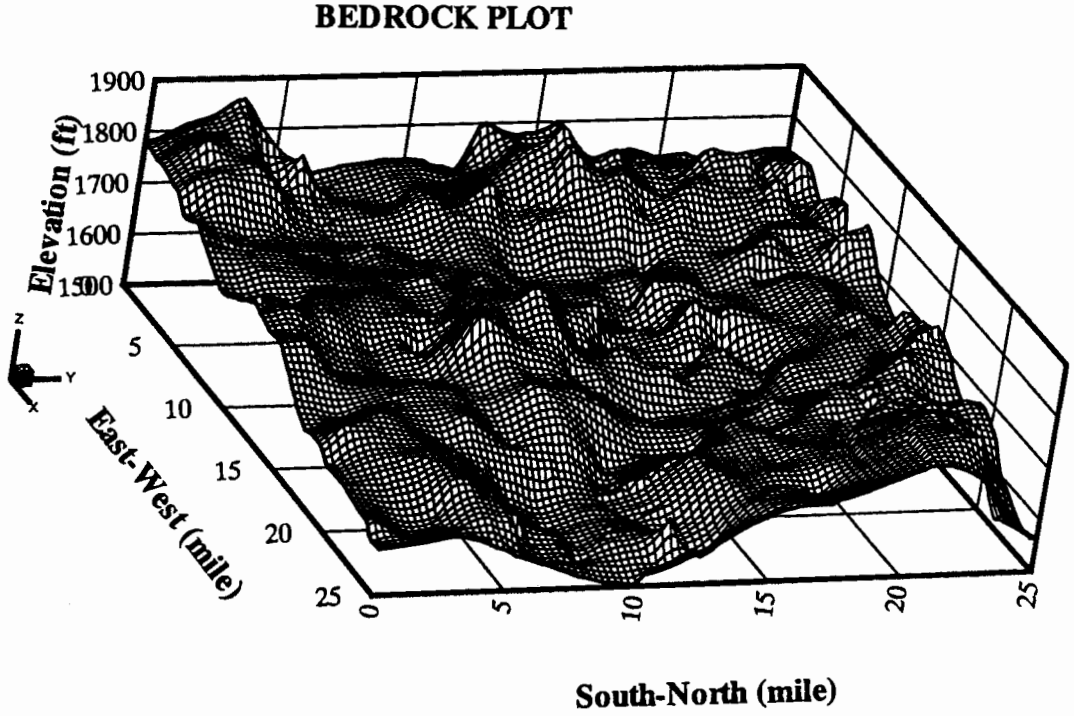

Figure 13. A three-dimensional plot of the kriged bedrock elevation.

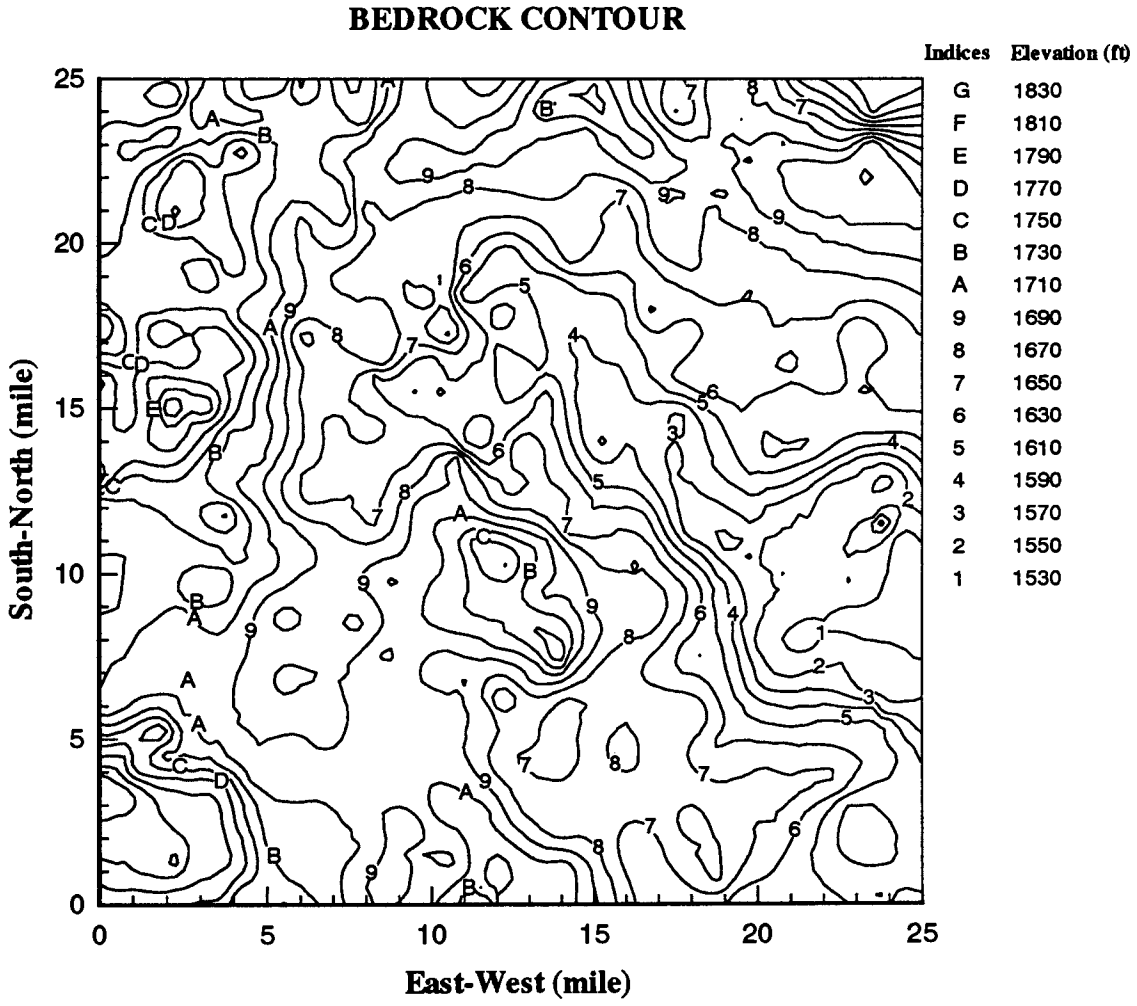

Figure 14. A plot of contours of the kriged bedrock elevation.

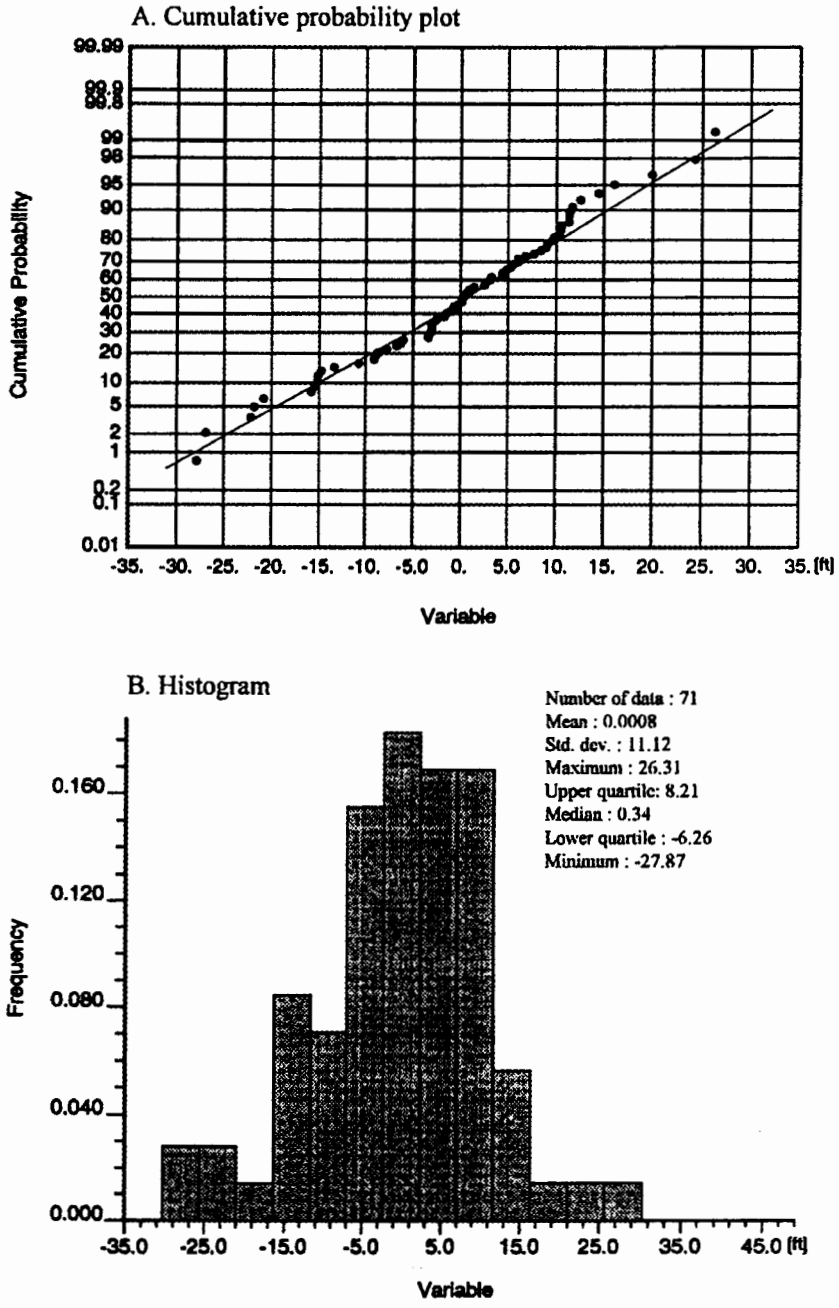

Figure 15. Cumulative probability and histogram of measurements at 71 observation wells in 1992.

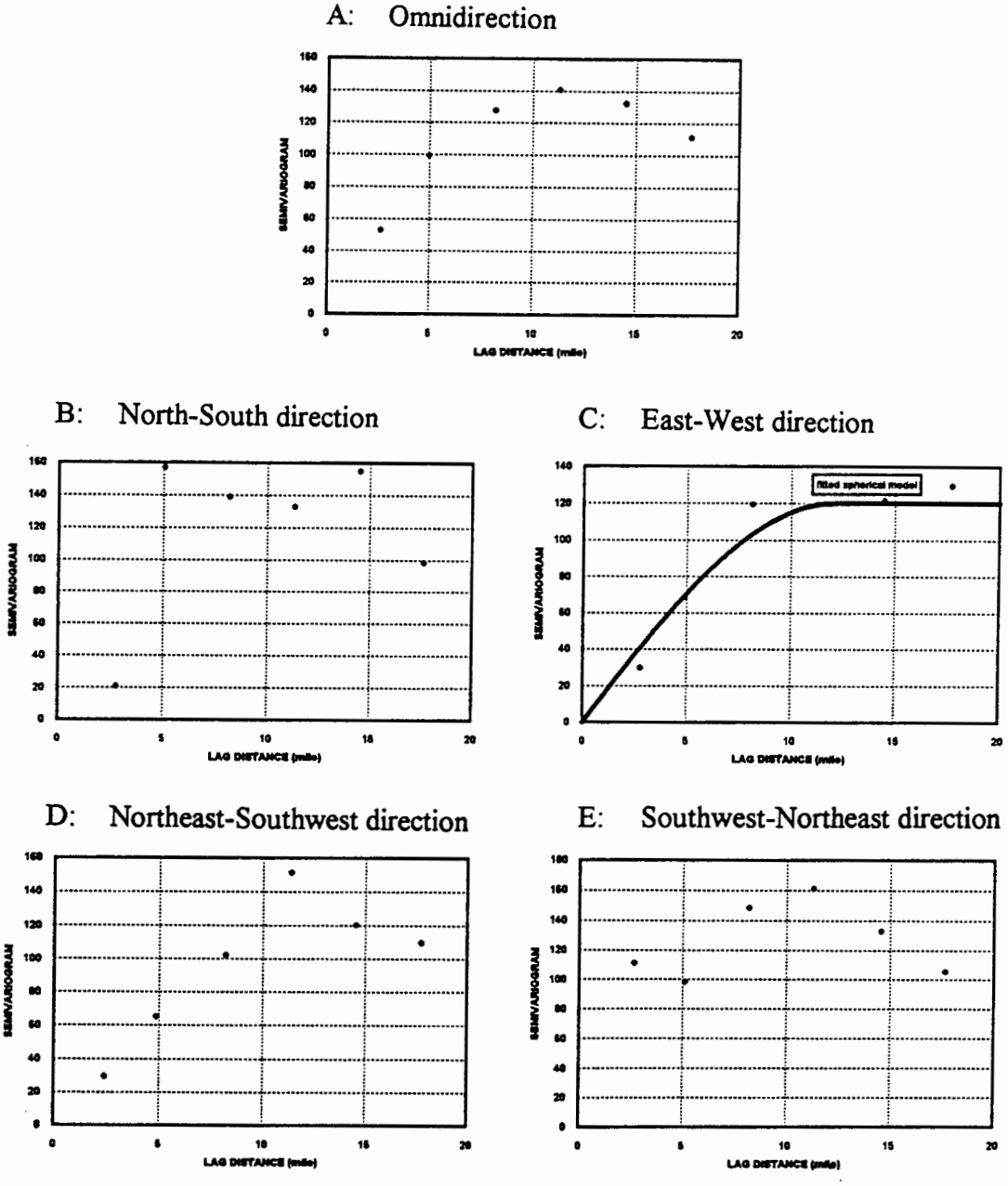

Figure 16. Plots of calculated semivariograms based on the sampled values of piezometric heads in 1992, and the fitted spherical model (C).

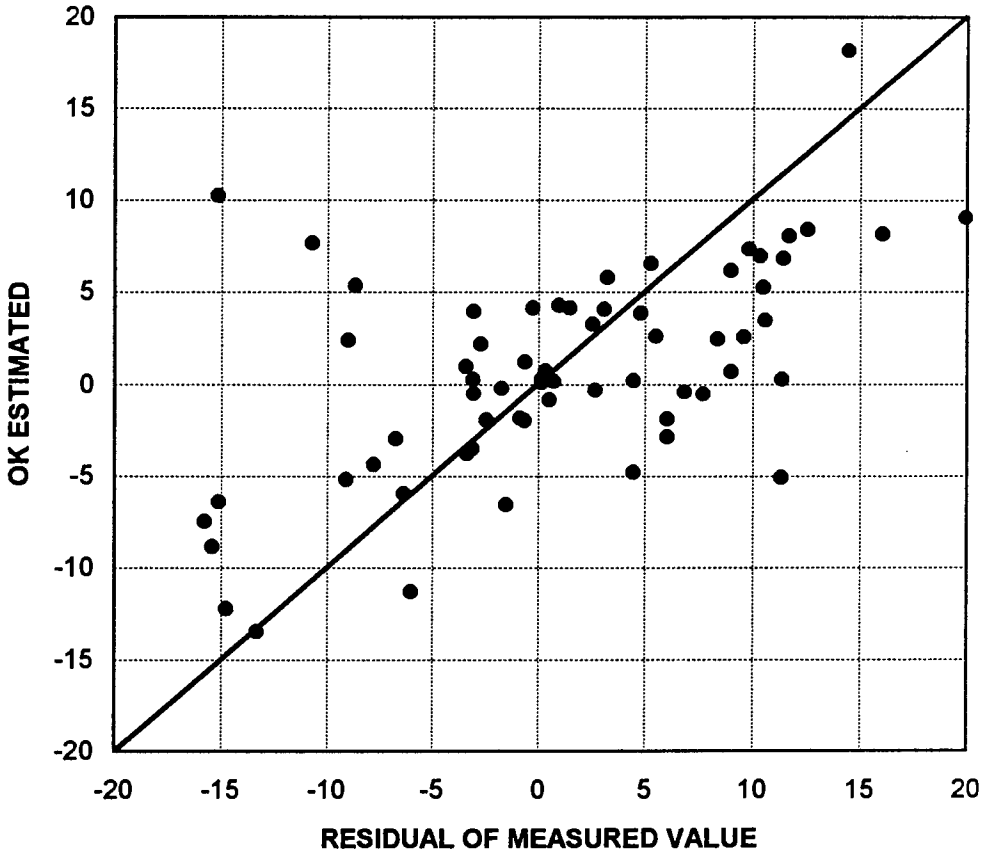

Figure 17. Scatter plot of measured 1992 water level residuals versus kriged residuals at sampled sites.

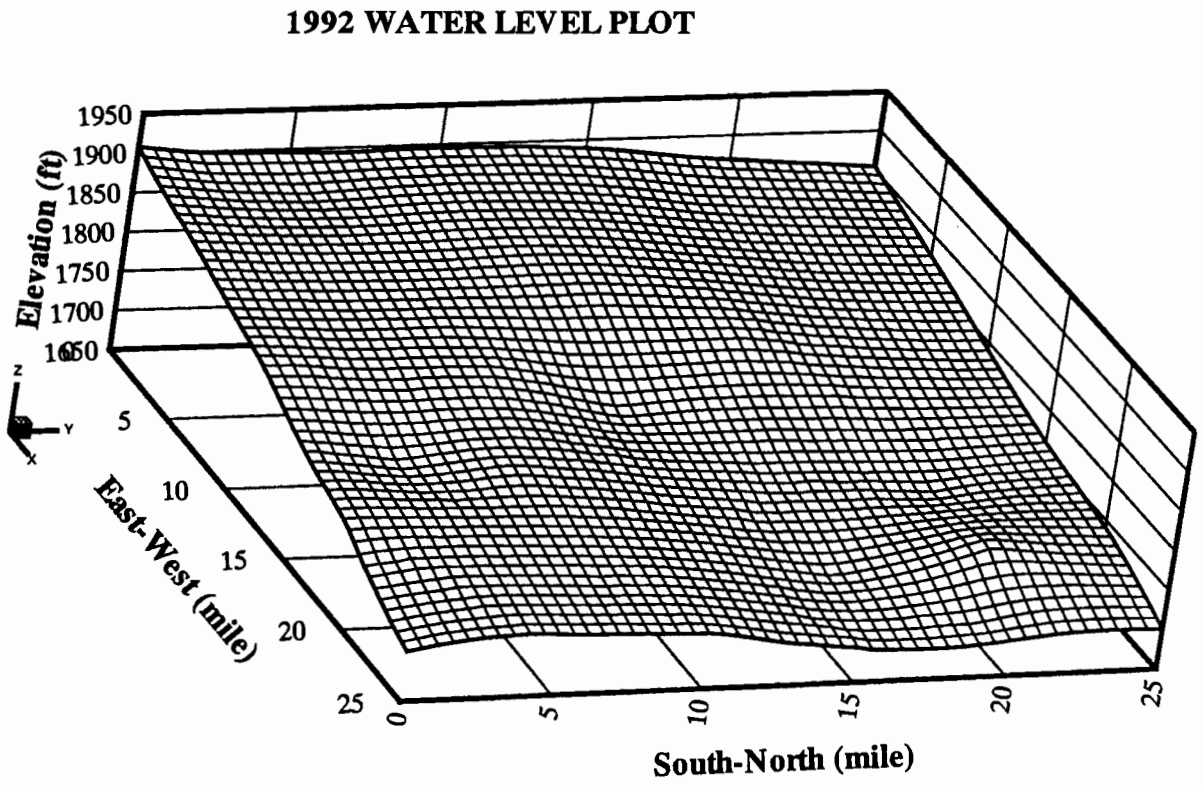

Figure 18. A three-dimensional plot of the kriged piezometric heads based on the 1992 data.

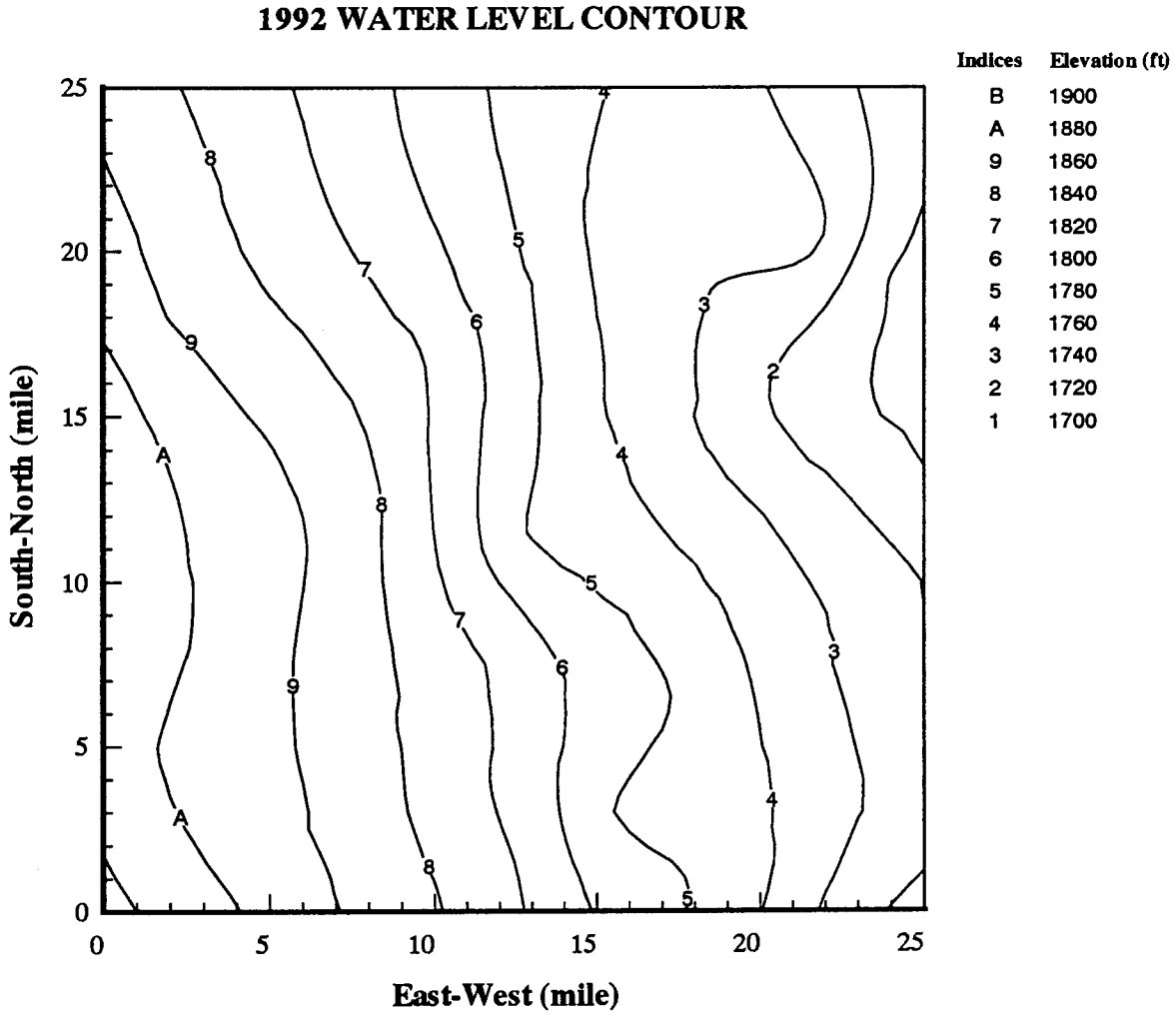

Figure 19. A plot of contours of the kriged piezometric heads based on the 1992 data.

Figure 20. A three-dimensional plot of the estimated saltwater-freshwater interface (data from Young et al., 1993) based on Eq. 4.25.

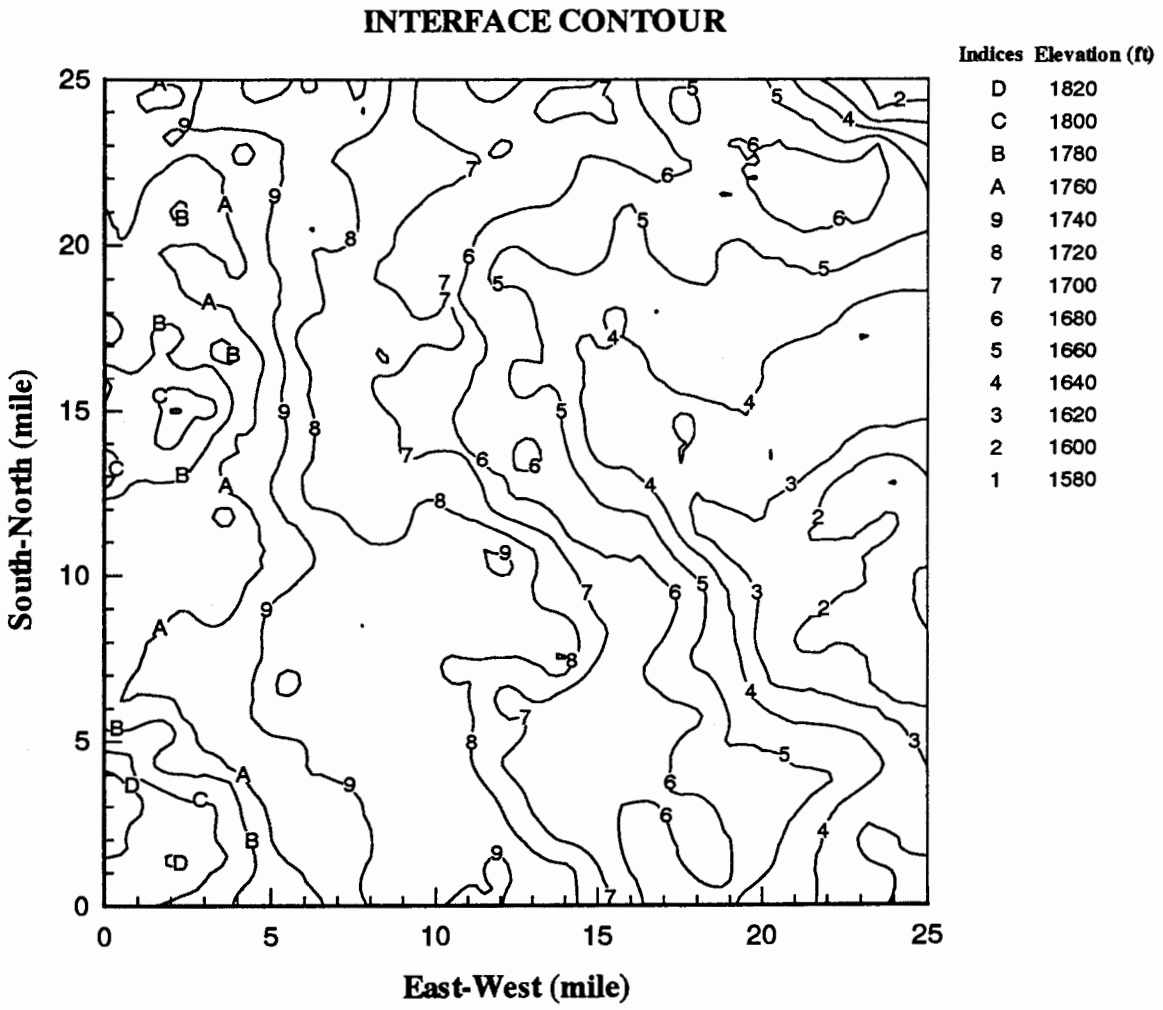

Figure 21. A plot of contours of the estimated saltwater-freshwater interface (data from Young et al., 1993) based on Eq. 4.25.

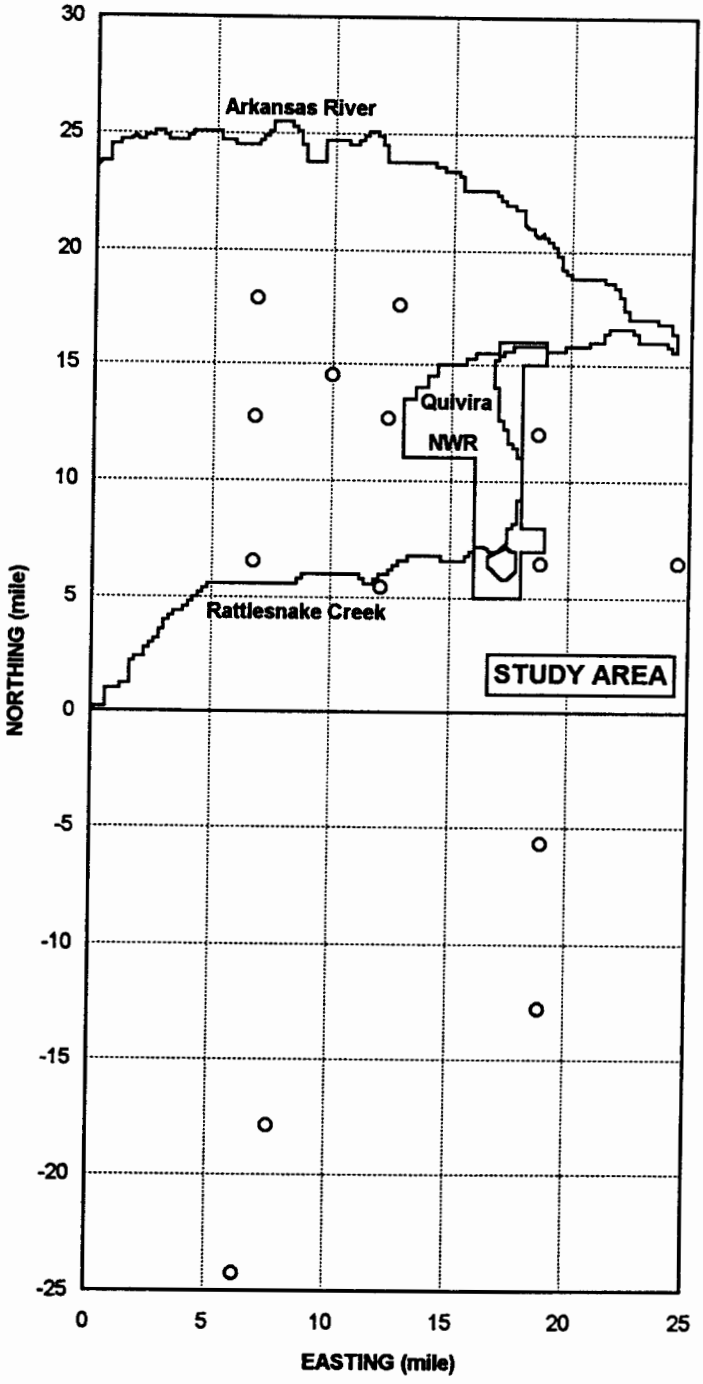

Figure 22. Locations of saltwater-freshwater interface measurements.

Table 1. Location of the saline transition zone sites at which the 100 mS/m Cm' level could be determined.

Site	Location	Land Elevation (ft)	Date	DTW (ft)	Depth to 100 mS/m Cm'	Depth to Bedrock (ft)	Water level Elevation (ft)	100 mS/m Cm' Elev. (ft)	Bedrock Elevation (ft)	COND (mS/m)	Cl (mg/L)
1	23-12-12BAA	1827.00	3/26/93	5.30	111.70	146.00	1821.70	1715.30	1681.00	3690.0	13200.0
5	23-12-06BBB	1855.00	9/17/93	1.80	79.60	181.00	1853.20	1775.30	1674.00	8550.0	41200.0
9	24-10-31CBC	1755.00	4/25/93	9.00	76.50	87.00	1746.00	1678.40	1668.00	1070.0	3280.0
11	22-10-06CBB	1763.00	3/27/93	13.50	146.40	208.00	1749.50	1616.70	1555.00	6690.0	25000.0
16	21-12-31CCC	1872.00	3/25/93	12.00	146.70	220.00	1860.00	1725.20	1652.00	8850.0	34800.0
17	21-12-36DDC	1804.00	3/25/93	11.60	84.00	114.00	1792.40	1719.90	1690.00	2890.0	9880.0
18	21-11-07BBB	1810.00	3/25/93	19.00	143.90	214.00	1791.00	1666.00	1596.00	3520.0	12200.0
21	26-11-01DDD	1801.00	5/20/93	21.60	112.40	137.00	1779.40	1688.00	1664.00	3510.0	11700.0
22	21-12-06CCB	1855.00	3/25/93	16.10	175.70	215.00	1838.90	1679.40	1640.00	8260.0	32500.0
25	23-10-06BBA	1780.00	3/28/93	6.30	25.00	98.00	1773.70	1754.80	1682.00	4100.0	17400.0
26	23-10-01AAA	1738.00	4/20/93	6.80	80.70	177.00	1731.20	1657.10	1561.00	3710.0	13470.0
36	27-12-06BAA	1892.00	4/21/93	28.00	164.00	195.00	1864.00	1727.80	1697.00	5680.0	21800.0
42	28-13-01CBA	1829.00	4/22/93	13.10	139.90	160.00	1815.90	1689.10	1669.00	1550.0	4900.0
SP	21-12-27DACC	1840.00	9/18/93	9.00	147.20	186.00	1831.00	1692.70	1654.00	7080.0	26670.0
SDA	21-12-27DADD	1840.00	9/18/93		145.70			1694.30		3840.0	13940.0

DTW- Depth to water (feet below land surface) in shallow wells. Some values estimated.
COND- Specific conductance of water from Permian wells and Siefkes deep aquifer well.
Cl- Chloride concentration of water from Permian wells and Siefkes deep aquifer well.

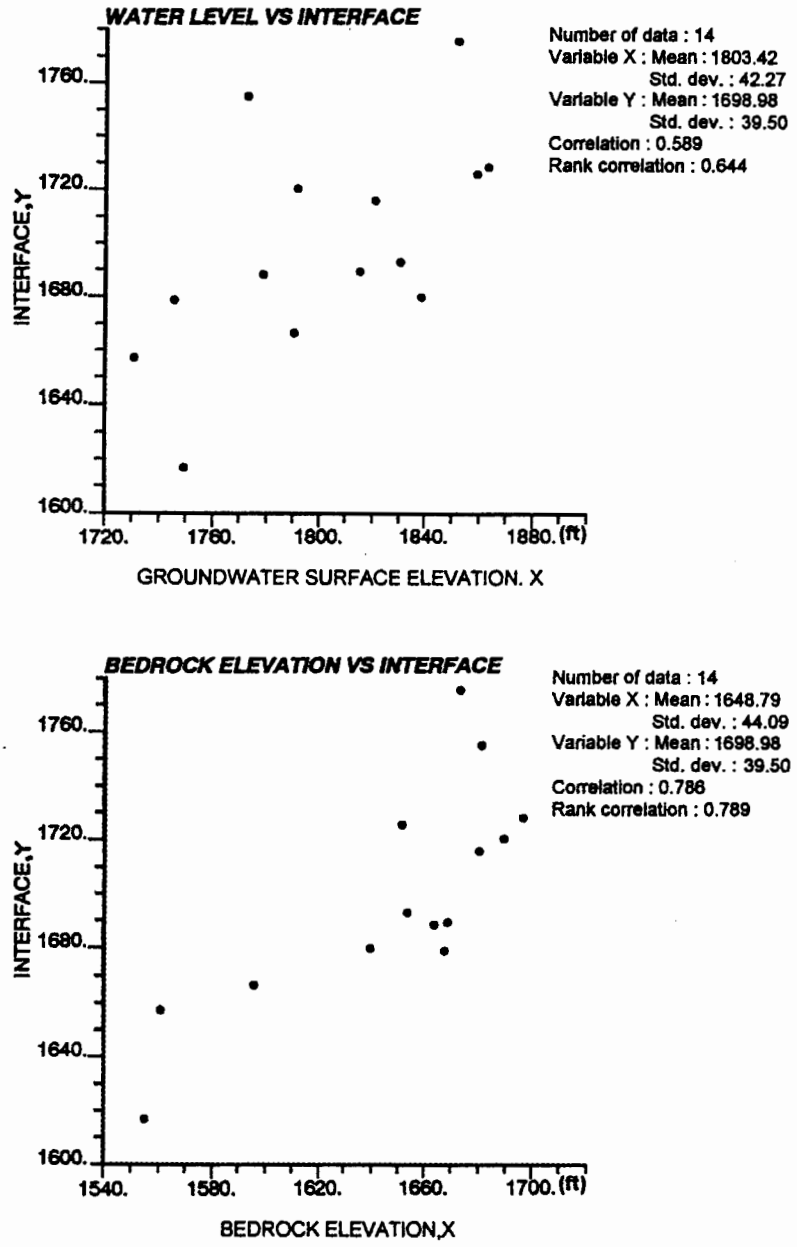

Figure 23. Correlation between the measured interface and piezometric head and between the interface and bedrock elevation.

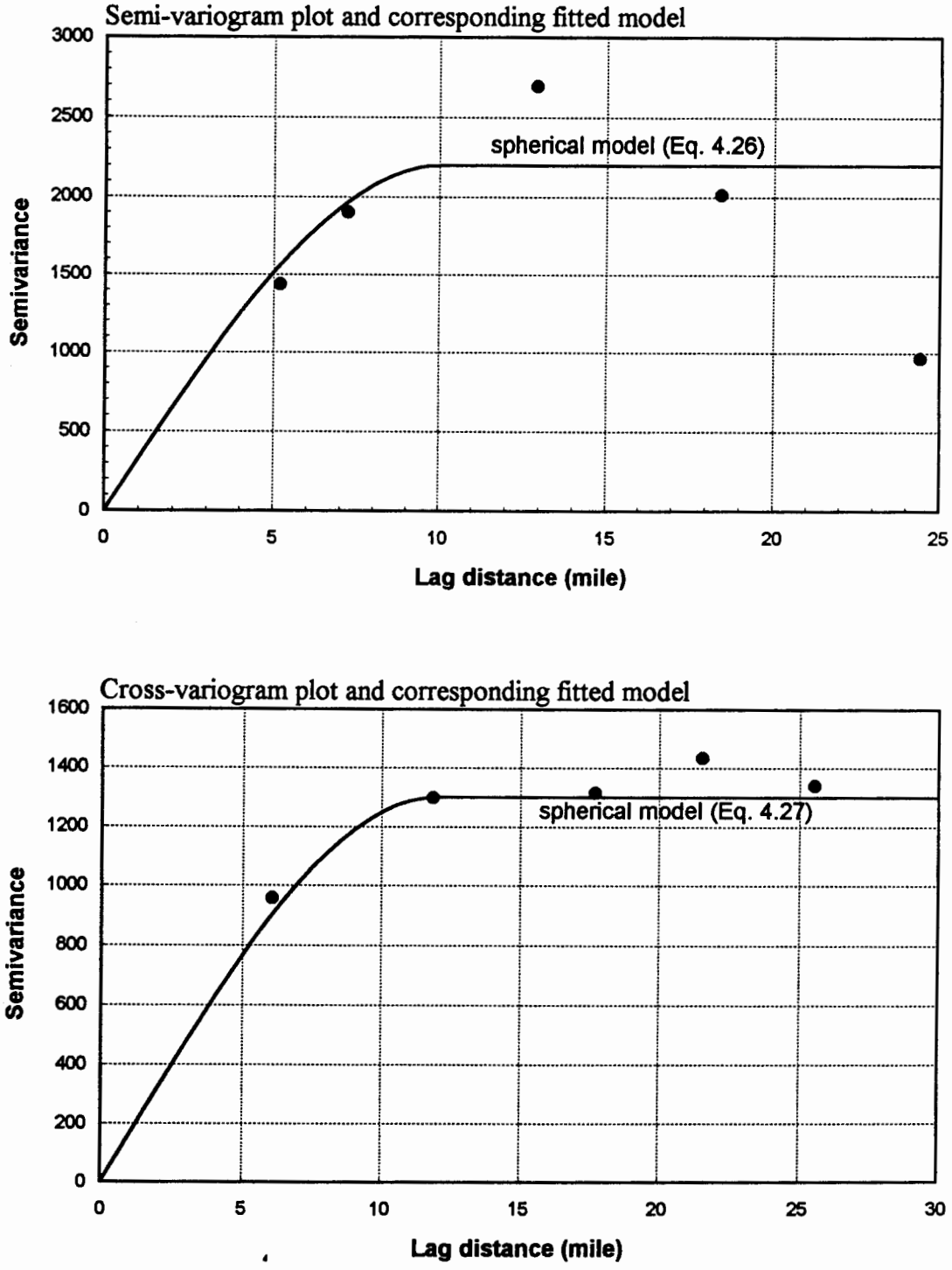

Figure 24. The calculated semi-variograms and cross-variograms and their corresponding fitted models.

Table 2. The calculated semi-variograms and cross-variograms for the interface and interface-bedrock, respectively.

Interface Semivariance				Interface-Bedrock Crossvariance		
mean distance	semivariance	pairs		mean distance	semivariance	pairs
5.19	1433.80	3		6.08	956.45	7
7.22	1902.00	18		11.88	1298.07	3
12.93	2692.60	17		17.70	1315.85	1
18.46	2013.10	12		21.54	1434.81	7
24.44	966.18	10		25.54	1340.53	2
				30.74	1476.70	5

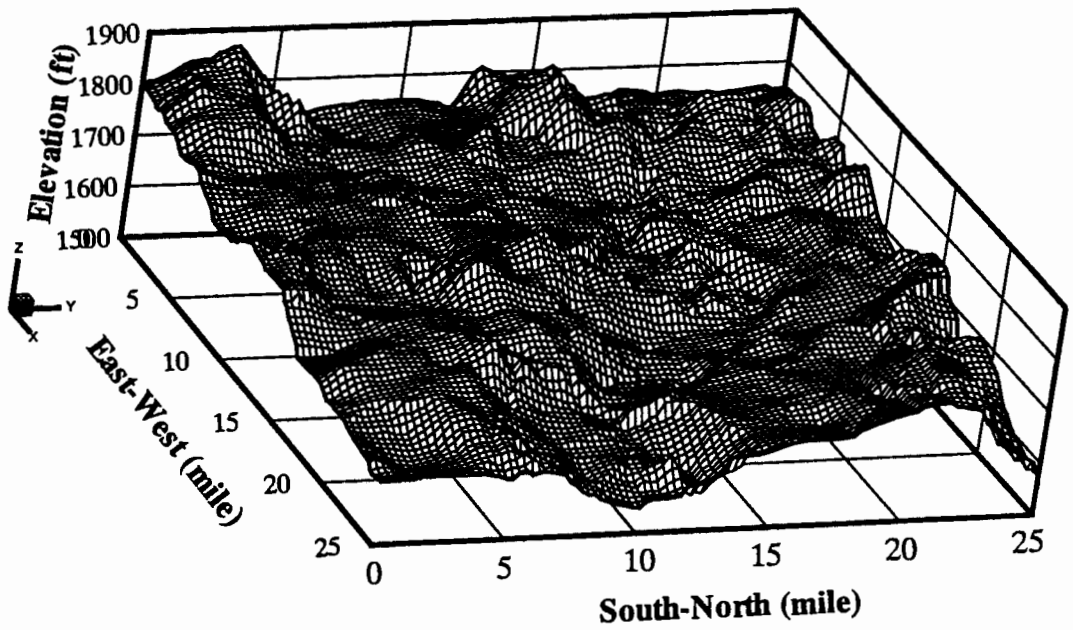

Figure 25. A three-dimensional plot of the kriged saltwater-freshwater interface elevation based on the measured interface and bedrock data.

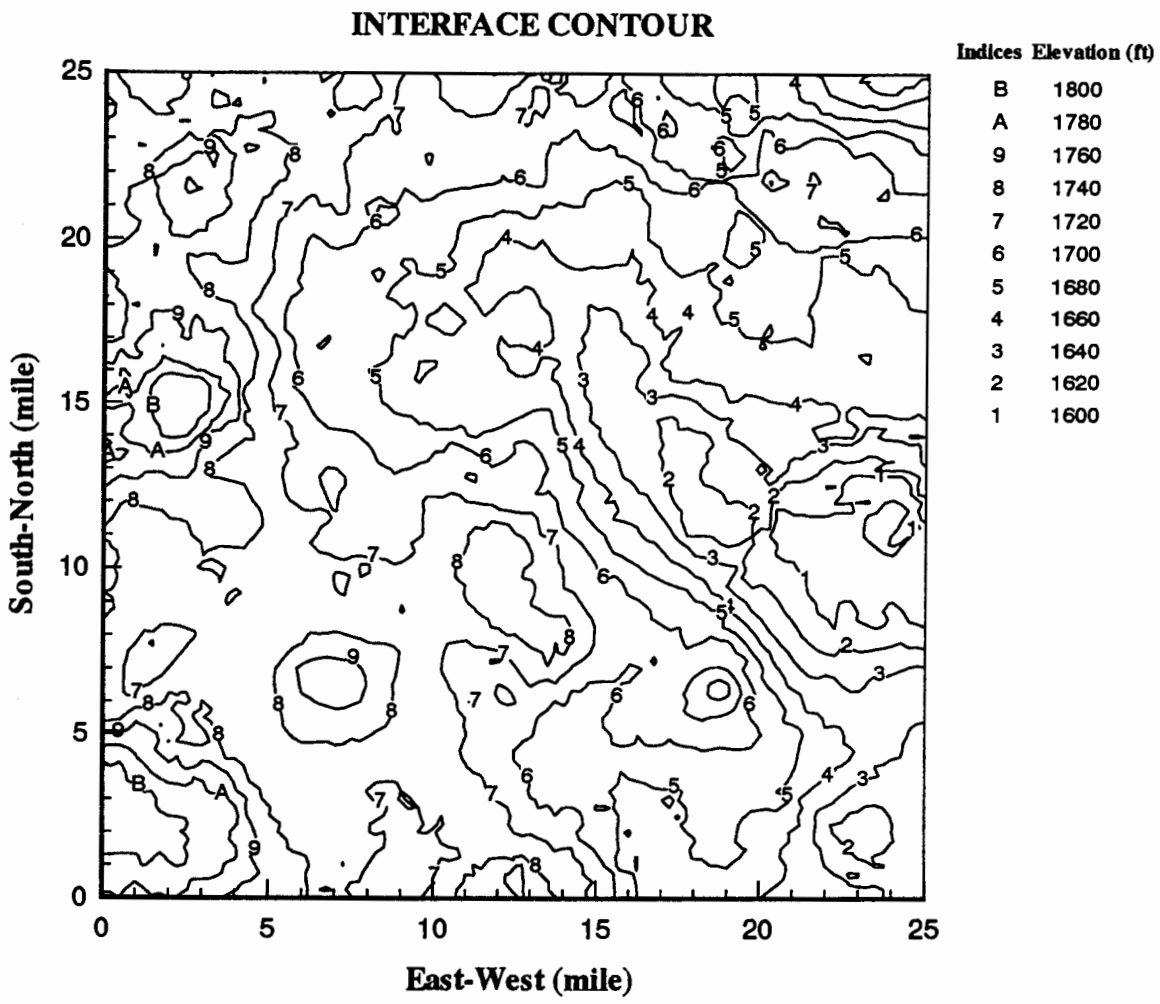

Figure 26. A plot of contours of the kriged saltwater-freshwater interface elevation based on the measured interface and bedrock data.

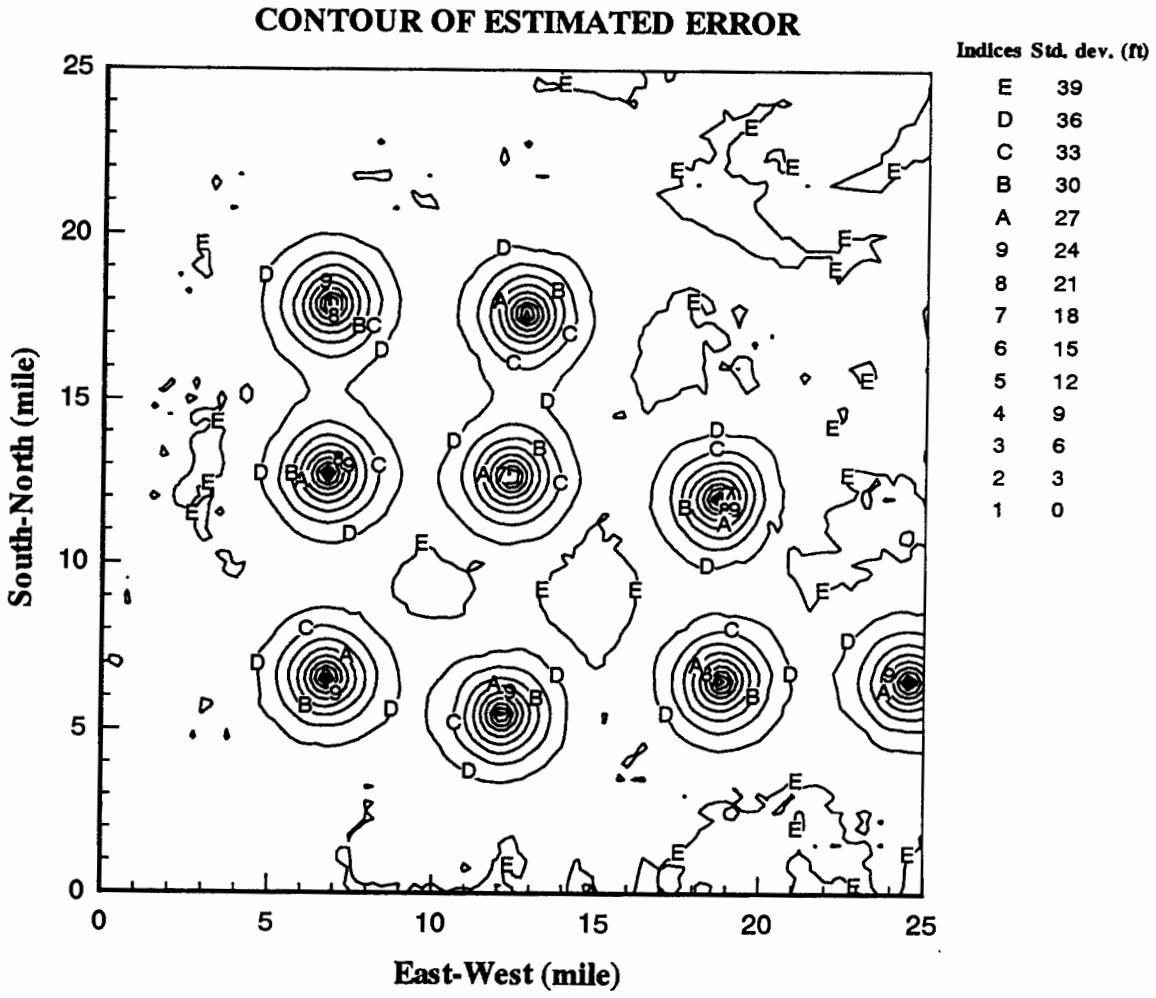

Figure 27. Contours of the estimated standard deviations based on the measured interface and bedrock data.

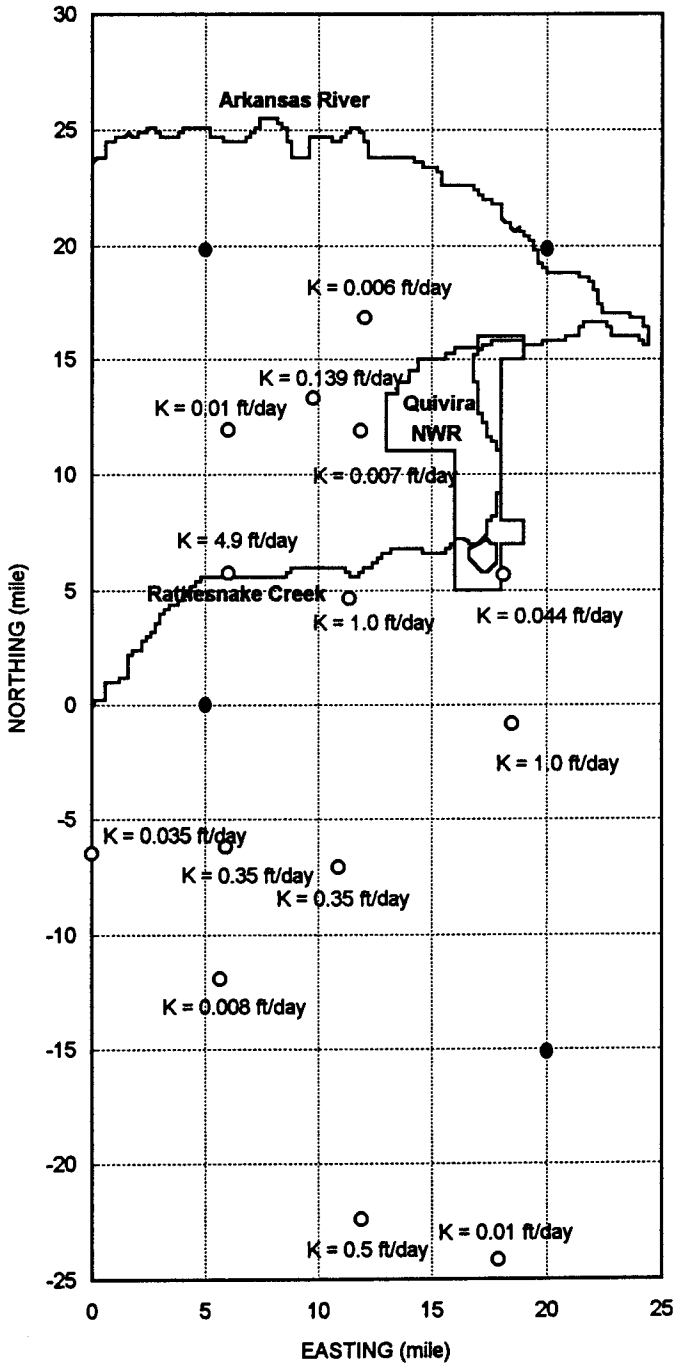

Figure 28. Locations and the corresponding values of the Permian bedrock permeability, shown as open circle, and the suggested sample sites, shown as solid circle.

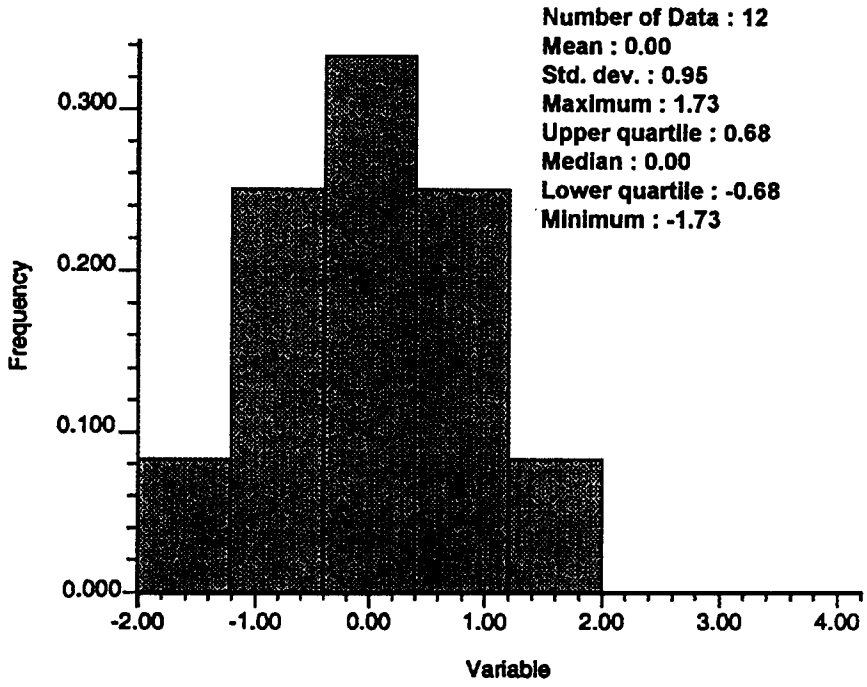

Figure 29. A plot of histogram of transformed normal scores from 12 measured Permian bedrock permeability.

Table 3. Calculated semivariograms based on the transformed normal scores.

No.	Lag	Semivariogram	No. of pairs
1	4.15	0.72	10
2	6.86	0.87	18
3	11.39	0.91	10
4	15.27	1.18	16
5	18.88	1.13	28
6	22.81	0.98	22
7	25.64	0.69	6
8	29.34	0.39	6
9	34.95	1.36	6
10	38.01	1.18	8

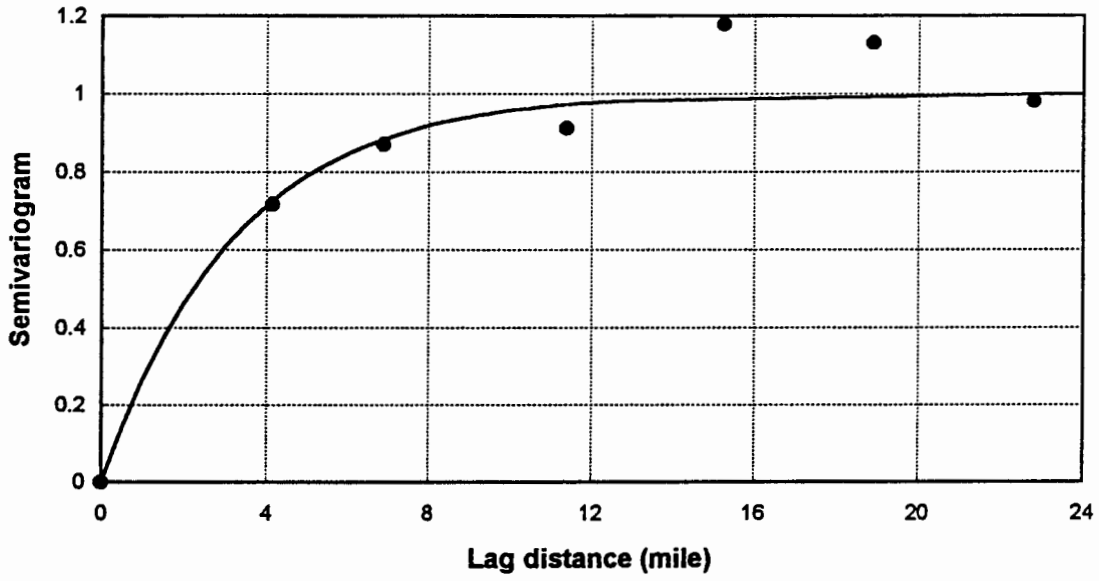

Figure 30. Plots of calculated semivariograms based on the transformed normal scores and the fitted exponential model.

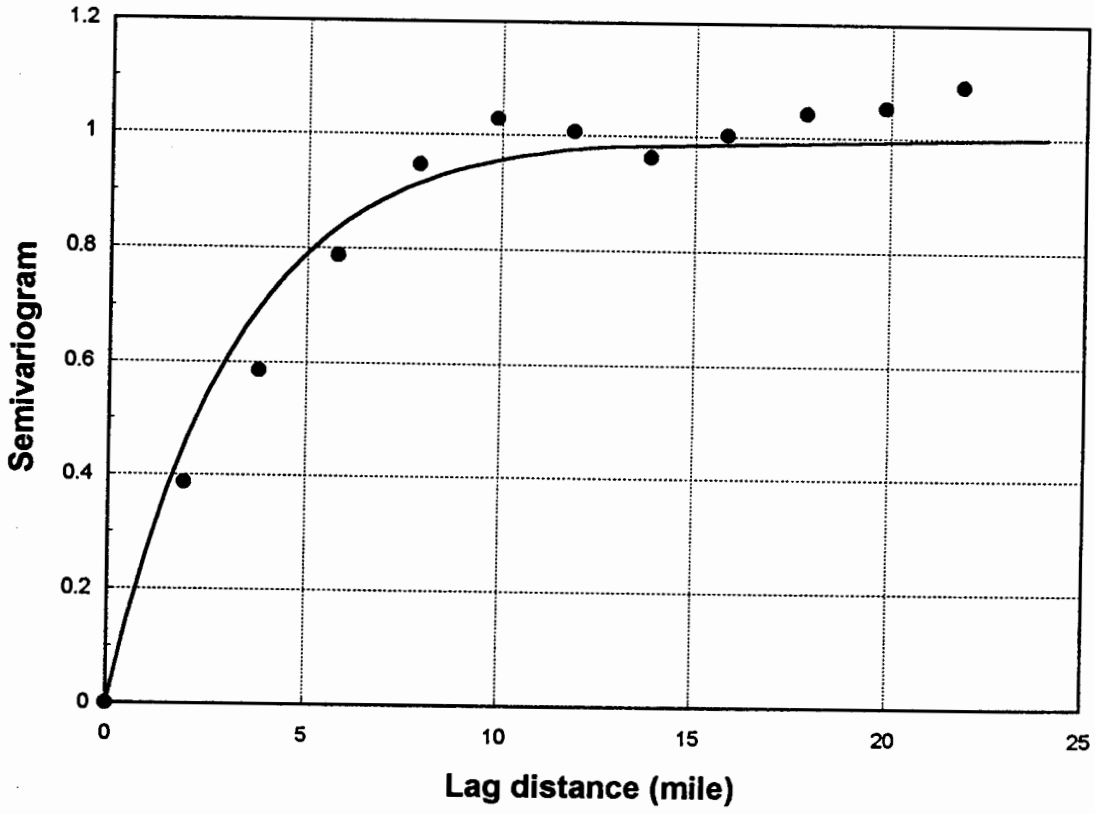

Figure 31. The calculated semivariograms of the simulated realization versus the exponential semivariogram model of the observed data.

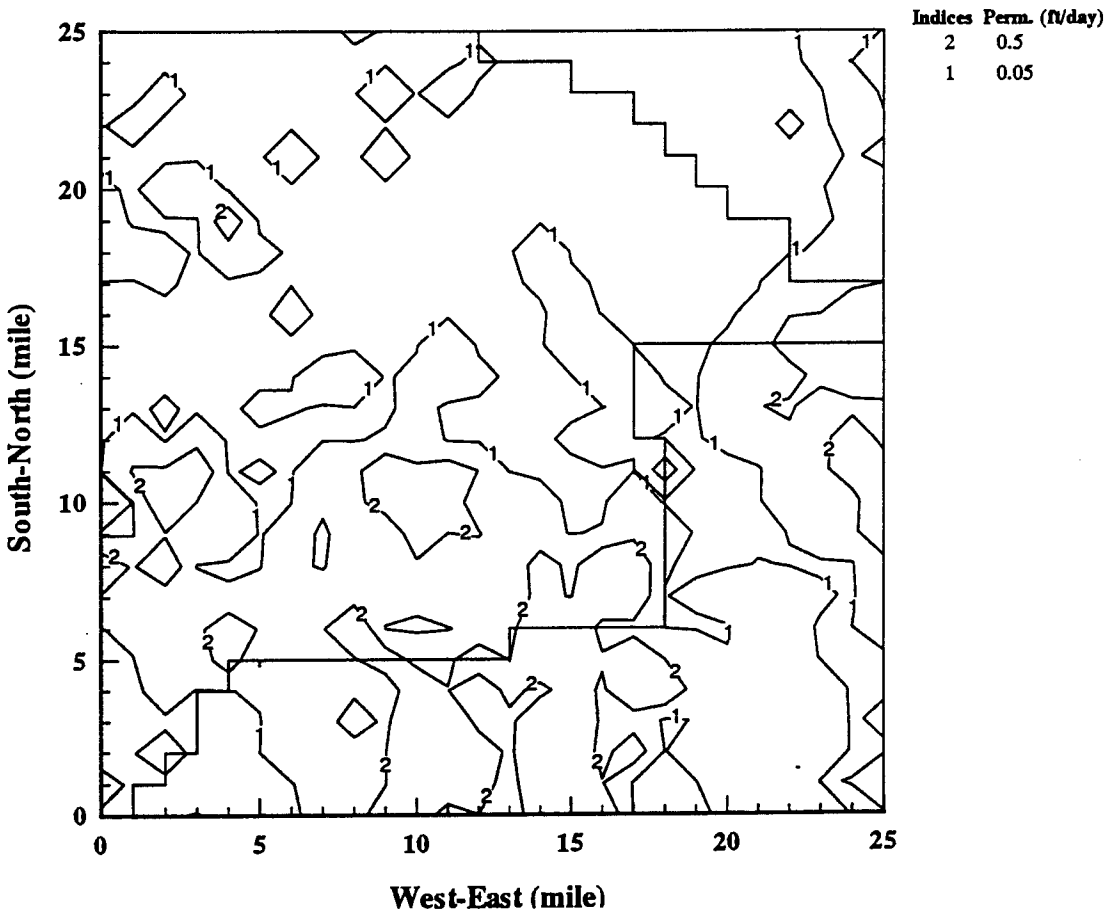

Figure 32. Contours of the simulated realization of the Permian bedrock permeability based on the simulated annealing technique.

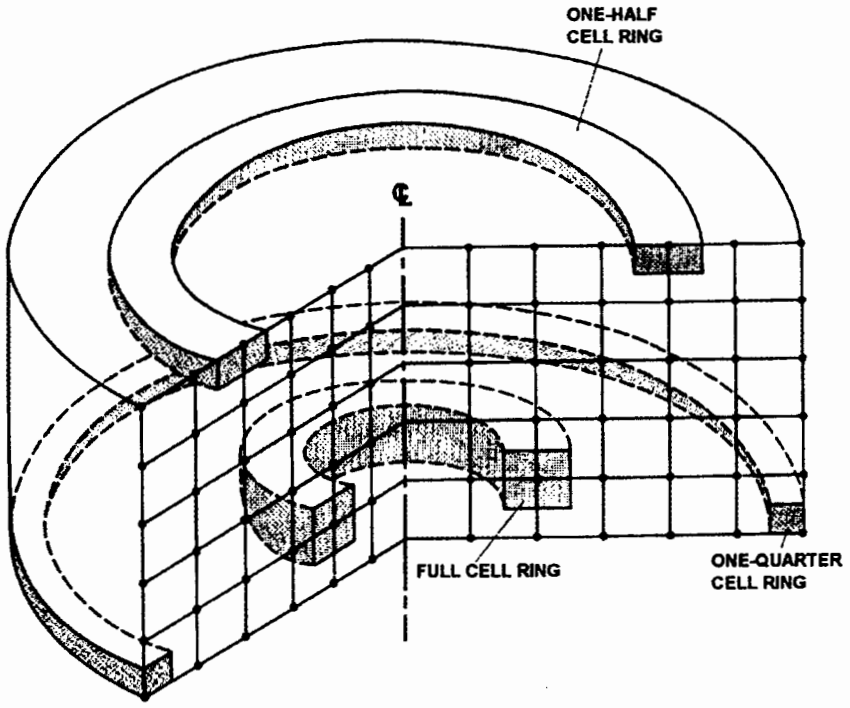

Figure 33. The finite-difference spatial discretization for a cylindrical-coordinate system.

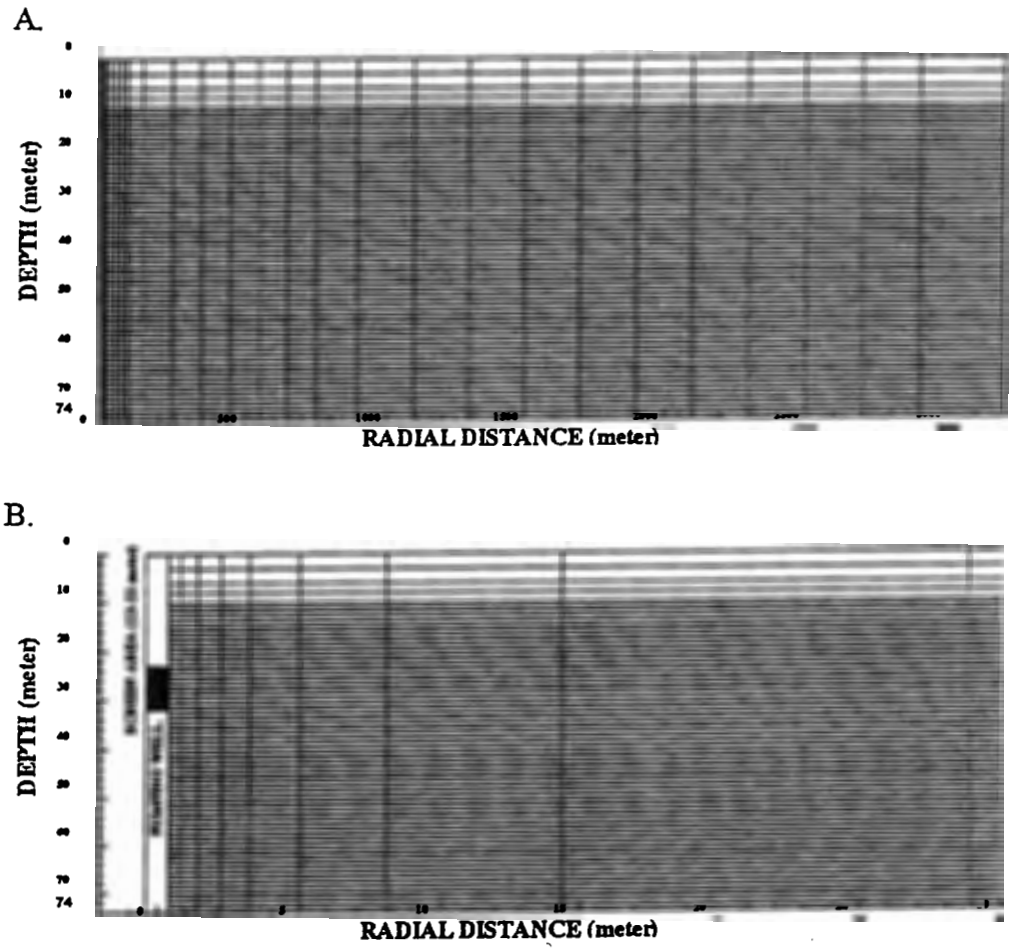

Figure 34. A. Mesh of the conceptual axisymmetrical model.
B. Mesh sizes near the pumping well.

Table 4. Simulation cases in two-dimensional saltwater upconing simulation.

Case No.	Descriptions	Figure
1.	Uniform aquifer system without clay layer (reference case). The input parameters, variables, and boundary conditions are described in Table 5 & Table 6 .	
2.	Investigation of the effect of the continuous and discontinuous clay layers.	
3.	Investigation of the effect of the porosity.	
4.	Investigation of the effect of the radial conductivity.	
5.	Investigation of the effect of the vertical conductivity.	
6.	Investigation of the effect of the location of the well screen.	
7.	Investigation of the effect of the recharge.	
8.	Investigation of the effect of the pumpage.	

Table 5. Variables and parameters used in the numerical model for saltwater upconing

Aquifer, Fluid, and other Parameters	
radial hydraulic conductivity	Kr = 23 m/d (75 ft/d)
vertical hydraulic conductivity	Kz = 23 m/d (75 ft/d)
porosity	$\phi = 0.20$
bulk porous matrix compressibility	$\alpha = 2.58 \times 10^{-7}[kg/(m\ s^2)]^{-1}$
water compressibility	$\beta = 4.40 \times 10^{-10}[kg/(m\ s^2)]^{-1}$
solute molecular diffusivity	$D_m = 1.0 \times 10^{-9}\ m^2/s$
longitudinal dispersivity	$\alpha_L = 1$ m
transverse dispersivity	$\alpha_T = 0.05$ m
fluid (water) density	$\rho_o = 1{,}000\ kg/m^3$
brine density	$\rho = 1{,}025\ kg/m^3$
solid grain density	$\rho_s = 2{,}650\ kg/m^3$
fluid (water) viscosity	$\mu = 1.0 \times 10^{-3}$ kg/(m s)
initial fluid (freshwater) salt concentration	$C_0 = 0$
initial brine fluid salt concentration	C (r,z,0)
initial specified pressure at the boundary	p(r, z, 0)
saturated thickness	b = 74 m
depth to freshwater-saltwater interface	54 m
depth to Permian boundary	74 m
volumetric pumping rate	$Q_p = 50\ m^{-3}/s$ (~800 gpm)
gravitational acceleration	$g = 9.81\ m/s^2$
total simulation time	1 yr.
Clay Layer Properties	
thickness	10 m
hydraulic conductivity	0.023 m/d (0.075 ft/d)
porosity	$\phi = 0.02$
Dependent Variables	
concentration	C(r, z, t)
pressure	p(r, z, t)

Table 6. Boundary conditions used in two-dimensional saltwater upconing simulation.

Top	Bottom	Outer radius	Inner radius
streamline (no flow)	constant pressure & brine concentration	constant pressure & brine concentration	specified volumetric flux at well $Q = 50\ m^{-3}/s$

A.

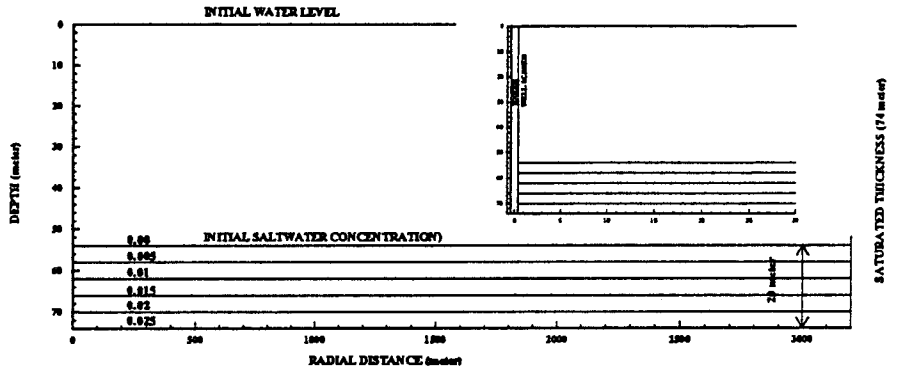

B.

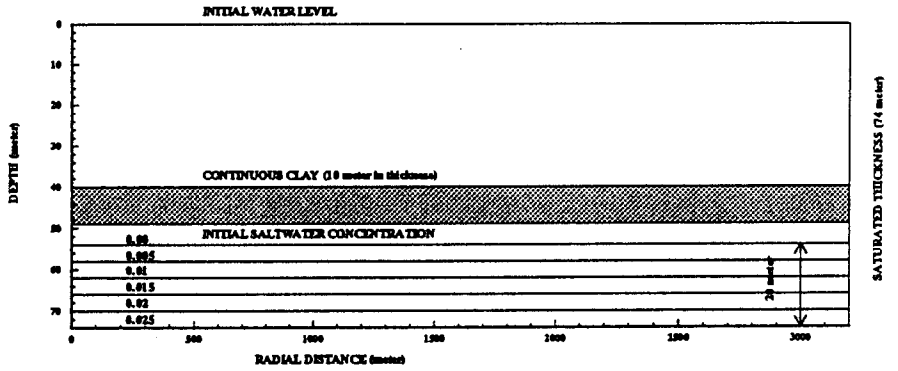

C.

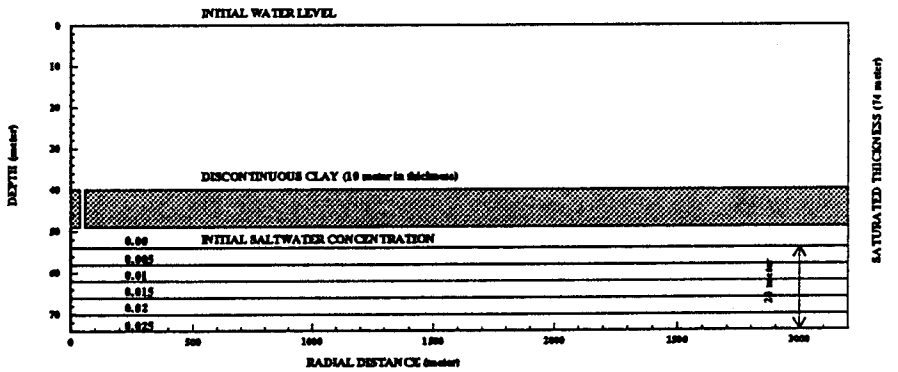

Figure 35. A. A conceptual homogeneous and isotropic aquifer with no clay layer for salt water upconing simulation.
B. A conceptual homogeneous and isotropic aquifer with continuous clay layer for salt water upconing simulation.
C. A conceptual homogeneous and isotropic aquifer with discontinuous clay layer for salt water upconing simulation.

A. No clay layer

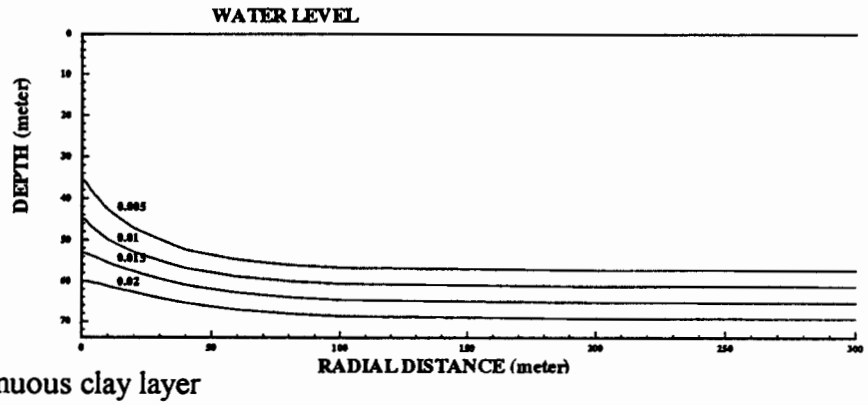

B. Continuous clay layer

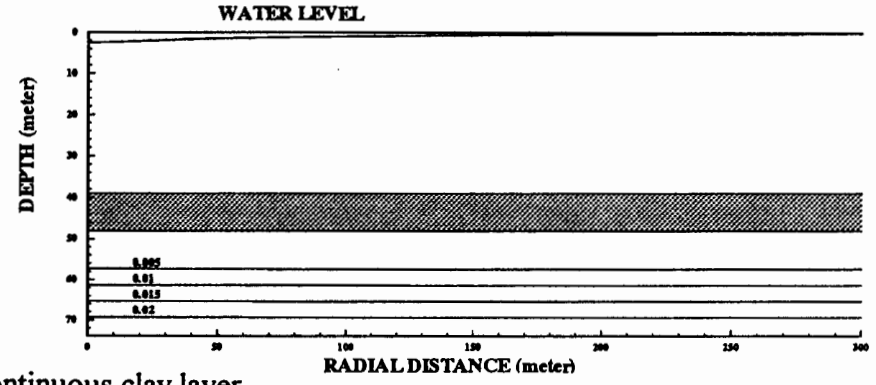

C. Discontinuous clay layer

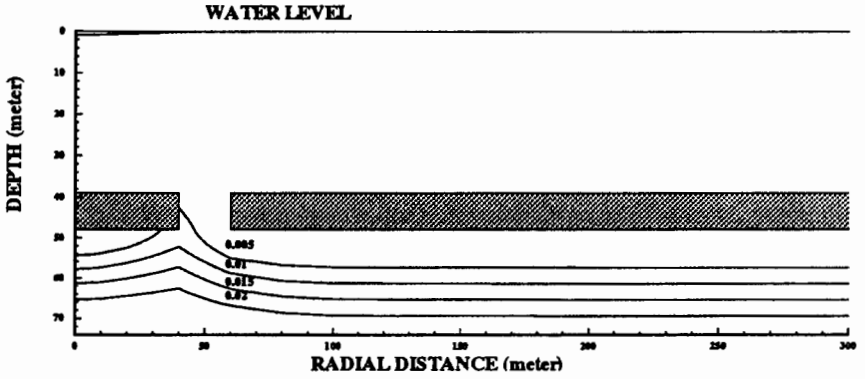

Figure 36. Isolines of brine concentration for no clay layer, continuous clay layer, and discontinuous clay layer cases at the 7th day after pumping started.
A. No clay layer case.
B. Continuous clay layer case.
C. Discontinuous clay layer case.

A. No clay layer

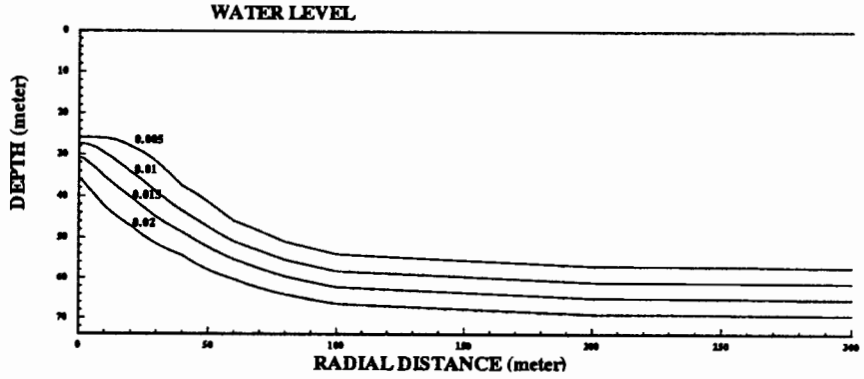

B. Continuous clay layer

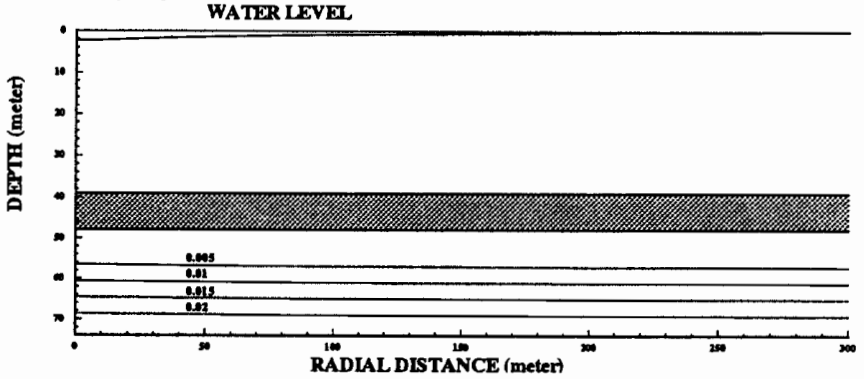

C. Discontinuous clay layer

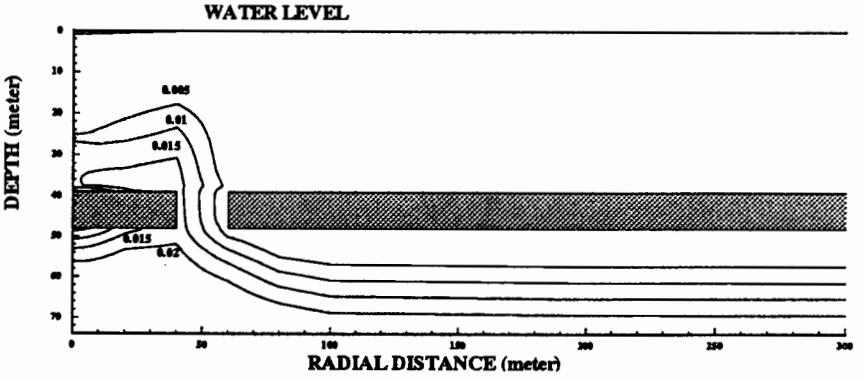

Figure 37. Isolines of brine concentration for no clay layer, continuous clay layer, and discontinuous clay layer cases at the 30th day after pumping started.
A. No clay layer case.
B. Continuous clay layer case.
C. Discontinuous clay layer case.

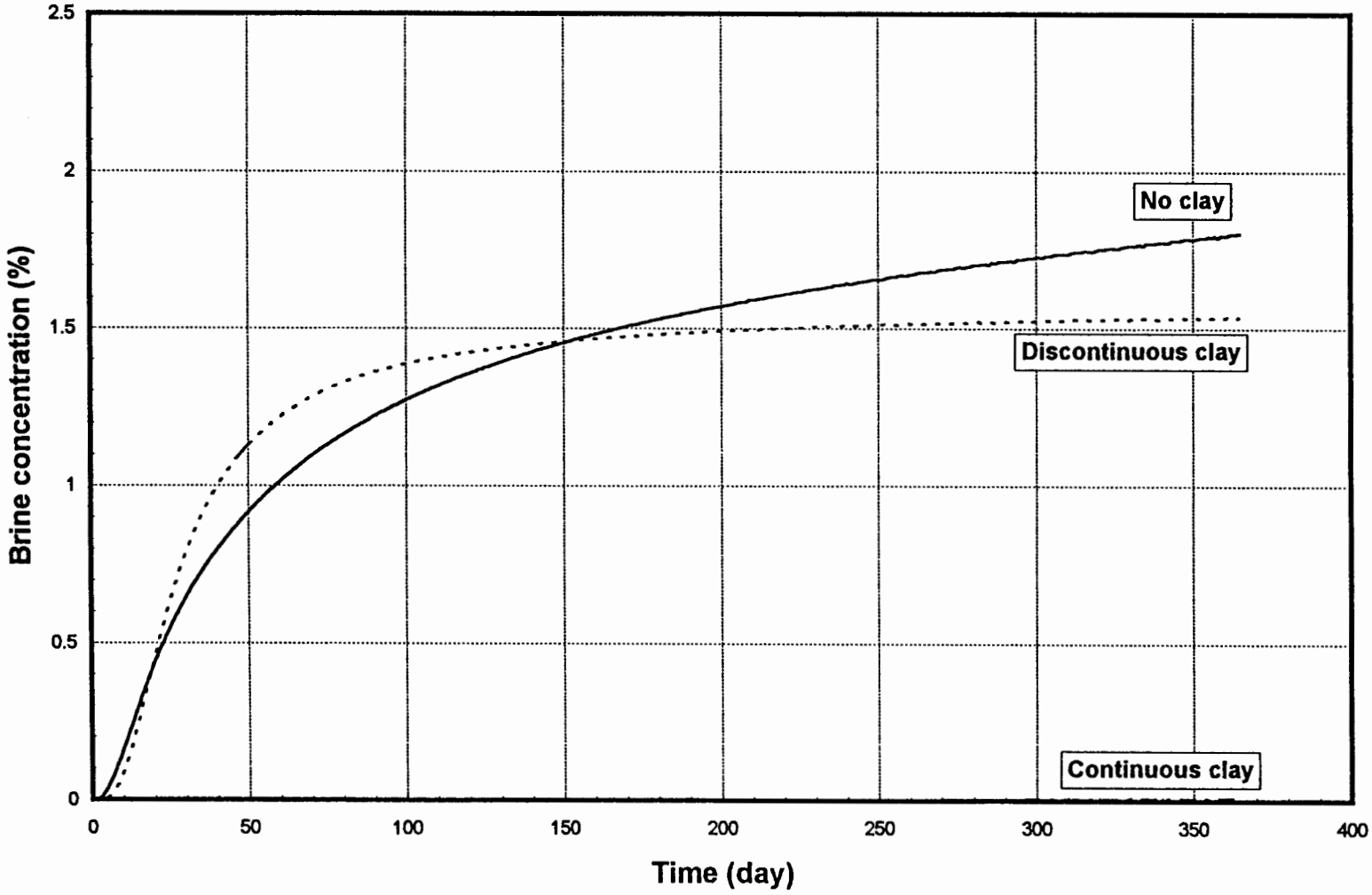

Figure 38. Comparison of discharged brine concentration vs. time for the simulated system with continuous, discontinuous, and no clay layers.

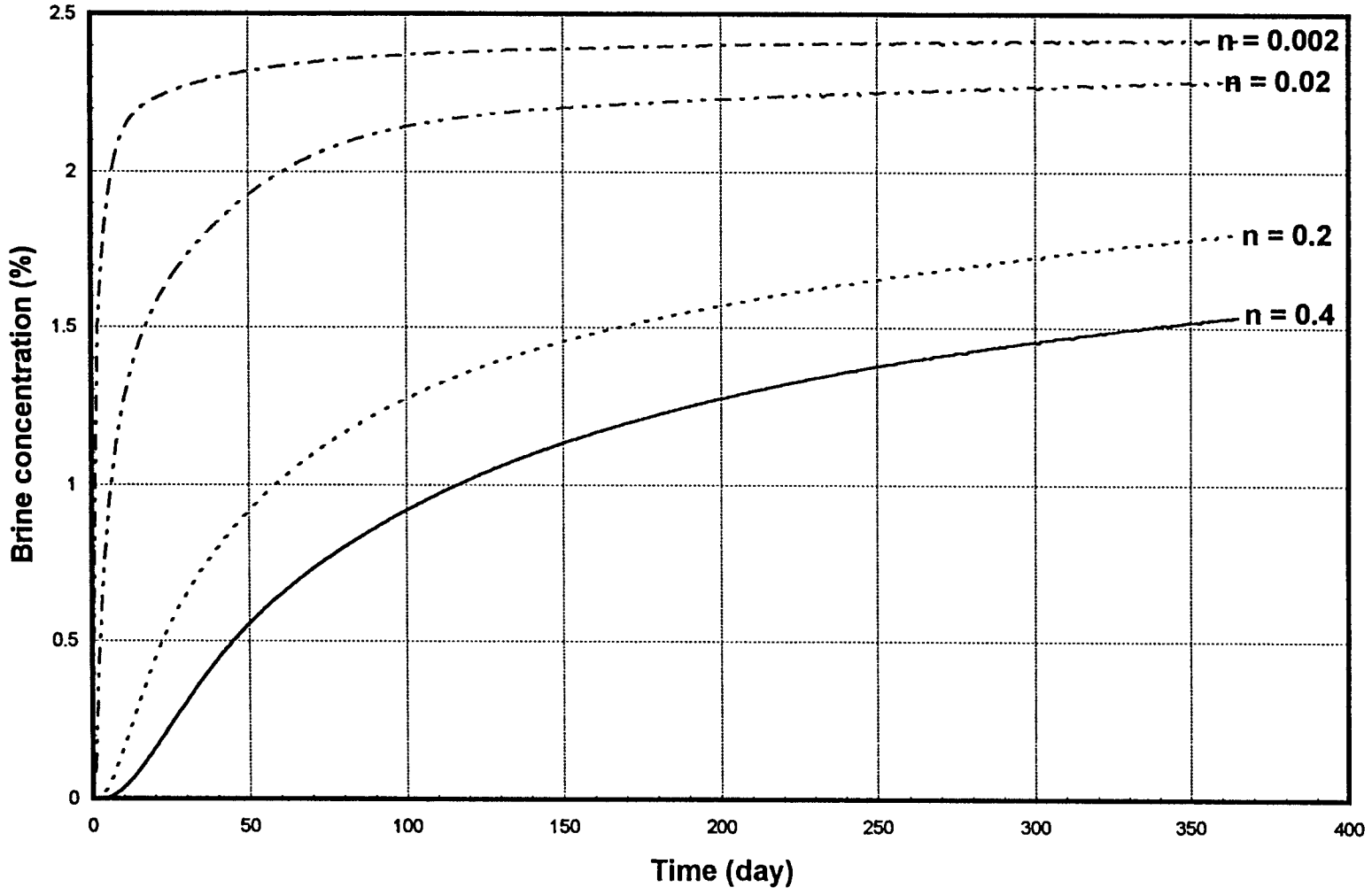

Figure 39. Comparison of discharged brine concentration vs. time for the simulated system with 4 different porosity (0.002 ~ 0.4).

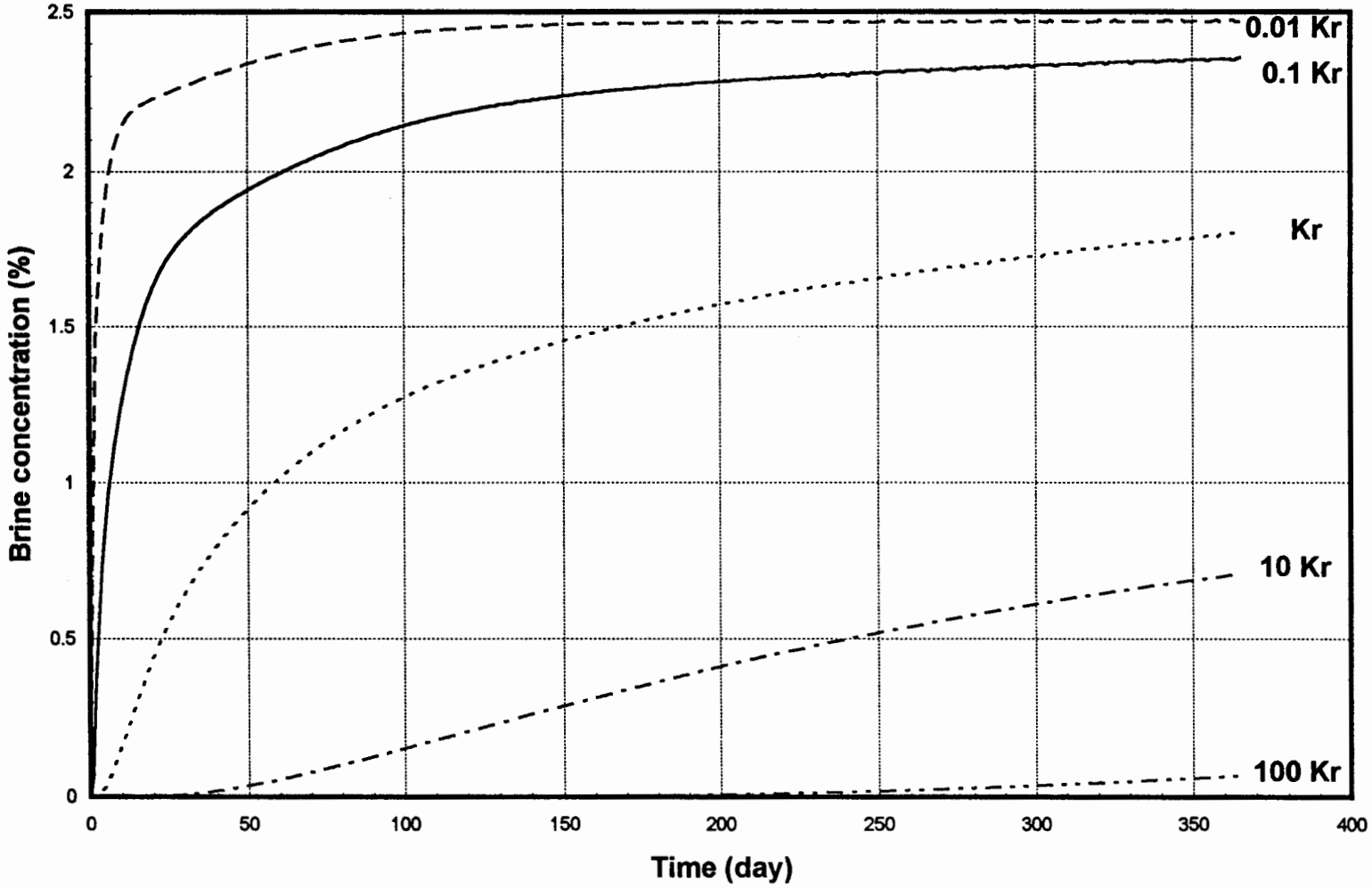

Figure 40. Comparison of discharged brine concentration vs. time for the simulated system with 5 different radial hydraulic conductivity, where Kr = 23 m/d.

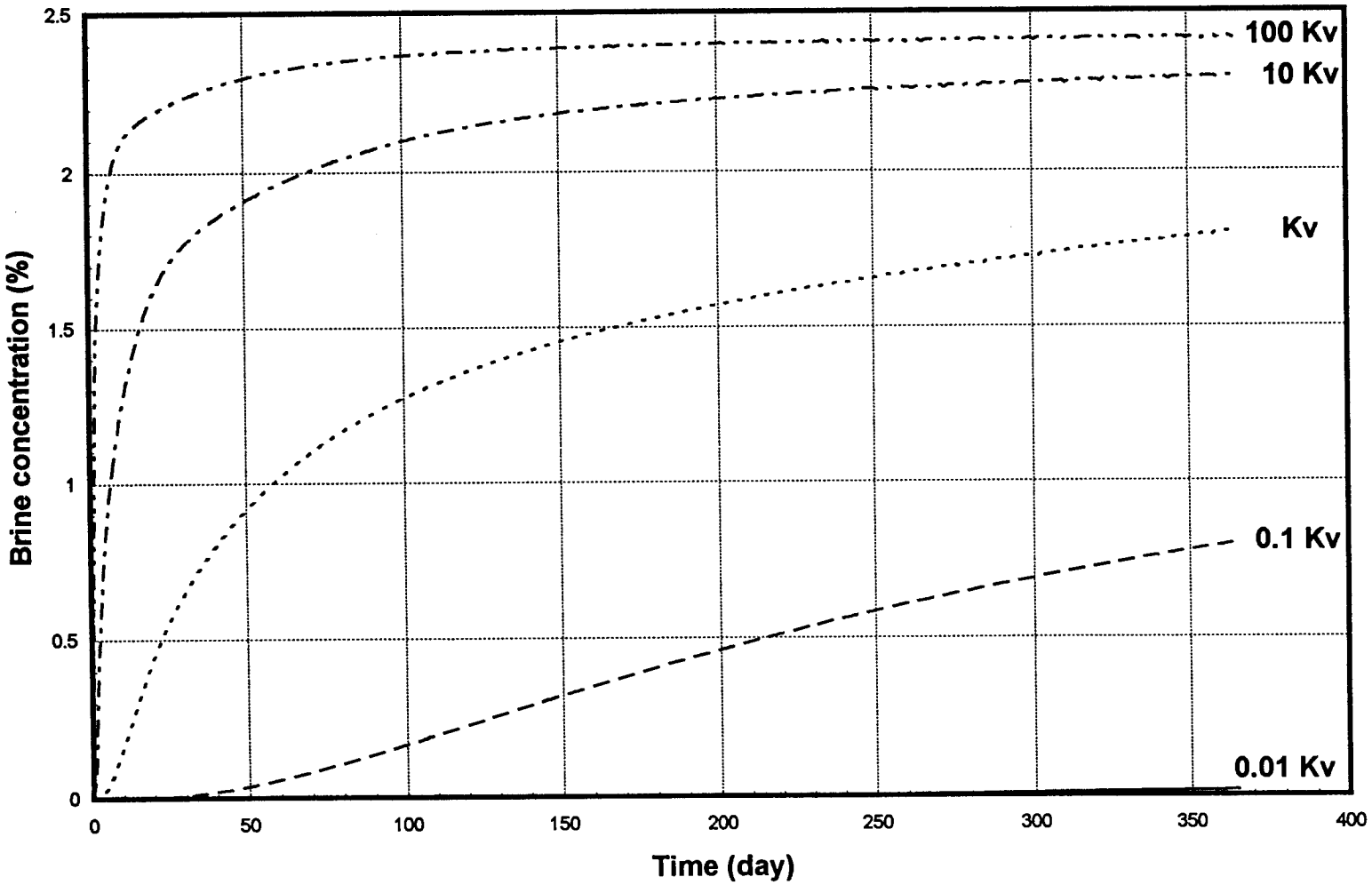

Figure 41. Comparison of discharged brine concentration vs. time for the simulated system with 5 different radial hydraulic conductivity, where Kv = 23 m/d.

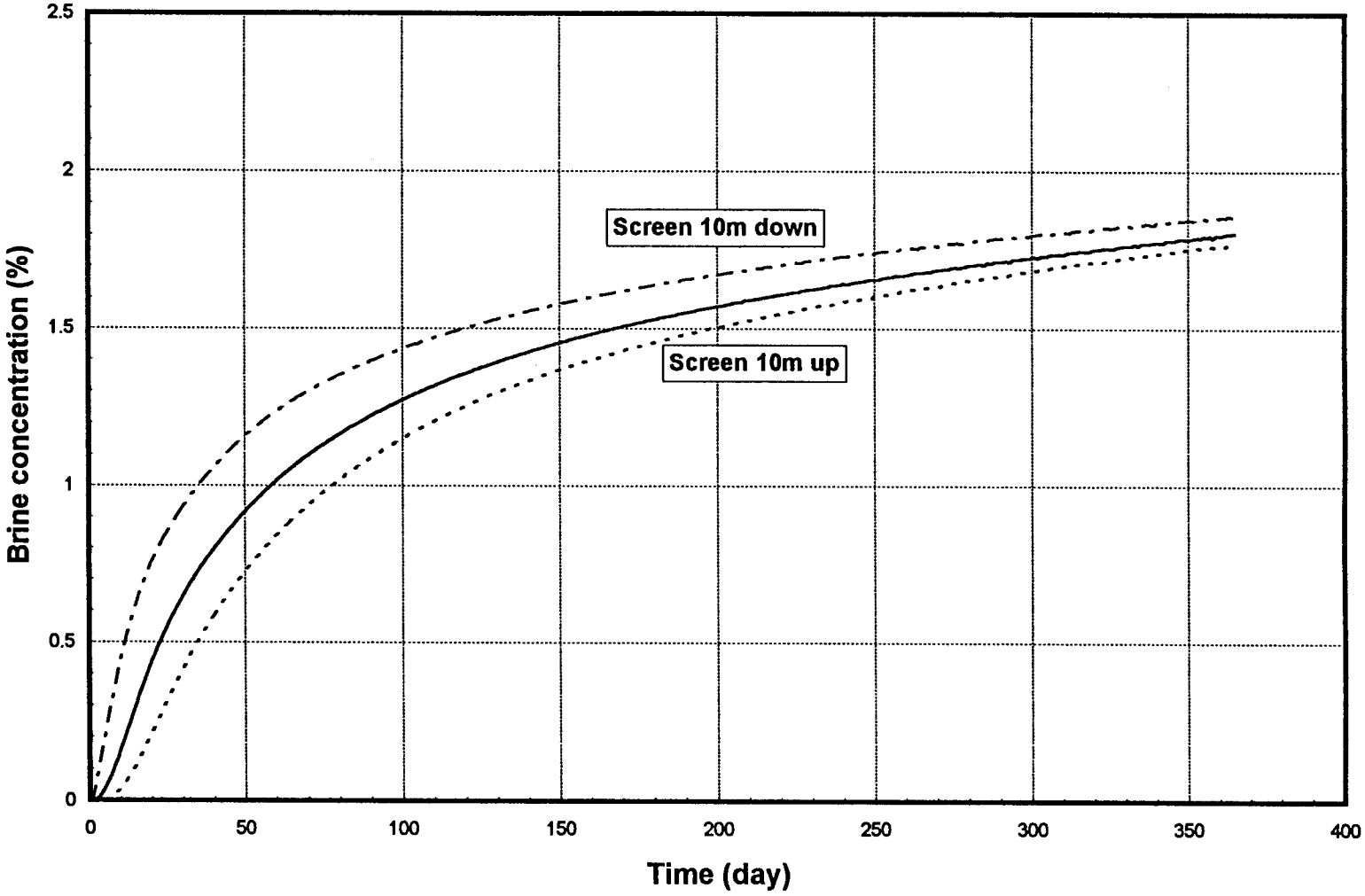

Figure 42. Comparison of discharged brine concentration vs. time for the simulated system with 3 different well screen locations.

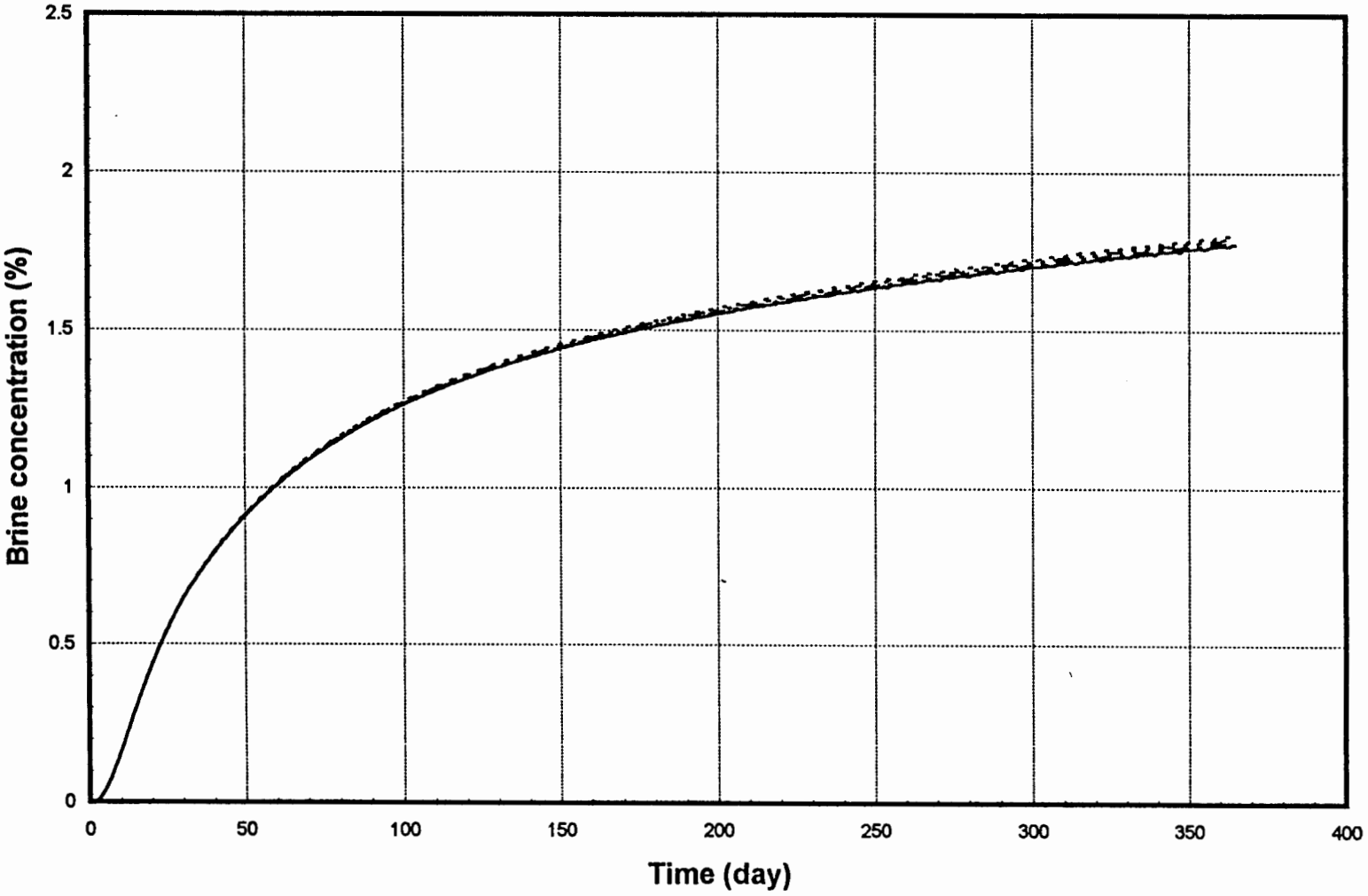

Figure 43. Comparison of discharged brine concentration vs. time for the simulated system with 4 different recharges.

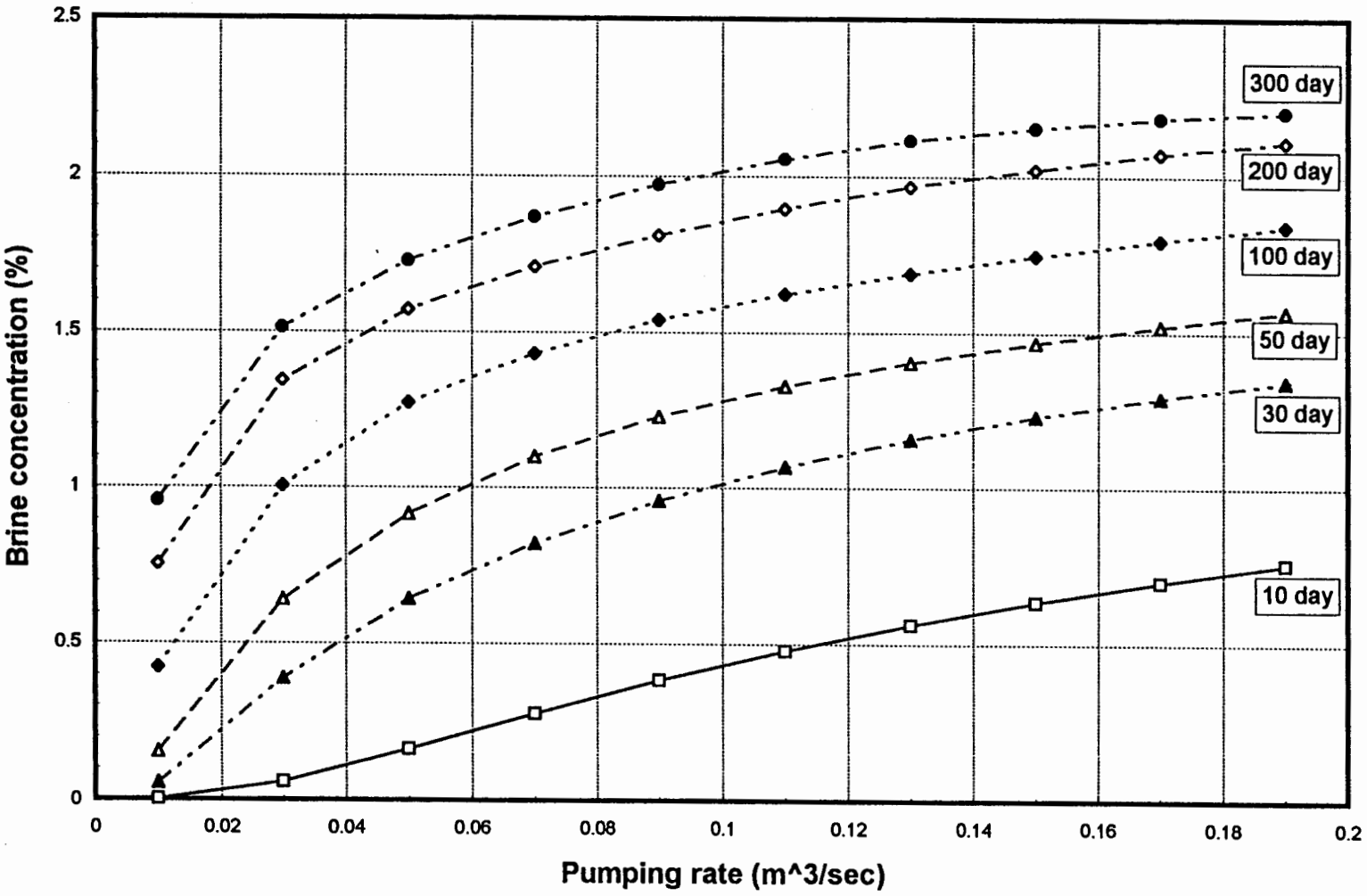

Figure 44. Comparison of discharged brine concentration vs. time for the simulated system with various pumping rates.

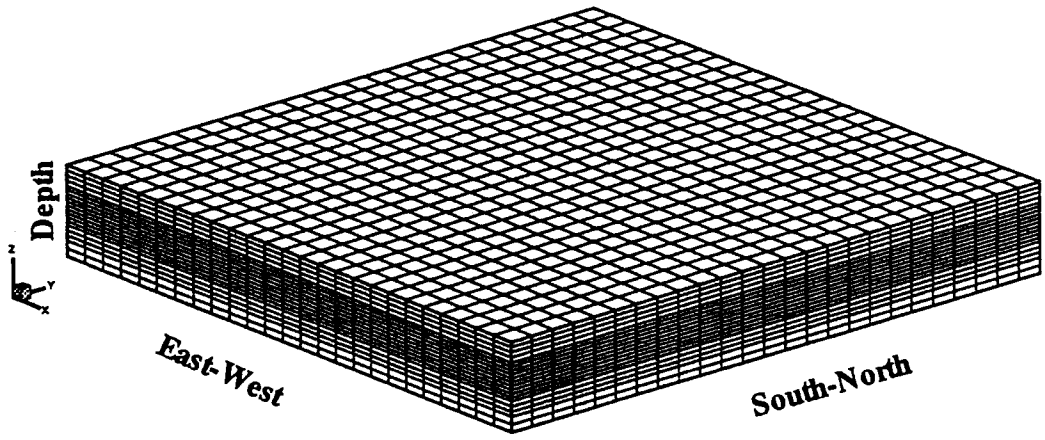

Figure 45. A three-dimensional mesh of the study area with uniform spacing in both X and Y directions and variable spacing in the vertical, Z, direction.

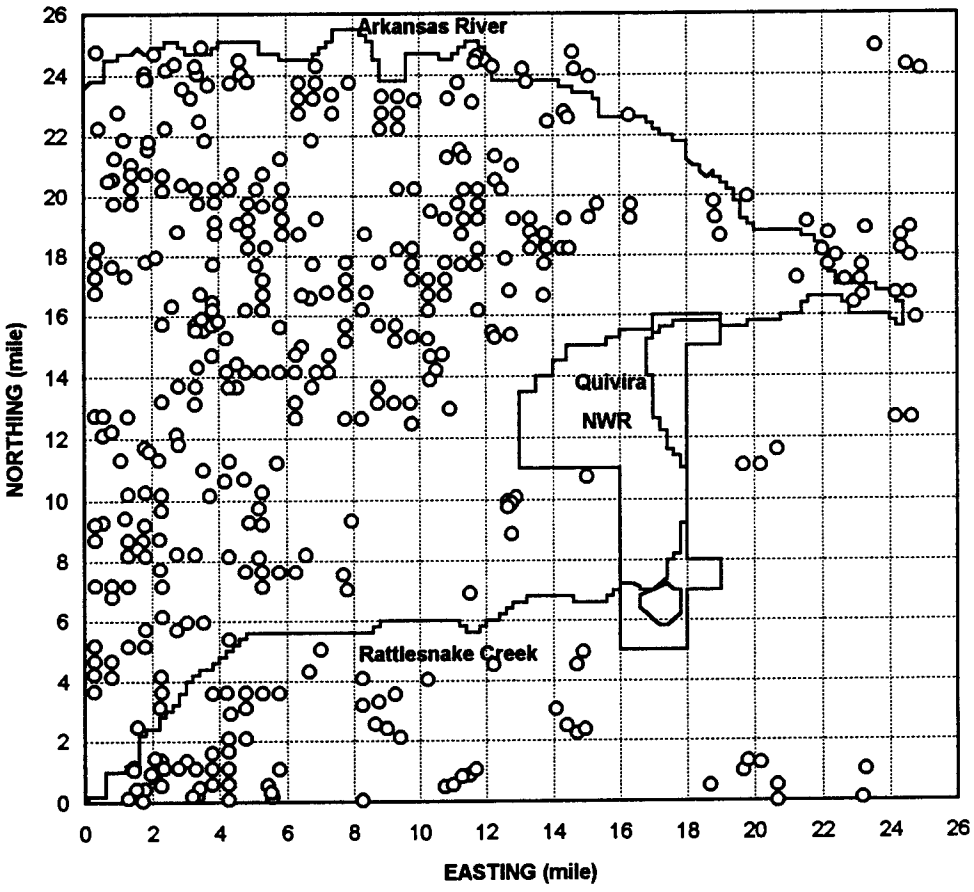

Figure 46. The distribution of the 1990 irrigation well in the study area.

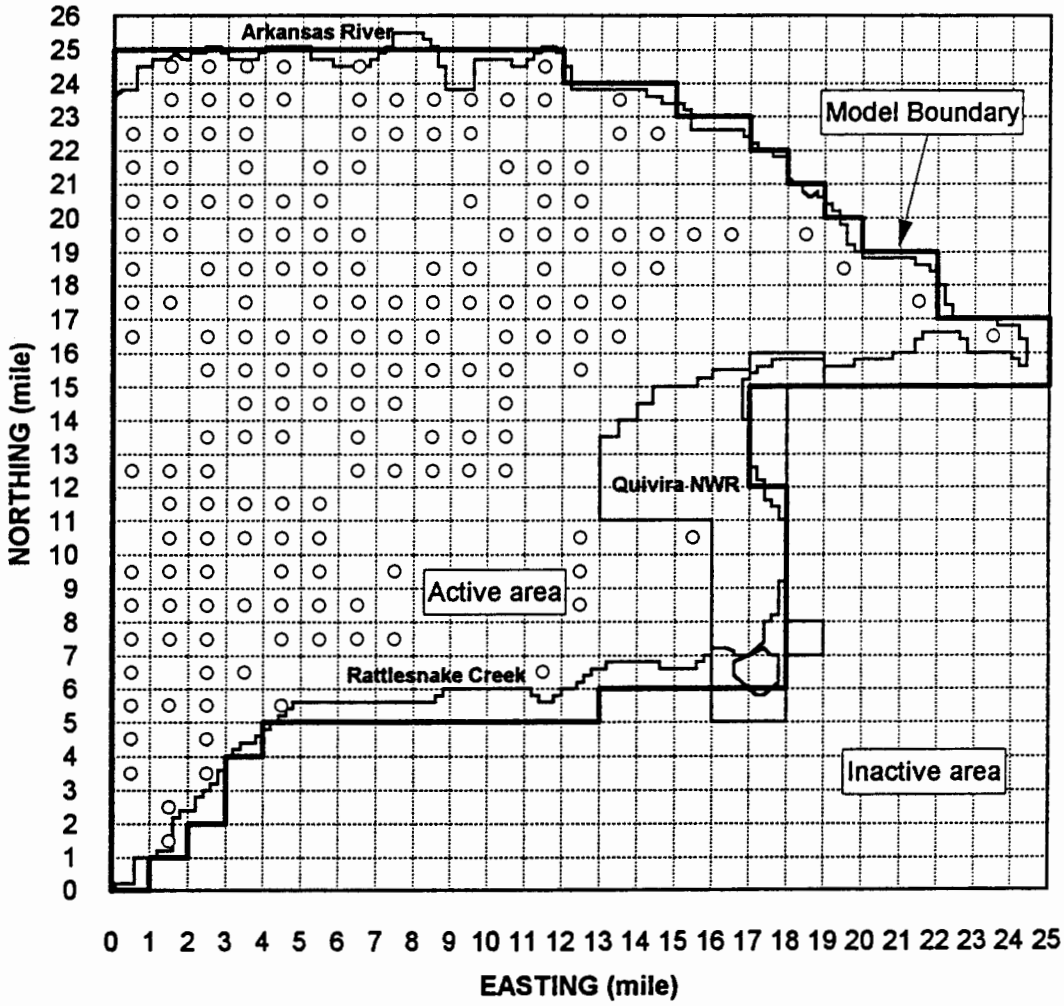

Figure 47. The distribution of the lumped 1990 irrigation well in the study area and the active and inactive are also indicated.

Table 7. The lumped pumpage (m^3/sec) for the three-dimensional numerical simulation.

No.	EAST.	NORTH.	Pump. (m^3/sec)	No.	EAST.	NORTH.	Pump. (m^3/sec)
1	1	4	0.00738	89	6	18	0.0102
2	1	5	0.02514	90	6	19	0.0121
3	1	6	0.00735	91	6	20	0.01699
4	1	7	0.00272	92	6	21	0.02106
5	1	8	0.01026	93	6	22	0.00732
6	1	9	0.00516	94	7	8	0.00404
7	1	10	0.01349	95	7	9	0.0048
8	1	13	0.01777	96	7	13	0.00629
9	1	17	0.00579	97	7	14	0.00917
10	1	18	0.01101	98	7	15	0.01806
11	1	19	0.00648	99	7	16	0.0061
12	1	20	0.00619	100	7	17	0.00737
13	1	21	0.0118	101	7	18	0.00751
14	1	22	0.01192	102	7	19	0.00751
15	1	23	0.00751	103	7	20	0.00591
16	2	2	0.00595	104	7	22	0.00493
17	2	3	0.00598	105	7	23	0.00751
18	2	6	0.02254	106	7	24	0.02504
19	2	8	0.0061	107	7	25	0.00582
20	2	9	0.03023	108	8	8	0.00066
21	2	10	0.0179	109	8	10	0.00001
22	2	11	0.01295	110	8	13	0.0061
23	2	12	0.00757	111	8	15	0.00917
24	2	13	0.00619	112	8	16	0.01502
25	2	18	0.00776	113	8	17	0.01362
26	2	20	0.0061	114	8	18	0.0122
27	2	21	0.01311	115	8	23	0.00751
28	2	22	0.01621	116	8	24	0.01314
29	2	23	0.00507	117	9	13	0.00594
30	2	24	0.0289	118	9	14	0.01126
31	2	25	0.02524	119	9	16	0.00751
32	3	4	0.01302	120	9	17	0.01114
33	3	5	0.00394	121	9	18	0.0056
34	3	6	0.00732	122	9	19	0.00619
35	3	7	0.00751	123	9	23	0.01282
36	3	8	0.01221	124	9	24	0.0061
37	3	9	0.01207	125	10	13	0.00751
38	3	10	0.00751	126	10	14	0.01502
39	3	11	0.0061	127	10	16	0.02254
40	3	12	0.00738	128	10	18	0.01502
41	3	13	0.00266	129	10	19	0.01218
42	3	14	0.01342	130	10	21	0.01282
43	3	16	0.00375	131	10	23	0.01142
44	3	17	0.00347	132	10	24	0.00689
45	3	19	0.01198	133	11	13	0.00002

46	3	21	0.01656	134	11	14	0.0061
47	3	23	0.00557	135	11	15	0.0185
48	3	24	0.00657	136	11	16	0.00619
49	3	25	0.00694	137	11	17	0.02254
50	4	7	0.01329	138	11	18	0.01389
51	4	9	0.00751	139	11	20	0.01162
52	4	11	0.0091	140	11	22	0.00454
53	4	12	0.00413	141	11	24	0.0061
54	4	14	0.00707	142	12	7	0.00072
55	4	15	0.00754	143	12	17	0.00751
56	4	16	0.01876	144	12	18	0.02118
57	4	17	0.01126	145	12	19	0.01133
58	4	18	0.00751	146	12	20	0.02347
59	4	19	0.00751	147	12	21	0.01323
60	4	20	0.01846	148	12	22	0.00935
61	4	21	0.01164	149	12	24	0.01014
62	4	22	0.00629	150	12	25	0.00093
63	4	23	0.0061	151	13	9	0.00001
64	4	24	0.00948	152	13	10	0.00002
65	4	25	0.0167	153	13	11	0.00004
66	5	6	0.00274	154	13	16	0.0001
67	5	8	0.00751	155	13	17	0.00751
68	5	9	0.0055	156	13	18	0.00075
69	5	10	0.00075	157	13	20	0.00751
70	5	11	0.01311	158	13	21	0.00615
71	5	12	0.00626	159	13	22	0.01502
72	5	14	0.01915	160	14	17	0.00635
73	5	15	0.01972	161	14	18	0.00466
74	5	16	0.01117	162	14	19	0.02372
75	5	17	0.00751	163	14	20	0.00563
76	5	19	0.01221	164	14	23	0.00723
77	5	20	0.02138	165	14	24	0.00732
78	5	21	0.00929	166	15	19	0.01042
79	5	24	0.01167	167	15	20	0.00751
80	5	25	0.00105	168	15	23	0.01502
81	6	8	0.01972	169	16	11	0.00001
82	6	9	0.00626	170	16	20	0.01098
83	6	10	0.01251	171	17	20	0.01302
84	6	11	0.00354	172	19	20	0.0103
85	6	12	0.00657	173	20	19	0.00222
86	6	15	0.01362	174	22	18	0.00774
87	6	16	0.00629	175	24	17	0.00858
88	6	17	0.01502				

Table 8. Variables and parameters used in the three-dimensional numerical model.

Aquifer, Fluid, and other Parameters	
radial hydraulic conductivity	Kr = 23 m/d (75 ft/d)
vertical hydraulic conductivity	Kz = 23 m/d (75 ft/d)
porosity	$\phi = 0.20$
bulk porous matrix compressibility	$\alpha = 2.58 \times 10^{-7}[kg/(m\ s^2)]^{-1}$
water compressibility	$\beta = 4.40 \times 10^{-10}[kg/(m\ s^2)]^{-1}$
solute molecular diffusivity	$D_m = 1.0 \times 10^{-9}\ m^2/s$
longitudinal dispersivity	$\alpha_L = 1$ m
transverse dispersivity	$\alpha_T = 0.05$ m
fluid (water) density	$\rho_o = 1{,}000\ kg/m^3$
brine density	$\rho = 1{,}025\ kg/m^3$
solid grain density	$\rho_s = 2{,}650\ kg/m^3$
fluid (water) viscosity	$\mu = 1.0 \times 10^{-3}\ kg/(m\ s)$
initial fluid (freshwater) salt concentration	$C_0 = 0$
initial brine fluid salt concentration	C(x,y,z,0)
initial specified pressure at the boundary	p(x,y,z, 0)
pumping rate	Q_p (x,y,z,t)
gravitational acceleration	$g = 9.81\ m/s^2$